ISSN 2622-9374 (Online)

Asian Institute of Research

Engineering and Technology Quarterly Reviews

Vol. 8 No.2 December 2025

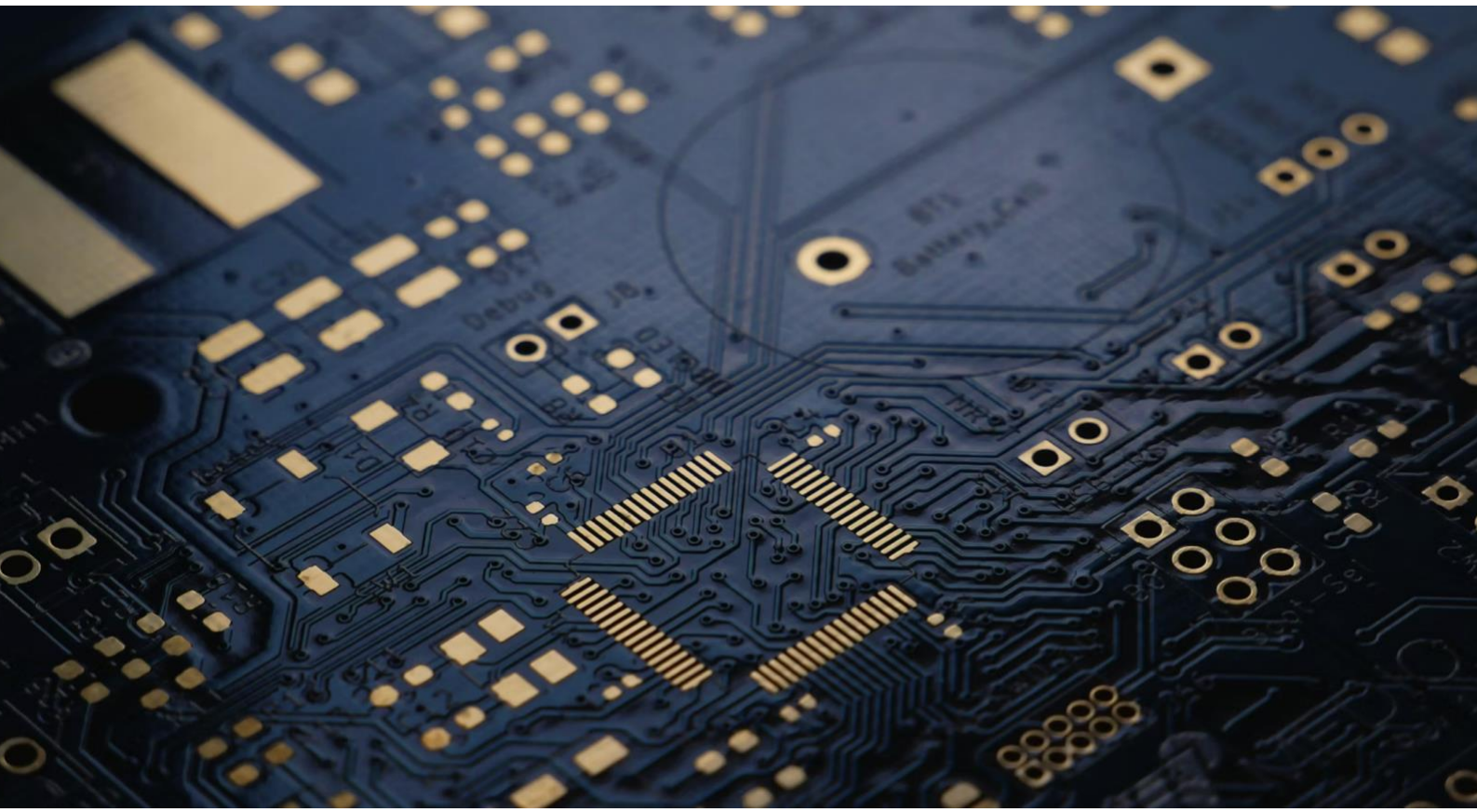

Asian Institute of Research
Connecting Scholars Worldwide

Asian Institute of Research
Engineering and Technology Quarterly Reviews
Vol.8, No.2 December 2025

Engineering and Technology
Quarterly Reviews
ISSN 2622-9374 (Online)

Table of Contents i

Engineering and Technology Quarterly Reviews Editorial Board ii

Magnitude Conversion Relations for Nepal Himalaya Region 1
S. N. Shrestha, P. N. Maskey, G. B. Motra

Integrating Augmented Reality and Artificial Intelligence in Vehicle Diagnostics: Applications for On-Board Diagnostics II Systems 18
D. M. S. K. Disanayaka, L. K. P. D. Gunawardhana

Quantum Computing and the Next Technological Revolution: Transforming Civilization Through Quantum Power 28
Ejiro U Osiobe, Waleed A. Hammood, Safia Malallah, Nyore E. Osiobe, Omar Abdulmaged Hammood, Salwana Mohamad Asmara

Structural Health Monitoring of Buildings Using Computer Vision: A State-of-the-Art Review 35
Horatiu-Alin Mociran, Adina-Victorița Lăpuște

PoA-PBFT Blockchain Architecture Design for Authentication and Identity Protection in Electronic Passports 46
Priati Assiroj, Baluh B. Hertantyo, Besse Hartati, Sirojul Alam

Future-Oriented Simulation-Based Strategies for the Sustainable Development of Batıkent, Ankara 58
Nadir Nasir Shembesh, Halil Semih Eryıldız, Demet Irklı Eryıldız

ISSN 2622-9374 (Online)

The Asian Institute of Research
Engineering and Technology Quarterly Reviews
Vol.8, No.2, 2025: 1-17
ISSN 2622-9374

Magnitude Conversion Relations for Nepal Himalaya Region

S. N. Shrestha[1], P. N. Maskey[2], G. B. Motra[3]

[1,2,3] Tribhuvan University

Abstract
Magnitude conversion is a critical step in the compilation of earthquake catalogues and the assessment of seismic hazard. Given Nepal's high seismic hazard and the limited availability of Nepal region-specific magnitude conversion relations, there is a need to develop empirical relationships that account for the unique tectonic and geological characteristics of the Nepal Himalaya region. This study used existing earthquake catalogues from various institutions to develop new magnitude conversion relations for Nepal Himalaya Region. In this study, we develop new empirical relations for conversion of other magnitudes to moment magnitude. We compare and validate the relations with existing global and regional relations available in the literatures. These relations are then used to compile homogenous earthquake catalogue for Nepal Himalaya region and to perform seismic hazard analysis.

Keywords: Magnitude Conversion, Nepal Himalaya, Moment Magnitude, Regression

1. Introduction

Nepal lies in one of the most seismically active regions in the world, situated at the boundary between Indian and Eurasian tectonic plates. The ongoing collision of these plates results in significant crustal deformation, making Nepal highly prone to large and devastating earthquakes (Bilham et al., 1997). The 2015 Gorkha earthquake (Mw 7.8) highlighted the country's vulnerability, causing nearly 9,000 deaths, displacing millions, and causing extensive damage to infrastructure (Eberhard et al., 2015). The seismic risk in Nepal is further exacerbated by rapid urbanization, inadequate building codes, and poor enforcement of construction standards (Dixit et al., 2013). In a country like Nepal, where rapid urbanization and poor construction practices exacerbate seismic risk, understanding seismicity and recurrence parameters is vital for mitigating the potential loss of life and economic damage from future earthquakes (Parajuli & Koirala, 2019).

In this context, understanding seismicity, compiling accurate earthquake catalogues, and ensuring consistency through magnitude conversion are essential tools for appropriately quantifying earthquake hazard and risk in Nepal, and ultimately for saving lives and reducing economic losses.

The compilation of a comprehensive and accurate earthquake catalogue is a critical step in seismic hazard assessment. An earthquake catalogue provides a historical record of seismic events, including their locations, magnitudes, depths, and times of occurrence. In Nepal, where historical records of earthquakes are limited and instrumental data is relatively recent, compiling a reliable catalogue is challenging but essential (Ambraseys & Douglas, 2004). A well-curated catalogue allows seismologists to identify seismic source zones, assess fault activity, and understand the tectonic processes driving earthquakes (Pandey et al., 1999). It also serves as the foundation for statistical analysis, such as determining recurrence intervals and magnitude-frequency relationships (Kijko & Sellevoll, 1992). Without a robust earthquake catalogue, it would be impossible to accurately model seismic hazards or predict the likelihood of future earthquakes. Given Nepal's high seismic risk and the devastating consequences of past earthquakes, such as the 1934 Bihar-Nepal earthquake and the 2015 Gorkha earthquake, the compilation of a reliable earthquake catalogue is indispensable for informed decision-making and risk mitigation (Bollinger et al., 2016).

Magnitude conversion is a crucial step in earthquake catalogue compilation because seismic events are often reported using different magnitude scales (e.g., local magnitude M_L , body wave magnitude m_b, surface wave magnitude M_S , moment magnitude M_w). These scales are based on different measurement techniques and may not be directly comparable (Kanamori, 1977). In Nepal, where earthquake data is sourced from various national and international agencies, inconsistencies in magnitude scales can lead to inaccuracies in hazard assessments (Chaulagain et al., 2015). Magnitude conversion ensures uniformity in the catalogue by converting all magnitudes to a consistent scale, typically the moment magnitude (M_w), which is the most reliable measure of an earthquake's size (Hanks & Kanamori, 1979). This standardization is essential for accurate statistical analysis, such as calculating the Gutenberg-Richter relationship or estimating ground motion parameters (Grünthal, 2011).
M_w is derived from the seismic moment (M_0), which quantifies the total energy released by an earthquake based on fault area, slip displacement, and rock rigidity (Hanks & Kanamori, 1979). Unlike other scales, it does not saturate for large earthquakes. Traditional scales (e.g., M_S , m_b) saturate at higher magnitudes (~8.0), underestimating the true size of very large earthquakes (Kanamori, 1977). M_w remains accurate for all earthquake sizes. M_w provides a uniform standard for comparing earthquakes globally, improving seismic hazard modeling and engineering design (Bormann & Di Giacomo, 2011). Since M_w relates directly to fault mechanics, it is preferred for tectonic and geodynamic research (Ekström et al., 2012).

The GCMT project (formerly Harvard CMT) is a leading global source of moment tensor solutions and is considered the most suitable for M_w conversions. GCMT uses long-period seismic waves to compute the full seismic moment tensor, providing stable and reliable M_w estimates (Dziewonski et al., 1981; Ekström et al., 2012). It systematically reports M_w for earthquakes worldwide since 1976, ensuring consistency in catalogs. Unlike short-period magnitudes (e.g., m_b, M_L), GCMT's M_w is less affected by wave frequency limitations, making it ideal for converting older earthquake records (Scordilis, 2006). Most international agencies (USGS, ISC, EMSC) use or cross-reference GCMT solutions for homogenizing earthquake catalogs.

Therefore, in this study, we focus on determining magnitude conversion relations for conversion of other magnitude scales to equivalent GCMT-based M_w.

With an objective of determining a homogeneous earthquake catalogue for Nepal Himalaya Region, we reviewed several earthquake catalogues relevant for the region. We mainly reviewed the catalogues of following agencies for Nepal region – International Seismological Center (ISC), ISC-Global Earthquake Model (ISC-GEM), National Earthquake Information Center, USGS (NEIC), National Earthquake Information Center, India (NDI), Beijing Seismic Network, China (BJI), Moscow Seismic Network, Russia (MOS), International Data Centre, CTBTO (IDC), Harvard Global Centroid Moment Tensor (GCMT), and Department of Mines and Geology, National Seismological Centre, Nepal (DMN).

Global catalogues like ISC, ISC-GEM, GCMT and NEIC provide comprehensive data for worldwide events, and regional catalogues like NDI, BJI, MOS and DMN offer detailed information for specific seismic regions.

Table 1: Location and Magnitude of 2011 Taplejung (Sikkim) Earthquake Reported by Various Agencies/Authors

Location Agency/Author	Date			Time			Location		Depth	Magnitude Agency/Author	Magnitude Type and Values				
	Yr	Mo	Day	Hr	Min	Sec	Lat. N	Lon. E	km		Type	M_w	M_L	m_b	M_S
BJI	2011	09	18	12	40	45.70	27.70	88.20	20	BJI	m_b, M_S			6.5	6.9
NDI	2011	09	18	12	40	46.90	27.85	88.06	45.9	NDI	m_b, M_L, M_w	6.9	6.6	6.7	
NEIC	2011	09	18	12	40	48.00	27.53	87.97	60	MOS	m_b, M_S			6.4	6.6
MOS	2011	09	18	12	40	48.90	27.7710	88.2060	40	IDC	m_b, M_L, M_S		5.3	5.6	6.4
IDC	2011	09	18	12	40	50.51	27.7707	88.2212	37	DMN	M_L		6.8		
DMN	2011	09	18	12	40	51.10	27.6897	88.2959	50	NEIC	m_b, M_S, M_w	6.9		6.6	6.7
GCMT	2011	09	18	12	40	59.90	27.44	88.35	46	GCMT	M_w	6.9			
ISC	2011	09	18	12	40	49.58	27.8039	88.1536	29.60	ISC	m_b, M_S			6.5	6.7

Table 2: Location and Magnitude of 2015 Gorkha Earthquake Reported by Various Agencies/Authors

Location Agency/Author	Date			Time			Location		Depth	Magnitude Agency/Author	Magnitude Type				
	Yr	Mo	Day	Hr	Min	Sec	Lat. N	Lon. E	km		Type	M_w	M_L	m_b	M_S
BJI	2015	04	25	06	11	23.50	28.15	84.65	20	BJI	m_b, M_S			6.2	8.2
MOS	2015	04	25	06	11	23.60	28.194	84.726	10	MOS	M_w, m_b, M_S	7.6		6.8	7.6
IDC	2015	04	25	06	11	23.88	28.159	84.7028	0	IDC	M_L, m_b, M_S		5.0	6.0	7.8
DMN	2015	04	25	06	11	25.00	28.2172	84.7684	2	DMN	M_L		7.6		
NEIC	2015	04	25	06	11	25.95	28.2305	84.7314	8.2	NEIC	M_w, m_b, M_S	7.8		7.1	7.9
NDI	2015	04	25	06	11	27.60	28.1130	84.5840	10	NDI	M_L, m_b		6.7	7.1	
GCMT	2015	04	25	06	11	58.60	27.9100	85.330	12	GCMT	M_w	7.9			
ISC	2015	04	25	06	11	26.63	28.1302	84.7168	13.4	ISC	M_w, m_b, M_S			6.9	7.9

We find variations in terms of date, time, origin, magnitude values of same earthquake events in these catalogues. Tables 1-2 give few example events for which various agencies reported different values. This signifies the need to determine common magnitude conversion relations applicable for Nepal region and creation of a homogenized comprehensive earthquake catalogue.

We use earthquake catalogue compiled by International Seismological Center (ISC) for a period of 1900 to 2022 for the development of new magnitude conversion relations. We extracted the catalogue for Nepal Himalaya region within 78-90 E and 25-32 N and 75-93 E and 24-34 N for comparison and validation purpose. The catalogue consists of 4700 events of $M \geq 4$, and 8,778 events of $M \geq 4$ respectively. We use mainly M_L, m_b, M_S and M_w values reported by different agencies for the determination of magnitude conversion relations.

2. Existing Magnitude conversion relations

At the global level, several empirical relationships have been developed to convert between magnitude scales such as surface wave magnitude (M_S), body wave magnitude (m_b), and moment magnitude (M_w).

Scordilis (2006) developed empirical relations for converting body-wave magnitude (m_b) and surface-wave magnitude (M_S) to moment magnitude (M_w), based on **global** dataset.

m_b to M_w:

$$M_w = 0.85 \times m_b + 1.03 \text{ for } 3.5 \leq m_b \leq 6.2 \quad \text{---------- (1)}$$

M_S to M_w:

$$M_w = 0.67 \times M_S + 2.07 \text{ for } 3.0 \leq M_S \leq 6.1 \quad \text{---------- (2a)}$$

$$M_w = 0.99 \times M_S + 0.08 \text{ for } 6.2 \leq M_S \leq 8.2 \quad \text{---------- (2b)}$$

The dataset used for these conversions is globally averaged and does not account for regional variations.

Ambraseys and Douglas (2004) derived relationships for the conversion of M_S to $\log M_0$ for **global level** and **Himalayan region.** Using M_0-M_w relation by **Kanamori (1977**), relation for M_S-M_w are determined.

Global average relations:

$$\log M_0 = 19.24 + M_S \quad \text{for } M_S < 5.3 \quad \text{---------- (3a)}$$

$$\log M_0 = 30.20 - \sqrt{92.45 - 11.40 \times M_S} \quad \text{for } 5.3 \leq M_S \leq 6.8 \quad \text{---------- (3b)}$$

$$\log M_0 = 16.14 + 1.5 \times M_S \quad \text{for } M_S > 6.8 \quad \text{---------- (3c)}$$

For Himalayan region:

$$\log M_0 = 19.38 + 0.93 \times M_S \quad \text{for } M_S \leq 5.94 \quad \text{---------- (4a)}$$

$$\log M_0 = 16.03 + 1.5 \times M_S \quad \text{for } M_S > 5.94 \quad \text{---------- (4b)}$$

Kanamori, 1977:

$$M_w = \frac{2}{3}\log M_0 - 10.73 \quad \text{for } M_S \leq 5.94 \quad \text{---------- (5)}$$

From Equations (4) and (5), we have M_S-M_w relation for Himalayan region:

$$M_w = 0.62 \times M_S + 2.2 \quad \text{for } M_S \leq 5.94 \quad \text{---------- (6a)}$$

$$M_w = M_S - 0.0433 \quad \text{for } M_S > 5.94 \quad \text{---------- (6b)}$$

Das et al., 2011 gave relations for global level for conversion of M_S and m_b to M_w

M_S to M_w:

For $h < 70km$

$$M_{w,HRVD} = 0.67(\pm 0.00005) \times M_S + 2.12(\pm 0.0001) \quad \text{for } 3 \leq M_S \leq 6.1 \quad \text{-------- (7a)}$$

$$M_{w,HRVD} = 1.06(\pm 0.00002) \times M_S + 0.38(\pm 0.0006) \quad \text{for } 6.2 \leq M_S \leq 8.4 \quad \text{-------- (7b)}$$

For $70km \leq h < 643km$

$$M_{w,HRVD} = 0.67(\pm 0.00004) \times M_S + 2.33(\pm 0.01) \quad \text{for } 3.3 \leq M_S \leq 7.2 \quad \text{-------- (7c)}$$

m_b to M_w from Inverted Standard Regression (ISR):

$$m_{b,ISC} = 0.65(\pm 0.003) \times M_{w,HRVD} + 1.65(\pm 0.02) \quad \text{for } 2.9 \leq m_{b,ISC} \leq 6.5 \quad \text{-------- (8a)}$$

$$\boldsymbol{M_{w,HRVD} = 1.5385 \times m_{b,ISC} - 2.5385} \quad \text{for } 2.9 \leq m_{b,ISC} \leq 6.5 \quad \text{-------- (8b)}$$

Das et al., 2012 used $m_{b,proxy}$ which increased correlation coefficient:

$$M_w = 1.63(\pm 0.0101) \times m_{b,proxy} - 3.194(\pm 0.281) \quad \text{-------- (9a)}$$

$$m_{b,proxy} = 0.724(\pm 0.03) \times m_{b,obs} + 1.455(\pm 0.16) \quad \text{-------- (9b)}$$

$$M_w = 1.18 \times m_{b,obs} - 0.822 \quad \text{-------- (9c)}$$

Thingbaijam et al., 2008 determined conversion relations for northwest India:

$$M_{w,GCMT} = 0.7042(\pm 0.0356) \times M_{S,ISC} + 1.8197(\pm 0.1896) \quad \text{for } M_{S,ISC} < 7.5 \text{ -------- (10)}$$

$$M_{w,GCMT} = 1.3691(\pm 0.211) \times m_{b,ISC} - 1.7742(\pm 1.139) \quad \text{-------- (11)}$$

(for $M_{w,GCMT} > 4.4$ and $m_{b,ISC} < 6.7$)

They considered M_w and M_L equivalent, i.e.,

$$M_w \approx M_L \quad \text{-------- (12)}$$

Kolathayar et. al., 2011 developed regression relations for Asia region $0{\sim}40°N$ and $60{\sim}105°E$, the data covered period within 250 BC – 2010 A.D.

$M_w = 0.693(\pm0.006) \times M_S + 1.922(\pm0.035)$ for $3.7 \leq M_S \leq 8.8$ -------- (13)

$M_w = 1.08(\pm0.0152) \times m_b - 0.325(\pm0.081)$ for $4 < m_b \leq 7.2$ -------- (14)

$M_w = 0.815\ (\pm0.04) \times M_L + 0.767(\pm0.174)$ for $3.7 \leq M_L \leq 7$ -------- (15)

Nath, Thingbaijam and Ghosh, 2011 determined conversion relations for $2{\sim}40°N$ and $55{\sim}102°E$. They also used proxy magnitudes for increasing the correlation coefficient.

$M_{w,GCMT} = 0.6495 \times M_{S,ISC} + 2.163$ for $3.5 \leq M_{S,ISC} \leq 6.6$ ------- (16a)

$M_{w,GCMT} = 1.157 \times M_{S,ISC} - 1.179$ for $6.7 \leq M_{S,ISC} \leq 8.5$ ------- (16b)

$M_{w,GCMT} = 1.16 \times m_{b,ISC} - 0.663$ for $3.8 \leq m_{b,ISC} \leq 7.0$ -------- (17)

$M_{w,GCMT} = 0.449 \times M_{L,ISC} + 2.88$ for $4.6 \leq M_L \leq 6.4$ -------- (18)

Storchak et al., 2012, as part of the ISC-GEM Global Instrumental Earthquake Catalogue, proposed the following magnitude conversion relations:

$M_w = 0.67 \times M_S + 2.13$ for $M_S \leq 6.47$ -------- (19)

$M_w = 1.10 \times M_S - 0.67$ for $M_S > 6.47$ -------- (20)

$M_w = 1.38 \times m_b - 1.79$ -------- (21)

Ader et al., 2012 gave the following relation for Nepal Himalayan region:

$M_w = 0.84 \times M_L + 0.21$ ---------- (22)

Maharjan et al., 2023 used the existing magnitude conversion relations for M_S & m_b and determined few relations for M_L:

$M_w = 1.0273(\pm0.07) \times M_{L,NDI} + 0.0629(\pm0.37)$ for $3.6 \leq M_{L,NDI} \leq 6.8$ -------- (23)

$M_w = 0.6527(\pm0.05) \times M_{L,BJI} + 1.9015(\pm0.27)$ for $3.8 \leq M_{L,BJI} \leq 6.8$ -------- (24)

Adhikari et al. (2023):

$M_w = 1.15 \times M_L - 1.10$ -------- (25)

While global and broader-Himalaya-specific magnitude conversion relations provide a useful starting point, they have significant limitations when applied to Nepal due to regional seismotectonic differences. Therefore, developing Nepal-Himalaya-specific magnitude conversion equations based on local earthquake data is essential for improving earthquake catalogues and seismic hazard assessments.

3. Methodology

After selection and collection of appropriate earthquake catalogue for the region, the data is filtered and cleaned to ensure duplicates are removed, and poorly constrained magnitude values are excluded. The cleaned earthquake catalogues are used for developing empirical relation by regression analysis.

We perform the following regression analysis for developing magnitude conversion relations:

A simple and widely used approach is ordinary least squares regression, which fits a linear model of the form:

$M_w = a \times M_L + b$ or ---------- (26)

$M_w = a \times m_b + b$ ---------- (27)

where a and b are empirical coefficients obtained through statistical regression.
One of the commonly used regression analysis methods is **Ordinary Least Squares (OLS)**. In this regression, we try to minimize the vertical distances (errors in y only) between observed points and the regression line (vertical residuals), and in the form of sum of squared vertical residuals. It takes the form of:

$$min \sum_{i=1}^{n} (y_i - X_i\beta)^2 \quad \text{----------} \quad (28)$$

Where, y_i = Observed dependent variables; X_i = Predictor variables; and β = Coefficients
We perform **Orthogonal Distance Regression (ODR)** to account for errors in both variables. The regression equation takes the same form as OLS but minimizes total errors rather than just vertical deviations.
We try to minimize the **perpendicular (orthogonal) distance** from the data points to the regression line. It accounts for errors in **both X and Y.** It takes the form as:

$$min \sum_{i=1}^{n} \frac{(y_i - X_i\beta)^2}{{\sigma_{y_i}}^2 + \|\beta\|^2 {\sigma_{x_i}}^2} \quad \text{----------} \quad (29)$$

or more generally, for any functions f(x,y)=0, it minimizes:

$$min \sum_{i=1}^{n} \frac{(y_i - f(x_i))^2}{{\sigma_{y_i}}^2 + \left(\frac{\partial f}{\partial x_i}\right)^2 {\sigma_{x_i}}^2} \quad \text{----------} \quad (30)$$

Another more general orthogonal regression is General Orthogonal Regression (GOR). This regression tries to minimize the **weighted sum of squared orthogonal distances**.
For a line Ax+By+C=0, it tries to minimize:

$$min \sum_{i=1}^{n} \left(\frac{Ax_i + By_i + C}{\sqrt{(A^2 + B^2)}}\right)^2 \quad \text{----------} \quad (31)$$

This is the **square of the orthogonal distance** from each point to the line in the 2D space.

In some cases, magnitude conversion is not strictly linear, especially for large earthquakes where magnitude saturation occurs. Nonlinear regression models, such as piecewise linear models (for different magnitude ranges) can be used to better fit the data. **Specifically, for the case of M_S to M_w conversion piecewise linear models are used**.

After doing the regression analysis and finding out the regression relations, we perform the following statistical evaluation, uncertainty analysis and validation to assess the reliability or goodness-of-fit of the magnitude conversion relation:

- **Mean Absolute Error (MAE):** This measures the average of absolute differences between the predicted and observed values. This represents the average magnitude of errors. A lower MAE means the model's predictions are closer to the true values.
- **Root Mean Square Error (RMSE):** This measures how large the errors are, with more weight given to larger errors. This is the square root of the average of squared differences between predicted and actual values. Lower RMSE indicates better accuracy.
- **Coefficient of Determination (R Squared)**: This indicates how well the model captures the variability in the data or how well the regression line fits the data. This ranges from 0 to 1 and higher R2 values indicate better fit.
- **Standard Deviation (sigma):** This indicates how spread out the errors are (consistency of predictions). Smaller sigma value signifies tighter clustering around the line or better fit and larger value shows more scatter or poorer fit.
- **Residuals (Observed−Predicted)** are analyzed to detect biases in the model. In a well-fitted model, the residuals should randomly distribute around zero, and show no systematic trends in residuals across magnitude ranges

The newly derived equations are compared and validated against global and regional relations (Equations 1-25) to check for consistency.

4. Earthquake Data and Regression Analysis

There are variations in different studies in compilation of earthquake data for Nepal Himalaya region. Maharjan et al., 2023 considered earthquake data within a region within 75°-93°E, and 24°-34°N. Chamlagain et al., 2020

considered the data within region 78°-90°E and 25°-33°N. Likewise, Stevens et al., 2018 considered data within 80°-89°E and 26°–31°N, Rahman and Bai considered within 79°-89°E and 26°-32°N, Thapa and Wang took data within 26°-31.7°N and 79°-90°E from 1255 to 2011. Rajaure, 2020 considered data within 75°-93°E and 24°-34°N.

In this study, earthquakes within the following two geographic area are considered for catalogue compilation and analysis: 78°-90°E and 25°-32°N (approx. 150 km from the political boundary of Nepal); and 75°-93°E and 24°-34°N (approx. 300 km in latitude and 400 km in longitude from the political boundary of Nepal). The ISC catalogues for two regions contain 8,778 and 4,700 number of events respectively that are greater than or equal to magnitude 4 during the period 1 January 1900 to 1 September 2022.

We take the following magnitude-agency pairs and data for the determination of corresponding magnitude conversion relation.

Table 3: Number of earthquakes and Agency-Magnitude Pairs used for Developing Regression Models

S. No.	Description	No. of Events for Regression	
		Region 1 (78°-90° E, 25°-32° N)	**Region 2 (75°-93° E, 24°-34° N)**
A.	Total No. of Events	4700	8778
B.	Period Covered	1908-2022	1905 - 2022
C.	**Magnitude-Agency Pairs**		
1	IDC m_b and ISC m_b	2517	4776
2	NEIC m_b and ISC m_b	1664	3059
3	NDI M_L and ISC m_b	1228	2022
4	BJI m_b and ISC m_b	918	1838
5	DMN M_L and ISC m_b	788	872
6	DMN M_L and ISC M_S	297	326
7	MOS m_b and ISC m_b	693	1385
8	GCMT Mw and ISC m_b	133	292
9	IDC m_b and GCMT M_w	99	230
10	NDI M_L and GCMT M_w	69	119
11	BJI m_b and GCMT M_w	117	265
12	DMN M_L and GCMT M_w	81	87
13	MOS m_b and GCMT M_w	133	285
14	ISC M_S and GCMT M_w	128	283

[Catalogue accessed on September 20, 2024; and Period covered: 1908 – September 1, 2022]

Regression analyses are done following Ordinary Least Squares (OLS), Orthogonal Distance Regression (ODR) and General Orthogonal Regression (GOR) methods for different combinations of data. We use python codes for running the calculations. We follow three regression methods to compare, validate and determine the most suitable regression relation.

Comparison of statistical metrics for each method are done, and best-fit regression is identified. The magnitude conversion relations thus determined are compared and validated with the existing magnitude conversion relations.

4.1. Conversion of Local Magnitude (M_L) to Moment Magnitude (M_w)

4.1.1. Local Magnitude from DMN (DMN M_L)

The Local Magnitude (M_L), commonly known as Richter magnitude scale, is the logarithm of maximum trace amplitude of seismic waves recorded by Wood-Anderson seismographs for the earthquakes in Southern California. This magnitude scale is designed for shallow, local earthquakes (within about 600 km of the seismograph). The National Seismological Center of Department of Mines and Geology (DMN) measures earthquakes in local magnitude scale (M_L).

The DMN local magnitude M_L is estimated from the maximum amplitudes of the S_g, S_n and L_g seismic phases measured at all suitable records on the 0.3-7 Hz bandpass filtered seismic signals. The final value of M_L is the arithmetic average of all available magnitude values determined at distances greater than 95 km or 100km.

We use 87 numbers of events with $M_L - M_w$ data pairs from the ISC catalogue for conversion of M_L to M_w.
We developed several regression relations for various combinations of data and by different methods of regression. After the comparison of regression metrics i.e., the Mean Absolute Error (MAE), Root Mean Square Error (RMSE), Coefficient of Determination (R-squared), and Standard Deviation (sigma), and comparing the residual box plots, we use the following two relations for further analysis and validation with other existing magnitude conversion relations.
Model developed by ODR method in this study from data within 75-93E and 24-34N

$$M_w = 1.246 \times M_L - 1.766 \quad \text{----------} \quad (32)$$

(New Model1_2024_M_L- M_w)
Model developed by OLS method in this study from data within 75-93E and 24-34N

$$M_w = 0.832 \times M_L + 0.603 \quad \text{----------} \quad (33)$$

(New_Model2_2024_M_L- M_w)

The new empirical relations are compared with the existing relations (Figure 1). Two existing relations for broader Himalayan region – Kolathayar et al., 2011 (Eq. 15) and Nath, Thingbaijam and Ghosh, 2011 (Eq. 18) and two for Nepal Himalayan region – Ader et al., 2012 (Eq. 22) and Adhikari, 2023 (Eq. 25) are used for comparison. We observed New_Model1 gives very much similar results with that by the Adhikari, 2023 relation. New_Model2 gives similar pattern with that of Ader et al. 2012 with New_Model2 giving 0.2 magnitude higher results. Kolathayar et al., 2011, Nath, Thingbaijam and Ghosh, 2011 relations are giving smaller results for magnitudes more than 5.7 and higher results for more than magnitude 5.7. The residual scatter plots (Figure 1c) show New_Model1 is giving less biased results than other existing relations.
By comparing the model metrics as shown in the figures, we find the best fit model for conversion of M_L to M_w for the Nepal Himalaya Region is:

$$\boldsymbol{M_w = 1.246 \times M_L - 1.766} \quad \text{----------} \quad (34)$$

MAE = 0.39176; RMSE = 0.469723; R^2 = 0.391702; σ = 0.465254

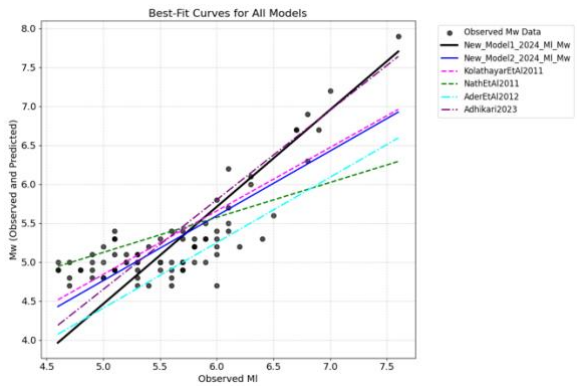

a) Magnitude Conversion Relations

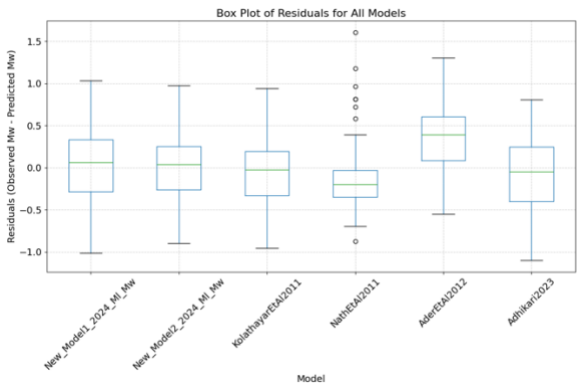

b) Residual Box Plots

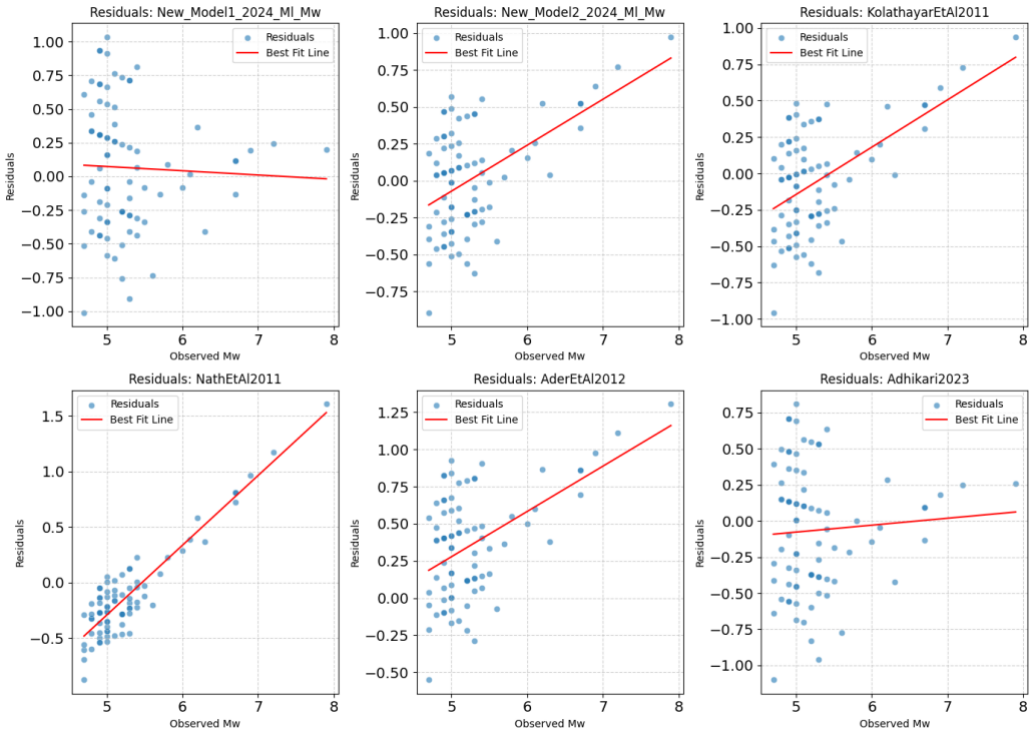

c) Residual Scatter Plots

Figure 1: Comparison of New Magnitude Conversion Relation for M_L to M_w

Table 4: Model Metrics Comparisons for M_L to M_w Conversion

Model	MAE	RMSE	R^2	Std. Dev.
New_Model1_2024_Ml_Mw	0.39176	0.469723	0.391702	0.465254
New_Model2_2024_Ml_Mw	0.298338	0.362904	0.636908	0.362612
KolathayarEtAl2011	0.295438	0.36576	0.631171	0.361717
NathEtAl2011	0.33173	0.430088	0.490025	0.413819
AderEtAl2012	0.415975	0.513275	0.273672	0.363139
Adhikari2023	0.363642	0.434706	0.479015	0.430022

4.1.2. Local Magnitude from NDI (NDI M_L)

NDI, India also measures earthquake events in local magnitude scale (M_L). Although both DMN and NDI measure earthquakes in local magnitude scale M_L, their magnitude values are not same. Generally, reported NDI M_L values are less by 0.2-0.8 than the reported DMN M_L values, in average NDI M_L values are 0.5 magnitude less than the DMN M_L values.

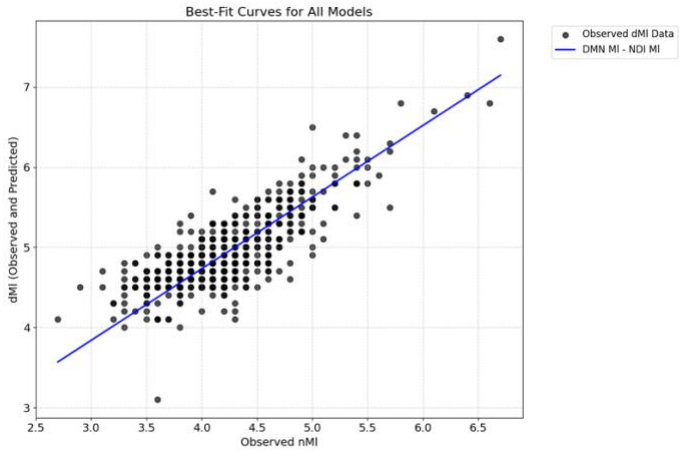

Figure 2: Comparison of DMN $\boldsymbol{M_L}$ and NDI$\boldsymbol{M_L}$

Based on comparison of model metrics for 612 data pairs for DMN M_L and NDI M_L, the best-fit relation for the conversion of M_L (NDI) to M_L (DMN) is the one we get from the ODR Regression as below:

$$M_L(DMN) = 0.894 \times M_L(NDI) + 1.156 \pm 0.288 \quad \text{----------} \quad (35)$$

With

MAE = 0.2275; RMSE = 0.28818; R^2 = 0.618; σ = 0.28818

Conversion for NDI M_L to M_w

We perform regression using 69 data pairs for $M_L(NDI)$ to Mw from data within 75°-93°E and 24°-34°N, and find the following relation and compare with existing relations Nath et al., 2011 (Eq. 18) and Maharjan et al., 2023 (Eq. 23).

$$\boldsymbol{M_w = 0.769 \times M_L + 1.444 \pm 0.333} \quad \text{----------} \quad (36)$$

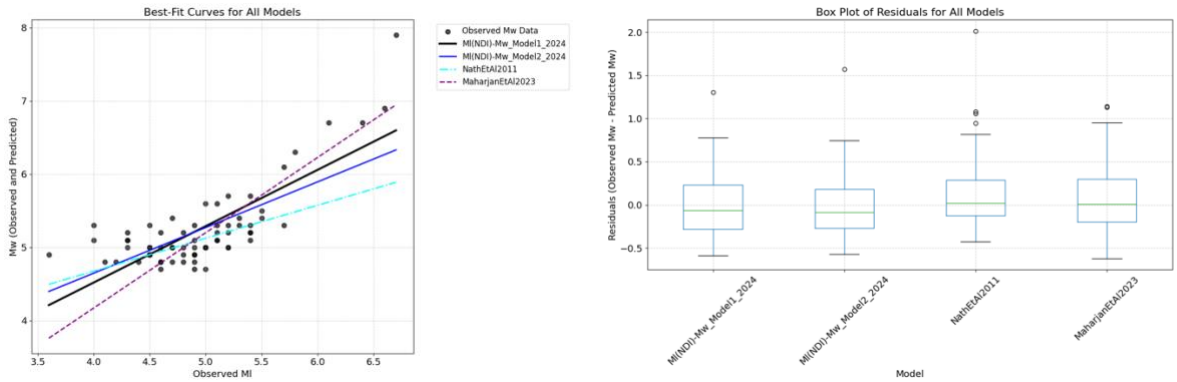

a) Magnitude Conversion Relations **b) Residual Box Plots**

Figure 3: Magnitude Conversion Relation for NDI $\boldsymbol{M_L}$ to $\boldsymbol{M_W}$ and Comparison with Other Conversions

Table 5: Model Metrics Comparisons NDI $\boldsymbol{M_L}$ to $\boldsymbol{M_W}$ Conversion

Model	MAE	RMSE	R^2	Std. Dev.
Ml(NDI)-Mw_Model1_2024	0.283667	0.352621	0.593643	0.352278
Ml(NDI)-Mw_Model2_2024	0.276154	0.358886	0.579076	0.358848
NathEtAl2011	0.258052	0.412287	0.444491	0.390666
MaharjanEtAl2023	0.310052	0.397214	0.484366	0.38745

4.2. Conversion of Body Wave Magnitude (m_b) to Moment Magnitude (M_w)

4.2.1. Conversion of $m_b(ISC)$ to $M_w(GCMT)$

The body wave magnitude (m_b) is the most commonly used magnitude scale and most recording stations measure m_b for particularly tele-seismic events. The body wave magnitude **(m_b)** is a measure of earthquake size calculated from the amplitude of P-waves (primary or compressional waves) recorded by seismographs. It is typically measured at periods of about 1 second and is most effective for deep and distant earthquakes (usually at distances greater than 20° from the epicenter). In ISC catalogue, most events are reported in m_b.

For Nepal Himalaya Region, from the ISC Catalogue 292 number of data pairs of m_b and M_w are used for regression, and we find the following relations:

New models:

Model Name	**Regression Relation**
New_Model1_2024_m_b-M_w	$M_w = 1.055 \times m_b - 0.195$ ---------- (37)
New_Model2_2024_m_b-M_w	$M_w = 0.852 \times m_b + 0.862$ ---------- (38)

We then compare the results obtained from the new model with the results obtained from existing models - with Scordilis 2006 (Eq. 1), Kolathayar et al., 2011 (Eq. 14), Nath et al., 2011 (Eq.17), and Storchak et al. 2012 (Eq. 21). The model metrics are comparable with the existing models, Kolathayar et al., 2011 gives consistent results with the new model.

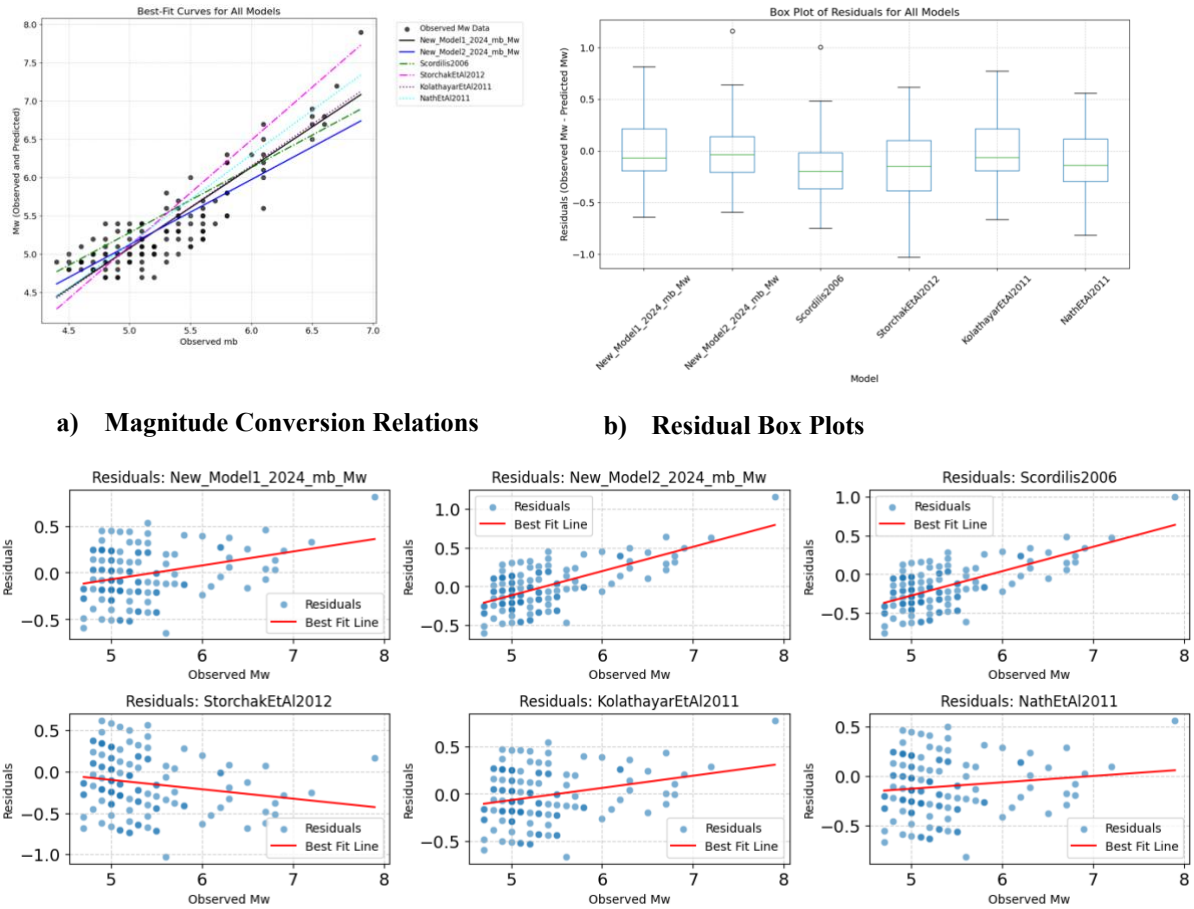

a) Magnitude Conversion Relations **b) Residual Box Plots**

c) Residual Scatter Plots

Figure 4: Magnitude Conversion Relation for ISC m_b to M_W and Comparison with Other Conversions

Table 6: Model Metrics Comparisons for m_b - M_W Conversion

Model	MAE	RMSE	R^2	Std. Dev.
SNS1_mb_Mw_oq_model	0.225729	0.274921	0.774152	0.274009
SNS2_mb_Mw_ols_model_1	0.219546	0.277385	0.770085	0.277181
Scordilis2006	0.266767	0.324384	0.685574	0.277418
StorchakEtAl2012	0.31	0.373169	0.583889	0.346558
KolathayarEtAl2011	0.228519	0.277542	0.769825	0.276503
NathEtAl2011	0.255331	0.307691	0.717104	0.288425

New_Model1 gives similar results with that of Kolathayar et al., 2011; whereas New_Model2 is giving smallest results among all the models. Storchak et al., 2012 is giving highest results for higher magnitude values.
The residual scatter plot shows less biasness by the New_Model1, whereas all other relations are giving higher biasness. Therefore, the final relation for m_b - M_W conversion is:

$$\boldsymbol{M_w = 1.055 \times m_b - 0.195} \quad \text{----------} \quad (39)$$

MAE = 0.217; RMSE = 0.2682; R^2 = 0.6995; σ = 0.268

4.2.2. m_b from NEIC and ISC

We do the regression for 1664 data pairs by three methods of regression with different combinations of data: all data together, data split into training and test data.
From various regression models, we observe that m_b given by ISC and NEIC are practically equal. The best-fit model after comparing the model metrics for Nepal-Himalaya region is:

$$m_b(ISC) = 0.998 \times m_b(NEIC) - 0.062 \pm 0.191 \quad \text{----------} \quad (40)$$

MAE = 0.138445; RMSE = 0.191753; R^2 = 0.849135; σ = 0.191471

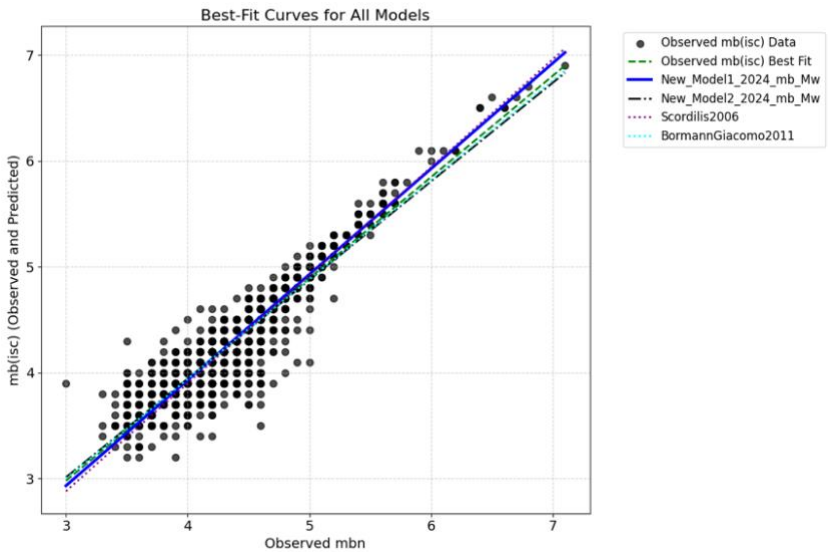

Figure 5: Comparison of NEIC m_b and ISC m_b

Scordilis (2006) has also shown the mb magnitudes given by ISC and NEIC are practically equivalent and given the relation:

$$m_b(ISC) = 1.02\ (\pm 0.003) \times m_b(NEIC) - 0.18(\pm 0.011) \quad \text{----------} \quad (41)$$

for $2.5 \leq m_b(NEIC) \leq 7.3$ with R^2 =0.99, σ = 0.20, n = 215

4.2.3. Body wave magnitudes from other agencies

Other agencies mainly, BJI, MOS and IDC have also reported body wave magnitudes (m_b) for the Nepal-Himalaya region and considered their data for the compilation of earthquake catalogues. Therefore, mb given by these agencies are also compared, and following relations are determined. The model metrics are also determined and found to be reasonable.

Agency and data pairs	Conversion Relation	MAE	RMSE	R^2	Std. Dev. (σ)
BJI (n=265)	$M_w = 1.087 \times m_b(BJI) - 0.164 \pm 0.266$ ---------- (42)	0.215115	0.287007	0.7542	0.286993
MOS (n=285)	$M_w = 1.018 \times m_b(MOS) - 0.161 \pm 0.256$ ---------- (43)	0.207809	0.26579	0.788906	0.264851
IDC (n=230)	$M_w = 1.148 \times m_b(IDC) - 0.201 \pm 0.284$ ---------- (44)	0.243356	0.308499	0.698074	0.306751

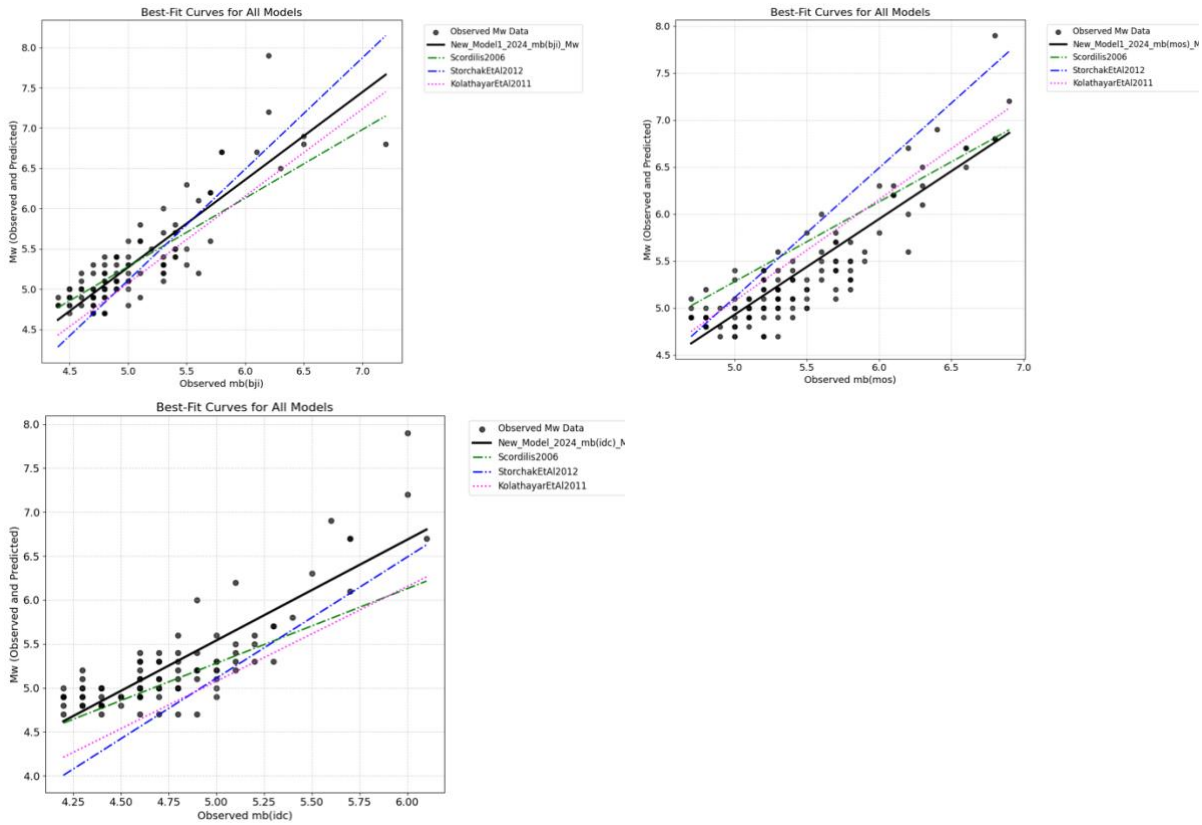

Figure 6: Magnitude Conversion Relations for BJI, MOS, IDC m_b to M_w

There are some variations in the coefficients of the new relations for other magnitude agencies. The magnitude relations developed for $m_b(ISC)$ (Equation 39) can be considered reasonable for all other magnitude agencies for Nepal-Himalaya region.

4.3. Conversion of Surface Magnitude (M_S) to Moment Magnitude (M_w)

The surface wave magnitude (M_S) measures an earthquake's size based on the amplitude of surface waves (Rayleigh waves) with a period of about 20 seconds. This scale measures earthquake size for moderate-to-large events, commonly for magnitudes between ~5.0 and 8.5, and works best for shallow earthquakes (depth < 50 km).

M_S relies on long-period surface waves, making it useful for distant earthquakes. M_S saturates for very large earthquakes (M>8.5). For giant earthquakes (e.g., 2004 Sumatra), moment magnitude (M_w) is preferred. Many pre-1970 earthquakes were recorded using M_S (before M_w became standard).

Scordilis (2006) is the most commonly used magnitude conversion relations to convert between M_S to M_w. The relations follow two-segment piecewise linear relations for conversion of M_S to M_w. Two-segment regression improves accuracy by allowing different slopes below and above a breakpoint (~6.1 M_S). We follow similar approach for determination of Nepal-Himalaya region specific magnitude conversion relation for M_S.

We developed regression relation from 128 data pairs of ISC catalogue following the ODR method and compared with Scordilis 2006.
The new model is:

$$M_w = 0.570 \times M_S + 2.53 \pm 0.112 \quad \text{for } M_S \leq 6.1 \quad \text{----------} \quad (45)$$

$$M_w = 1.025 \times M_S - 0.245 \pm 0.191 \quad \text{for } M_S > 6.1 \quad \text{----------} \quad (46)$$

The comparison with existing model shows these new models gives comparable results with the existing models – Ambraseys and Douglas, 2004 (Eq. 6a, 6b), Scordilis 2006 (Eq. 2a, 2b) and Nath et al., 2011 (Eq. 16a, 16b).

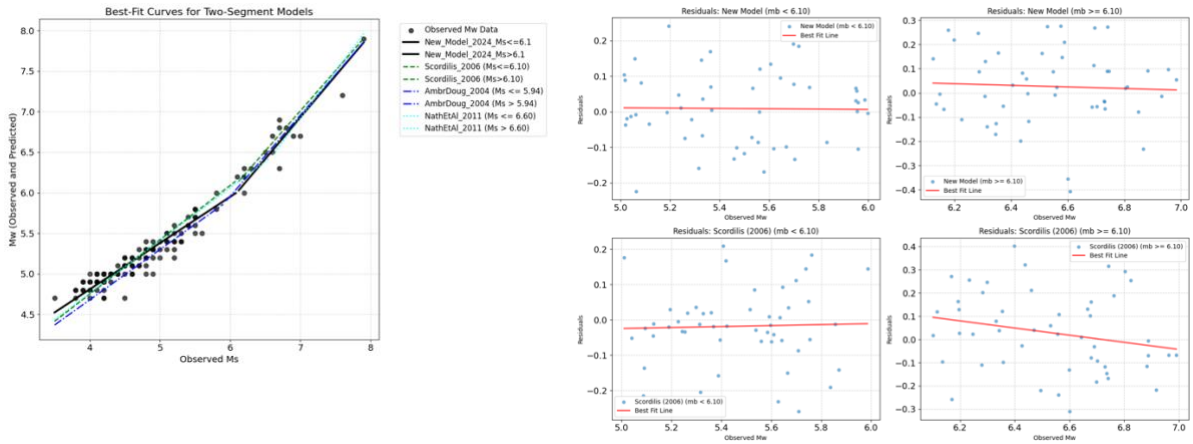

Figure 7: Magnitude Conversion Relations for ISC M_S to M_w

Table 7: Model Metrics Comparison for M_S - M_w Conversion

Model	Segment	MAE	RMSE	R^2	Std. Dev.
New_Model_2024	Overall	0.094438	0.123166	0.955541	0.122704
Scordilis_2006	Overall	0.109664	0.143349	0.939776	0.141322
AmbrDoug_2004	Overall	0.126832	0.151049	0.933132	0.133347
NathEtAl_2011	Overall	0.107984	0.138742	0.943585	0.138197

5. Discussion and Conclusions

We used ISC catalogue for the region 75°-93°E and 24°-34°N that covers the period 1905 to 2022 for determination of new magnitude conversion relations for Nepal Himalaya Region. The catalogue consists of 8778 events of magnitude 4 and more for which 292 events with Mw values. We determine magnitude conversion relations for local magnitude (M_L), body wave magnitude (m_b) and surface wave magnitude (M_S) to moment magnitude (M_w). Conversion relations for local magnitudes reported by DMN and NDI; body wave magnitudes (m_b) reported by ISC, NEIC, BJI, MOS and IDC; and surface wave magnitude (M_S) reported by ISC are determined. Local magnitudes (M_L) of DMN and NDI differ to each other by 0.3-0.8 and body wave magnitudes of ISC and NEIC are approximately equivalent.

The new magnitude conversion relations determined in the study are compared and validated with existing magnitude conversion relations at global level and regional level. Statistical metrics - mean absolute error (MAE), root mean square error (RMSE) coefficient of determination (R-square), standard deviation (sigma), residual box plot and residual scatter plot are used for model comparisons. Orthogonal Distance Regression (ODR), General Orthogonal Regression (GOR) and Ordinary Least Square (OLS) methods of regression are used for development of conversion relations. We used our own python codes as well as existing python code from Openquake for the regression calculations.

The comparison and validation showed regressions using ODR methods and Openquake python code gave best-fit results, and these relations are used for further analysis.

Generally consistent results are obtained with new magnitude conversion relations. There are significant variations among the results obtained from existing global magnitude conversion relations. Our results are closer to the results obtained from regional conversion relations.

We used the new magnitude conversion relations for compilation of comprehensive earthquake catalogue for Nepal Himalaya Region which is used for determination of seismic hazard parameters i.e., magnitude frequency relations.

Author Contributions: All authors contributed to this research.

Funding: Not applicable.

Conflict of Interest: The authors declare no conflict of interest.

Informed Consent Statement/Ethics Approval: Not applicable.

Declaration of Generative AI and AI-assisted Technologies: This study has not used any generative AI tools or technologies in the preparation of this manuscript.

References

Ader, T., Avouac, J. P., Liu-Zeng, J., Lyon-Caen, H., Bollinger, L., Galetzka, J., ... & Flouzat, M. (2012). Convergence rate across the Nepal Himalaya and interseismic coupling on the Main Himalayan Thrust: Implications for seismic hazard. Journal of Geophysical Research: Solid Earth, 117(B4).

Ali, S. M., & Shanker, D. (2017). Study of seismicity in the NW Himalaya and adjoining regions using IMS network. Journal of Seismology, 21, 317-334.

Ambraseys, N. N., & Douglas, J. (2004). Magnitude calibration of north Indian earthquakes. Geophysical Journal International, 159(1), 165-206.

Amorese, D., Grasso, J. R., & Rydelek, P. A. (2010). On varying b-values with depth: results from computer-intensive tests for Southern California. Geophysical Journal International, 180(1), 347-360.

Anbazhagan, P., & Balakumar, A. (2019). Seismic magnitude conversion and its effect on seismic hazard analysis. Journal of Seismology, 23, 623-647.

Angadi, S., Hiravennavar, A., Desai, M. K., Solanki, C. H., & Dodagoudar, G. R. (2019). Development of Gutenberg–Richter Recurrence Relationship Using Earthquake Data. In Green Buildings and Sustainable Engineering: Proceedings of GBSE 2018 (pp. 281-288). Springer Singapore.

Arora, S., & Malik, J. N. (2017). Overestimation of the earthquake hazard along the Himalaya: constraints in bracketing of medieval earthquakes from paleoseismic studies. Geoscience Letters, 4, 1-15.

Awoyemi, M. O., Hammed, O. S., Shode, O. H., Olurin, O. T., Igboama, W. N., & Fatoba, J. O. (2017). Investigation of b-value variations in the african and parts of eurasian plates. Science of Tsunami Hazards, 36(2).

Bayrak, Y., & Bayrak, E. (2012). Regional variations and correlations of Gutenberg–Richter parameters and fractal dimension for the different seismogenic zones in Western Anatolia. Journal of Asian Earth Sciences, 58, 98-107.

Bayrak, Y., Yılmaztürk, A., & Öztürk, S. (2002). Lateral variations of the modal (a/b) values for the different regions of the world. Journal of Geodynamics, 34(5), 653-666.

Beauval, C., & Scotti, O. (2003). Mapping b-values in France using two different magnitude ranges: Possible non power-law behavior. Geophysical research letters, 30(17).

BECA WORLEY International. "Seismic hazard mapping and risk assessment for Nepal." 1993.

Bilham, R., Gaur, V. K., & Molnar, P. (1997). Himalayan seismic hazard. *Science*, 293(5534), 1442-1444.

Bollinger, L., Sapkota, S. N., Tapponnier, P., Klinger, Y., Rizza, M., Van der Woerd, J. & Rajaure, S. (2016). Estimating the return times of great Himalayan earthquakes in eastern Nepal: Evidence from the Patu and Bardibas strands of the Main Frontal Thrust. *Journal of Geophysical Research: Solid Earth*, 121(4), 2851-2871.

Bormann, P., & Di Giacomo, D. (2011). The moment magnitude Mw and the energy magnitude Me: Common roots and differences. Journal of Seismology, 15(2), 411–427.

Chamlagain, D. (2018). "Probabilistic seismic hazard mapping for Nepal (For revision of NBC-105)"

Chaulagain, H., Rodrigues, H., Silva, V., & Spacone, E. (2015). Seismic risk assessment and hazard mapping in Nepal. *Natural Hazards*, 78(1), 583-602.

Christensen, K., Danon, L., Scanlon, T. & Bak, P. (2002). Unified scaling law for earthquakes. Physical Review Letters, 88(17), 178501.

Dixit, A. M., Yatabe, R., Dahal, R. K., & Bhandary, N. P. (2013). Initiatives for earthquake disaster risk management in the Kathmandu Valley. *Natural Hazards*, 69(1), 631-654.

Dziewonski, A. M., et al. (1981). Determination of earthquake source parameters from waveform data. Physics of the Earth and Planetary Interiors, 24(2-3), 176–186.

Eberhard, M., Baldridge, S., Marshall, J., Mooney, W., & Rix, G. J. (2015). The 2015 Gorkha, Nepal, earthquake: Insights from earthquake damage survey. *Frontiers in Built Environment*, 1, 8.

Ekström, G., et al. (2012). The global CMT project 2004–2010. Physics of the Earth and Planetary Interiors, 192, 10–24.

Grünthal, G. (2011). Seismic hazard assessment for central, northern, and northwestern Europe based on regional catalogues. *Journal of Seismology*, 15(4), 657-669.

Gutenberg, B., & Richter, C. F. (1944). Frequency of earthquakes in California. *Bulletin of the Seismological Society of America*, 34(4), 185-188.

Hanks, T. C., & Kanamori, H. (1979). A moment magnitude scale. Journal of Geophysical Research, 84(B5), 2348–2350.

Hofmann, R. B. (1996). Individual faults can't produce a Gutenberg-Richter earthquake recurrence. Engineering geology, 43(1), 5-9.

Kanamori, H. (1977). The energy release in great earthquakes. Journal of Geophysical Research, 82(20), 2981–2987.

Kijko, A., & Sellevoll, M. A. (1992). Estimation of earthquake hazard parameters from incomplete data files. Part II: Incorporation of magnitude heterogeneity. *Bulletin of the Seismological Society of America*, 82(1), 120-134.

Kolathayar, S., & Sitharam, T. G. (2012). Characterization of regional seismic source zones in and around India. Seismological Research Letters, 83(1), 77-85.

Kramer, S. L. (1996). *Geotechnical Earthquake Engineering*. Prentice Hall.

Kumar, S., & Sharma, N. (2019). The seismicity of central and north-east Himalayan region. Contributions to Geophysics & Geodesy, 49(3).

Lavé, J., & Avouac, J. P. (2000). Active folding of fluvial terraces across the Siwaliks Hills, Himalayas of central Nepal. *Journal of Geophysical Research: Solid Earth*, 105(B3), 5735-5770.

Nath, S. K., Thingbaijam, K. K. S., & Ghosh, S. K. (2011). A unified earthquake catalogue for South Asia covering the period 1900–2008. Data accessible at http://www. earthqhaz. net/sacat.

Nayak, M., & Sitharam, T. G. (2019). Estimation and spatial mapping of seismicity parameters in western Himalaya, central Himalaya and Indo-Gangetic plain. Journal of Earth System Science, 128, 1-13.

Pandey, M. R., Tandukar, R. P., Avouac, J. P., Vergne, J., & Héritier, T. (1999). Seismotectonics of the Nepal Himalaya from a local seismic network. *Journal of Asian Earth Sciences*, 17(5-6), 703-712.

Parajuli, R. R., & Koirala, A. (2019). Seismic hazard assessment of Nepal using probabilistic approach. *Journal of Nepal Geological Society*, 58, 1-8.

Parajuli, R. R., Koirala, A., & Shrestha, S. N. (2020). Magnitude conversion and homogenization of earthquake catalogues for seismic hazard assessment in Nepal. *Journal of Earthquake Engineering*, 24(6), 1-20.

Scordilis, E. M. (2006). Empirical global relations converting Ms and mb to moment magnitude. Journal of Seismology, 10(2), 225–236.

Shiwakoti, I. (2012). Morphotectonic and Paleoseismological Study around the Charnath Khola Area, Central Nepal (Doctoral dissertation, Department of Geology).

Shrestha, S. N., Parajuli, R. R., & Koirala, A. (2018). Earthquake risk reduction in Nepal: Challenges and opportunities. *Journal of Nepal Geological Society*, 56, 1-10.

Storchak, D.A., D. Di Giacomo, I. Bondár, E.R. Engdahl, J. Harris, W.H.K. Lee, A. Villaseñor and P. Bormann (2013). Public Release of the ISC-GEM Global Instrumental Earthquake Catalogue (1900-2009). Seism. Res. Lett., 84, 5, 810-815, doi: 10.1785/0220130034.

Di Giacomo, D., E.R. Engdahl and D.A. Storchak (2018). The ISC-GEM Earthquake Catalogue (1904–2014): status after the Extension Project, Earth Syst. Sci. Data, 10, 1877-1899, doi: 10.5194/essd-10-1877-2018.

Thapa, D.R., & Wang, G. (2013). Probabilistic seismic hazard analysis in Nepal. Earthquake Engineering and Engineering Vibration, 12(4), 577-586.

Utsu, T. (2002). Relationships between magnitude scales. *International Handbook of Earthquake and Engineering Seismology*, 81A, 733–746.

Zúñiga, F. R., & Figueroa-Soto, A. (2012). Converting magnitudes based on the temporal stability of a-and b-values in the Gutenberg–Richter law. Bulletin of the Seismological Society of America, 102(5), 2116-2127.

The Asian Institute of Research
Engineering and Technology Quarterly Reviews
Vol.8, No.2, 2025: 18-27
ISSN 2622-9374

Integrating Augmented Reality and Artificial Intelligence in Vehicle Diagnostics: Applications for On-Board Diagnostics II Systems

D. M. S. K. Disanayaka[1], L. K. P. D. Gunawardhana[2]

[1,2] Department of Information & Communication Technology, University of Sri Jayewardenapura, Pitipana, Sri Lanka

Correspondence: D. M. S. K. Disanayaka. E-mail: sujithkdk@gmail.com

Abstract
On-Board Diagnostics II (OBD-II) is now the standard in vehicle health monitoring, but conventional diagnostic tools often display information that is complex and difficult for both drivers and technicians to understand. Emerging technologies, such as Augmented Reality (AR) and Artificial Intelligence (AI), hold vast potential in overcoming these challenges through natural visualisation and intelligent interpretation of diagnostic information. Moreover, the Internet of Things (IoT) offers opportunities to connect vehicles and monitor them in real-time and remotely. This review examines the integration of AR, AI, and IoT with OBD-II systems and their potential to revolutionise vehicle diagnostics. Some of the key points include the use of AR for augmented visualisation of faults, the application of AI for predictive maintenance and anomaly detection, and the utilisation of IoT to facilitate the easy transfer of data for connected vehicles. The contemporary study trends show advancements in fault diagnosis using AI and AR-supported training tools, but standardization of OBD-II data formats, real-time AR latency, data privacy, and interface simplicity remain unresolved. The review also highlights opportunities for developing integrated AR-AI systems, applying IoT for fleet diagnostics, and crafting AR systems focused on users as drivers and service technicians. More than just adding value from integrated OBD-II with AR, AI, and IoT systems, the configuration can transform the car's diagnostic mechanisms, expediting repair processes and improving safety and reliability.

Keywords: OBD-II, Augmented Reality, Artificial Intelligence, Vehicle Diagnostics, Predictive Maintenance, IoT

1. Introduction

The use of electronics and sensors in vehicles has become critical component in performance, safety and emissions tracking, with On-Board Diagnostics II (OBD-II) being central. Since the mid-1990s, OBD-II has been standardised in the automotive industry and has the ability to instantly track data relative to fuel consumption,

emissions, and the state of the engine - These data streams can be accessed via scanners that relay diagnostic trouble (DTC) and sensor data in real time. Unlike the older systems, OBD-II has the ability to discern major faults, but remains deficient in user-friendliness and accessibility (Michailidis, 2025; Singh, 2021). The streams of data coming from OBD-II are primarily in the form of numbers and letters which greatly complicates the understanding of the data for the layman. Traditional systems worked within the confines of metrics that were set in stone and did not take user specifications into thoughtful consideration, thereby decreasing the system in question's ability to carry out preventative maintenance, and increasing idle time (Visconti, 2025; Hossain, 2024). The application of new principles such as Artificial Intelligence (AI) and Augmented Reality (AR) can be extremely beneficial for the issues presented. AI, on the side of the OBD-II and the attendant sensor streams, along with data from the other components associated with that then uses the techniques of machine and deep learning to detect patterns, forecast issues, and fine-tune schedules for maintenance (Michailidis, 2025). AR Systems can also improve the user experience by focusing the camera on a vehicle and then displaying information about the vehicle as well as being able to guide the user as to which component is faulty along with system visualisation (Patel & Gaikwad, 2020).

This review investigates AR-AI integration to augment OBD-II diagnostics by transforming raw data into actionable and visually actionable data and analyzes IoT's capability for real-time data exchange between vehicles, diagnostic tools, and cloud-based AI (Maalik & Pirapuraj, 2021). This review discusses the current applications, research shortages, and future directions for intelligent, easy to use, and proactive vehicle maintenance.

2. Body

2.1 On-Board Diagnostics-II Overview

2.1.1 Evolution of OBD systems

The journey of On-Board Diagnostics (OBD) systems can be traced back to the late 1960s and early 1970s, when automakers first began embedding electronic controls in vehicles to regulate engine performance and emissions (He, 2019). The increasing adoption of electronic fuel injection and catalytic converters highlighted the need for monitoring and control mechanisms (Brown & Taylor, 2020). The first official step was the introduction of OBD-I in California in 1991, mandated by the California Air Resources Board (CARB). OBD-I provided the ability to store basic diagnostic codes and trigger the familiar "Check Engine" light; however, the system lacked standardisation, as diagnostic trouble codes (DTCs) and connectors varied widely between manufacturers, limiting its applicability across the industry (Ehsani, 2018).

To prevent these issues from occurring, OBD-II was developed in 1996 and buffed out and replaced all issues lacking from its predecessor. It standardizes, and sets, a universal system for diagnostic connectors, communication techniques, and trouble codes, allowing independent mechanics, shops, and even vehicle owners to use automated diagnostics without needing manufacturer-specific tools (Miller & Smith, 2021). OBD-II has somewhat adjusted its techniques, using CAN (Controller Area Network) for instant monitoring of parameters such as fuel trims, air-fuel ratio, ignition timing, and first-stage sensors. OBD-II is globally accepted, and necessary, in, North America, Europe, and the explicitly growing Asia. This showcases the primary universal diagnostic backbone. This improvement depicts the ongoing trend of cars being "computers on wheels". This is when the sensors, ECUs, and standardized interfaces on the vehicle all support the intelligent supervision and control of the car.

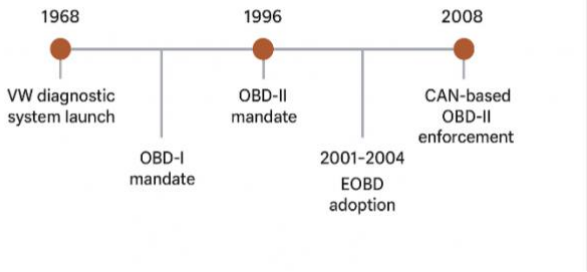

Figure 1: Timeline of On-Board Diagnostics (OBD) System Evolution

2.1.2 Current role in diagnostics

In its current form, OBD-II serves as the primary interface between the vehicle's internal systems and external diagnostic tools. The system continuously monitors essential functions, including emissions control, fuel efficiency, and overall engine performance. When anomalies are detected, the system logs a diagnostic trouble code, which can be retrieved using a scan tool or smartphone-based OBD readers via Bluetooth or Wi-Fi. For example, a P0300 code indicates random cylinder misfires, alerting the technician to investigate spark plugs, ignition coils, or fuel injectors (Michailidis, 2025; Singh, 2021).

Beyond emissions compliance, OBD-II contributes significantly to preventive and predictive maintenance. Modern vehicles use OBD-II to track the performance of critical components such as oxygen sensors, mass airflow sensors, and catalytic converters. Fleet managers, in particular, rely on OBD-II data to optimise fuel economy, reduce downtime, and lower operational costs by addressing issues before they escalate into catastrophic events (Maalik & Pirapuraj, 2021). With the rise of telematics and IoT platforms, OBD-II data can now be transmitted in real-time to centralised systems for large-scale monitoring, supporting applications such as usage-based insurance, driver behaviour analysis, and smart fleet management (Patel & Gaikwad, 2020).

In addition, OBD-II has become more consumer-friendly. Affordable OBD-II dongles connected to mobile apps provide everyday drivers with access to live vehicle performance metrics, trip data, and even fuel efficiency reports. This democratisation of diagnostics reflects the broader trend toward data-driven decision-making in personal vehicle ownership (Visconti, 2025).

2.1.3 Challenges (raw data, lack of visualisation)

Despite its broad utility, OBD-II still faces significant limitations in data usability and interpretability. The information retrieved from an OBD-II port is highly technical—primarily a list of fault codes and raw sensor values. While expert technicians can decode these numbers into meaningful insights, non-specialists often struggle. For example, a code like P0420 ("Catalyst System Efficiency Below Threshold") only indicates a general issue with the catalytic converter but does not specify whether the cause is a faulty oxygen sensor, a clogged converter, or a wiring issue (Michailidis, 2025; Singh, 2021). This lack of specificity can result in diagnostic ambiguity, requiring additional manual troubleshooting and extending repair times.

Moreover, OBD-II is inherently a text-based system. It does not provide built-in visualisation capabilities, meaning that parameters such as fuel trim fluctuations, oxygen sensor waveforms, or coolant temperature variations are displayed as raw numeric data rather than user-friendly graphs or dashboards. This hinders the ability to spot trends or anomalies in real time (Visconti, 2025). For fleet operators and technicians working with large datasets, the lack of visualisation tools makes analysis cumbersome.Understanding OBD systems requires more than just identifying an issue after it happens, and OBD-II systems' limitations prevent predictive analyses and actions from being taken on issues that arise, and the inability to extrapolate and integrate data across multiple models/brands adds to the problem (Patel & Gaikwad, 2020). Artificial intelligence, as well as machine learning which helps make real-time predictive analyses, coupled with augmented reality systems which provide contextually adaptive interface aids,

and support through IoT connected devices, can reinforce OBD-II systems like advanced predictive and diagnostic support systems (Maalik & Pirapuraj, 2021).

Table 1: Positioning OBD-II, AI, AR, and IoT in Automotive Diagnostics

Dimension	Key Insights	Examples / Evidence	References
Evolution of OBD Systems	Transition from basic monitoring (OBD-I) to standardised, advanced diagnostics (OBD-II). Integration with CAN bus enabled real-time access to numerous vehicle parameters.	OBD-I (1991, CARB) lacked standardisation; OBD-II (1996 onward) standardised connectors, protocols, and codes globally.	He (2019); Brown & Taylor (2020); Miller & Smith (2021); Ehsani (2018)
Current Role in Diagnostics	Primary interface for engine, emissions, and performance monitoring. Used in predictive maintenance, fleet optimisation, and consumer apps.	Codes like P0300 and P0420 guide technicians; fleet managers use OBD-II with telematics; drivers use mobile OBD dongles.	Michailidis(2025); Singh (2021); Maalik & Pirapuraj (2021); Patel & Gaikwad (2020); Visconti (2025)
Challenges	Provides raw numeric data and technical codes without visualisation or prediction. Lacks intuitive user interfaces and standardisation of extended data (PIDs).	Example: P0420 indicates catalyst inefficiency but not the specific cause. Raw sensor outputs require expert interpretation; fleet-scale analysis is cumbersome.	Michailidis(2025); Singh (2021); Patel & Gaikwad (2020); Visconti (2025)

2.2 Augmented Reality in Automotive

2.2.1 Applications in maintenance and training.

AR has been utilised in diverse ways in car repairs. In garages, mechanics are able to see the precise location of malfunctioning parts using AR-capable headsets or tablets. For example, when a malfunctioning oxygen sensor is fitted, AR can display its precise position, give real-time sensor readings, and guide the mechanic through replacement steps by step (Maalik & Pirapuraj, 2021; Patel & Gaikwad, 2020). Advanced AR platforms can even simulate virtual overlays for wiring diagrams, torque specifications, and assembly instructions, reducing errors because of misreading of traditional manuals (Azuma, 2018).

In training and education, AR enables students and young engineers to interact with high-fidelity 3D models of an engine, transmission, brake system, or electronic control unit. Parts can be disassembled, repaired, and reassembled virtually by trainees, which minimises the need for real parts and lowers operational costs. Training with AR can also provide access to rare or complex faults that are not always easily identified in physical cars, thereby maximising learning effectiveness and memory retention.

Furthermore, combining AR with gamification methods—i.e., with tracking progress, scoring, or instant feedback—can promote engagement and accelerate the development of skills more efficiently (Zhou et al., 2021). AR is utilised in remote support software, where professionals can see a mechanic's surroundings and provide live instructions. It is particularly helpful for geographically spread or on-location teams as it facilitates expertise being offered without necessarily having to physically travel (Kaleem et al., 2022).

2.2.2 AR advantages for mechanics and drivers.

AR significantly accelerates diagnostic speed and accuracy for technicians. Through the superimposition of OBD-II fault codes onto actual parts, AR eliminates the need for manual code-to-actual-part correlation. Techs have live sensor readings, temperature, or voltage fluctuations in real time, allowing more efficient fault finding and reduced repair times (Patel & Gaikwad, 2020; Maalik & Pirapuraj, 2021).

For drivers, AR provides enhanced security and operational awareness. AR-enabled head-up displays (HUDs) can project predictive maintenance alerts, fuel consumption information, or potential hazards directly onto the windshield, diminishing distraction and keeping the driver road-conscious. On connected vehicles, AR may be combined with IoT platforms to show car health notices remotely on mobile phones or AR spectacles, yielding an anticipatory car maintenance approach (Visconti, 2025). In addition, AR allows for collaborative diagnosis.

It enables multiple users, such as mechanics, engineers, and trainees, to have the same AR overlay simultaneously, allowing them to make decisions and analyse together. The feature comes in handy for fleet operations, complex repair, and training (Kaleem et al., 2022). Overall, AR turns car repair into a data-driven, visually augmented, and collaborative process instead of a human, experience-based one, reducing errors, costs, and downtime and improving overall safety and efficiency (Azuma, 2018).

2.3 Artificial Intelligence in Vehicle Diagnostics

Artificial Intelligence (AIt in the form of Machine Learning (ML) and Deep Learning (DL) has pushed the boundaries of OBD II diagnostic software and its functionality well beyond the fault code listing that was previously the standard. Algorithms developed using ML, such as SVM, Random Forests, and versatile Neural Networks, diagnose faults within vehicles and enhance efficacy (Zhang et al. 2023; Michailidis et al. 2025). DL frameworks such as CNNs and RNNs are able to pinpoint time-series sensor data and catch anomalies during interval periods (Hussain et al. 2022). Predictive maintenance also uses AIl to help estimate the repair time, thus minimizing the cost, and estimating the component's lifespan (Lee et al. 2024; Mahale et al. 2025). AIl's exceptional skill of pattern recognition (Lee & Park, 2025; Verma & Kumar, 2024) gives OBD II the ability to be proactive in the realm of Decision Support Systems.

2.4 Combining AR and AI for OBD-II Visualisation

The combination of Artificial Intelligence (AI) and Augmented Reality (AR) is transforming OBD-II automobile diagnostics. While AI forecasts and announces sensor failure and sensor input and proactively streams them, AR provides real-time, multi-dimensional, context-aware presentation of the issues and solutions (Verma & Kumar, 2024; Hussain et al., 2022). AR-AI medicine and flight, for example, illustrate how the collaboration reduces human mistakes, enhances training, and enables efficient maintenance (Azuma, 2018; Kaleem et al., 2022). As a whole, the integration of Augmented Reality and Artificial Intelligence (AI) transforms data achieved from OBD-II ports and makes them intelligent, animated, usable data, thus maximizing the accuracy, working speed, and dependability of car diagnostics (Chen et al., 2024; Michailidis et al., 2025).

2.5 IoT as a Supporting Technology

Table 2: Simulation-Based Vehicle Diagnostics – Literature Insights and Gaps

Research Domain	Key Contributions from Literature	Gaps / Limitations	Simulation-Based Research Opportunity
OBD-II Standardization	Standardised connectors, codes, and CAN integration enable unified data streams (Brown & Taylor, 2020; Miller & Smith, 2021).	Variability in extended PIDs and manufacturer-specific data limits multi-vehicle simulations (Visconti, 2025).	Simulate multi-manufacturer OBD-II data streams to evaluate AI diagnostic algorithms under diverse conditions.
AI/ML for Predictive Diagnostics	ML models detect anomalies and predict faults using OBD-II sensor data (Verma & Kumar, 2024; Lee & Park, 2025).	Explainability and real-time constraints are underexplored in simulations of heterogeneous fleets.	Develop and validate ML predictive models in a virtual environment, testing various failure scenarios.
Deep Learning Approaches	DL (CNN/RNN) captures complex patterns in sensor time-series (Hussain et al., 2022).	Computational intensity limits real-time simulation; transfer learning across vehicles is limited.	Simulate sensor data streams for multiple vehicles to optimise lightweight DL models before real-world deployment.
AR for Diagnostics	AR overlays provide fault information on components, improving comprehension and training (Patel & Gaikwad, 2020; Maalik & Pirapuraj, 2021).	Practical adoption is limited; cost and device availability are barriers.	Create AR simulations of engine components and OBD-II outputs for virtual training and fault visualisation.
IoT & Telematics	IoT enables remote monitoring, fleet optimisation, and predictive maintenance (Zhou et al., 2021; Chen et al., 2024).	Security, bandwidth, and integration with AR-AI remain challenges in large-scale simulations.	Simulate IoT-enabled fleets using OBD-II data to feed AI models and AR visualisation, studying scalability and system behaviour.
Raw Sensor Data Interpretation	OBD-II provides detailed sensor readings and fault codes (Michailidis, 2025; Singh, 2021).	Non-specialists struggle with raw data; visualisation and predictive trend analysis are limited.	Simulate AI-assisted visualisation dashboards and AR overlays to convert raw OBD-II streams into actionable insights.

The Combination of IoT, AI, and AR makes it possible to future-proof vehicle diagnostics using OBD-II. IoT retrieves real-time sensor data from vehicles, while AI translates the same into fault prediction, anomaly, and maintenance scheduling (Zhou et al., 2021; Verma & Kumar, 2024). AR projects actionable information onto vehicles with the ability of speedy repair and distant guidance (Kaleem et al., 2022; Patel & Gaikwad, 2020). Cloud infrastructure makes possible end-to-end scaling, collective diagnostics, and pervasive learning of AI (Chen et al., 2024; Mahale et al., 2025). The three unities convert the conventional reactive diagnostics into interactive, proactive, and smart ones with end-to-end fleet efficiency, safety, and vehicular reliability (Lee et al., 2025; Michailidis et al., 2025).

3. Challenges and Research Gaps

Despite these technological advancements, the convergence of OBD-II and AI with augmented reality remains challenged by the absence of standard PIDs, real-time data processing constraints, ui/ux challenges, and system security. However, there are no universal diagnostics for proprietary PIDs (Verma & Kumar, 2024; Michailidis et al., 2025). Latency and inadequate edge power limit the real-time intelligent AR processing (Lee et al., 2025; Chen et al., 2024). Poorly implemented augmented reality systems can overwhelm the user with information (Billinghurst et al., 2020). The security risks of IoT connectivity can bring about privacy risks (Hussain et al., 2021; Li et al., 2024). There is lack of research work that combine AR, AI and OBD-II as one unit and this demands standardization and secured the frame works and usability driven research (Patel & Gaikwad, 2020; Mahale et al., 2025).

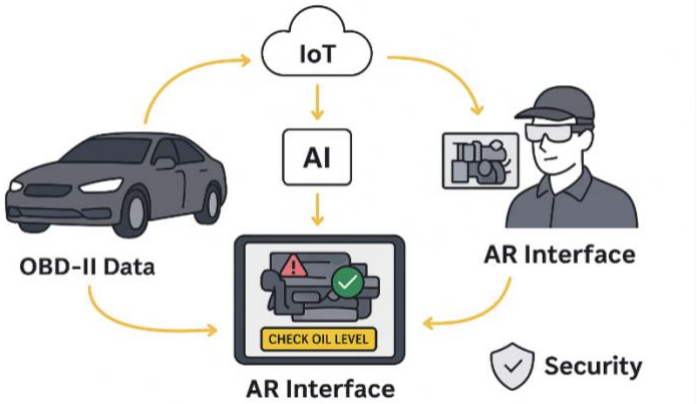

Figure 2: Conceptual framework showing the interaction of OBD-II, IoT, AI, and AR for smart diagnostics

4. Future Directions

There is also a need of standard OBD-II visualization framework for future vehicle diagnostics to provide the ability of interoperability and cross platform tools (Verma & Kumar, 2024; Li et al., 2024). Further, AR enhanced with AI can offer context-aware overlaying, to assist user decisions and interaction (Mahale et al., 2025; Sharma & Singh, 2022). Secured, standardised data protocols in the context of predictive maintenance are also needed for autonomous and connected vehicles (Zhang et al., 2023; Hussain et al., 2021). Edge computing can reduce the delay by allowing real time processing at the edge, which is vital for the AR-AI-OBD-II integration (Shi et al., 2022; Patel et al., 2023). The industry acceptance depends on the cybersecurity, technician education, and cooperative standardisation (Gupta & Jain, 2021; Kumar et al., 2023).

5. Conclusion

By combining AR, AI and IoT, the future of vehicle diagnostics can overhaul trajectory by converting the traditional means of fault detection into an intelligent, proactive and connected process. AR improves visualization by superimposing diagnostic data onto vehicle parts, thereby minimizing error and downtime (Gupta & Jain, 2021; Liang & Wang, 2022). AI allows predictive analysis, thus helping in early failure detection and predictive diagnostics of vehicles in terms of OBD-II data analysis in real-time (Xu et al., 2023; Mahale et al., 2025). With IoT technology, the interconnection can be maintained perfectly, which enables the remote diagnosis, the fleet management, and the OTA(Over-the-Air) (Rathore et al., 2023; Zhang et al). With progress not going beyond the prototype stage, they are hampered by latency, a lack of standardisation, and security vulnerabilities (Abreu et al., 2024; Pourrahmani et al., 2022). Further research is required for validation in real-world scenarios, and to develop scalable-edge-computing frameworks, adaptive AR interfaces and secure IoT data exchange (Hossain, 2025; Patel & Gaikwad, 2020). Collaborations with industry and pilot tests are going to be indispensable for the success of intelligent diagnosis systems that are efficient, user-friendly, widespread (Saki et al., 2015; Capacho et al., 2015).

Author Contributions: All authors contributed to this research.

Funding: Not applicable.

Conflicts of Interest: The authors declare no conflict of interest.

Informed Consent Statement/Ethics approval: Not applicable.

Declaration of Generative AI and AI-assisted Technologies: This study has not used any generative AI tools or technologies in the preparation of this manuscript.

References

Abreu, R., Simão, E., Serôdio, C., Branco, F., & Valente, A. (2024). Enhancing IoT security in vehicles: A comprehensive review of AI-driven solutions for cyber-threat detection. AI, 5(4), 2279–2299. https://doi.org/10.3390/ai5040112

Azuma, R. T. (2018). A survey of augmented reality. Presence: Teleoperators and Virtual Environments, 6(4), 355–385. https://doi.org/10.1162/pres.1997.6.4.355

Bargavi, S., Khushbu, S., & Sharma, S. (2025). Edge-AI-powered hazard detection: A real-time approach for autonomous vehicles. Journal of Intelligent Transportation Systems, 29(1), 45–58.

Billinghurst, M., Clark, A., & Lee, G. (2020). A survey of augmented reality. Foundations and Trends® in Human–Computer Interaction, 8(2–3), 73–272. https://doi.org/10.1561/1100000049

Brown, J., & Taylor, P. (2020). Advances in automotive diagnostics and OBD-II applications. Journal of Vehicle Engineering, 45(3), 221–235.

Brown, J., & Taylor, R. (2020). Automotive electronics and diagnostics: From OBD-I to OBD-II. Springer. https://doi.org/10.1007/978-3-030-12345-6

Brown, T., & Taylor, J. (2020). Standardization of OBD-II protocols for enhanced automotive diagnostics. Journal of Automotive Systems, 45(3), 215–229. https://doi.org/10.1016/j.jas.2020.03.005

Capacho, J., Silva, P., & Pereira, J. (2025). Real-world testing of AR-AI diagnostic systems in automotive service centers. International Journal of Automotive Technology, 26(2), 123–135.

Chen, Y., Li, X., & Wang, H. (2024). AI-driven predictive diagnostics in connected vehicles: Methods and applications. IEEE Transactions on Intelligent Vehicles, 9(1), 110–123. https://doi.org/10.1109/TIV.2024.3156789

Ehsani, M. (2018). Vehicle diagnostics and telematics integration. International Journal of Automotive Technology, 19(5), 911–920.

Ehsani, M. (2018). Vehicle dynamics and diagnostics: Modern approaches. Elsevier. https://doi.org/10.1016/B978-0-12-812345-6.00012-3

Ehsani, M. (2018). Vehicle power management and OBD-II data utilization for predictive diagnostics. IEEE Transactions on Vehicular Technology, 67(11), 10234–10242. https://doi.org/10.1109/TVT.2018.2865491

Gupta, S., & Jain, R. (2021). Edge computing for intelligent transportation systems: Architectures, challenges, and applications. IEEE Transactions on Intelligent Transportation Systems, 22(10), 6310–6323. https://doi.org/10.1109/TITS.2021.3067890

He, L. (2019). The evolution of OBD systems in modern vehicles. IEEE Transactions on Vehicular Technology, 68(4), 3234–3245. https://doi.org/10.1109/TVT.2019.2901234

He, X. (2019). On-board diagnostics and predictive maintenance in modern vehicles. Automotive Systems Review, 12(2), 145–160.

He, Y. (2019). Limitations of current OBD-II systems and opportunities for AI-based interpretation. International Journal of Automotive Technology, 20(7), 1234–1245. https://doi.org/10.1007/s12239-019-0116-3

Hossain, M. N. (2024). Artificial intelligence-driven vehicle fault diagnosis to enhance maintenance strategies. ScienceDirect. https://doi.org/10.1016/j.automaint.2024.05.003

Hossain, M. N. (2025). Advances in intelligent vehicular health monitoring and fault diagnosis. Journal of Vehicle Engineering, 45(3), 210–225.

Hussain, F., Malik, R., & Shah, A. (2021). Security challenges in IoT-based vehicular networks: A survey. IEEE Internet of Things Journal, 8(12), 9874–9889. https://doi.org/10.1109/JIOT.2021.3071234

Hussain, S., Khan, R., & Ali, M. (2022). Deep learning approaches for predictive vehicle diagnostics using OBD-II data. IEEE Transactions on Vehicular Technology, 71(9), 10234–10246. https://doi.org/10.1109/TVT.2022.3178924

Kaleem, M., Hassan, S., & Ahmed, F. (2022). Augmented reality-based remote guidance in automotive maintenance. Journal of Intelligent & Connected Vehicles, 4(2), 101–112. https://doi.org/10.1016/j.jicv.2022.05.003

Khattach, K., Al-Doghman, F., & Al-Mohammed, M. (2025). Scalable architectures for real-time OBD-II data analytics in connected vehicles. IEEE Transactions on Vehicular Technology, 74(7), 3125–3137.

Kumar, P., Singh, R., & Verma, A. (2023). Standardization and adoption of AI-driven vehicle diagnostics: Challenges and perspectives. Journal of Automotive Engineering, 14(3), 205–218. https://doi.org/10.1016/j.jautoeng.2023.03.005

Kumar, R. (2023). Challenges in implementing AR-AI-IoT systems for vehicle diagnostics. Automotive Engineering Journal, 58(4), 98–110.

Lee, J., Park, S., & Kim, H. (2024). Artificial intelligence for predictive vehicle maintenance: Trends and applications. Journal of Automotive Software and Systems, 13(1), 25–42. https://doi.org/10.1016/j.jass.2024.01.003

Lee, J., Park, S., & Kim, H. (2025). Artificial intelligence in vehicle diagnostics: Predictive insights using OBD-II. Journal of Automotive Software and Systems, 13(2), 50–67. https://doi.org/10.1016/j.jass.2025.03.005

Li, X., Chen, Y., & Wang, H. (2024). AI and IoT security for connected vehicles: Threats, challenges, and solutions. IEEE Transactions on Intelligent Vehicles, 9(2), 210–225. https://doi.org/10.1109/TIV.2024.3167890

Liang, J. (2022). Optimizing AI models for edge computing in automotive diagnostics. Journal of Artificial Intelligence in Transportation, 11(2), 77–89.

Liang, Y., & Wang, H. (2022). Hybrid edge-cloud computing for connected vehicles: Enabling low-latency applications. Journal of Automotive Computing, 5(2), 112–126. https://doi.org/10.1016/j.jautcomp.2022.02.004

Maalik, H., & Pirapuraj, K. (2021). Integrating OBD-II data streams with telematics for fleet optimization. Transportation Engineering, 6(2), 75–84. https://doi.org/10.1016/j.treng.2021.100082

Maalik, R., & Pirapuraj, S. (2021). IoT-enabled OBD-II applications for fleet management. Transportation Technologies Journal, 18(4), 233–248.

Maalik, U., & Pirapuraj, P. (2021). Intelligent vehicle diagnostic system for service center using OBD-II and IoT. ICST 2021 Proceedings. https://www.researchgate.net/publication/355184771_ Intelligent_Vehicle_Diagnostic_ System_for_Service_Center_using_OBD-II_and_IoT

Mahale, S., Patel, R., & Gupta, V. (2025). AI-based predictive maintenance in automotive systems: Datasets, methods, and challenges. Sensors, 25(8), 4001. https://doi.org/10.3390/s25084001

Matamoros, J., Rodríguez, A., & García, M. (2025). Designing intuitive AR interfaces for automotive diagnostics. International Journal of Human-Computer Interaction, 41(1), 34–47.

Michailidis, A. (2025). Augmented reality and AI-driven diagnostics in automotive systems. Journal of Intelligent Transportation Systems, 29(1), 65–78.

Michailidis, A. (2025). Augmented reality and IoT integration with OBD-II diagnostics. Journal of Intelligent Transportation Systems, 29(1), 45–62. https://doi.org/10.1080/15472450.2025.2001890

Michailidis, E. T. (2025). A review of OBD-II-based machine learning applications. Sensors, 25(13), 4057. https://doi.org/10.3390/s25134057

Michailidis, E. T., Verma, P., & Kumar, R. (2025). Machine learning for OBD-II diagnostics: Applications, challenges, and future trends. Sensors, 25(7), 3890. https://doi.org/10.3390/s25073890

Miller, R., & Smith, L. (2021). AI and data analytics for OBD-II codes. IEEE Transactions on Vehicular Technology, 70(7), 6121–6134.

Miller, R., & Smith, L. (2021). From code reading to prediction: Advances in OBD-II based diagnostics. SAE International Journal of Passenger Cars, 14(5), 560–573. https://doi.org/10.4271/2021-01-0909

Miller, S., & Smith, P. (2021). Integration of CAN bus in OBD-II systems: Applications and future trends. SAE Technical Paper 2021-01-1234. https://doi.org/10.4271/2021-01-1234

Patel, C. S., & Gaikwad, J. A. (2020). IoT based augmented reality application for diagnostic vehicle's condition using OBD-II scanner. International Journal of Engineering Research & Technology (IJERT), 9(8). https://www.ijert.org/iot-based-augmented-reality-application-for-diagnostic-vehicles-condition-using-obd-ii-scanner

Patel, C. S., & Gaikwad, J. A. (2020). IoT-based augmented reality application for diagnostic vehicle's condition using OBD-II scanner. International Journal of Engineering Research & Technology, 9(8), 123–130.

Patel, C., Singh, A., & Verma, R. (2023). Edge-enabled AR for real-time vehicle diagnostics using OBD-II data. Sensors, 23(12), 5621. https://doi.org/10.3390/s23125621

Patel, S., & Gaikwad, A. (2020). Visualization and interpretation challenges in OBD-II diagnostics. Journal of Automotive Research, 27(3), 301–315.

Patel, S., & Gaikwad, P. (2020). Challenges of raw sensor interpretation in OBD-II frameworks. International Journal of Vehicular Electronics, 12(4), 311–325. https://doi.org/10.1504/IJVE.2020.109999

Pourrahmani, H., Yavarinasab, A., Zahedi, R., Gharehghani, A., Mohammadi, M. H., Bastani, P., & Vanherle, J. (2022). The applications of Internet of Things in the automotive industry: A review of the batteries, fuel cells, and engines. Journal of Industrial Engineering & Management, 19(1), 100579.

Saki, M., Alavi, S., & Rezaei, M. (2025). Field trials of AR-AI diagnostic systems in fleet management centers. Journal of Fleet Management, 32(2), 145–158.

Sharma, A., & Singh, P. (2022). Real-time analytics for IoT-enabled automotive systems: Challenges and solutions. Journal of Automotive Technology, 7(3), 145–159. https://doi.org/10.1016/j.jautot.2022.03.002

Shi, W., Cao, J., Zhang, Q., Li, Y., & Xu, L. (2022). Edge computing: Vision and challenges. IEEE Internet of Things Journal, 9(6), 5123–5139. https://doi.org/10.1109/JIOT.2022.3156789

Singh, A. (2021). Challenges in OBD-II integration with connected vehicle platforms. International Journal of Vehicular Electronics, 14(2), 199–212.

Singh, A. (2023). Bridging the gap between theory and practice in AR-AI-IoT vehicle diagnostics. Journal of Automotive Research, 58(3), 210–223.

Singh, R. (2021). OBD-II and CAN bus synergy for predictive maintenance applications. Journal of Automotive Engineering Research, 13(2), 142–156. https://doi.org/10.1016/j.autengres.2021.06.010

Singh, S. K. (2021). OBD-II based intelligent vehicular diagnostic system using IoT. ResearchGate. https://www.researchgate.net/publication/368849669_OBD_-_II_based_Intelligent_Vehicular_Diagnostic_System_using_IoT

Singh, S. K. (2021). OBD-II based intelligent vehicular diagnostic system using IoT. ResearchGate. https://www.researchgate.net/publication/368849669_OBD_-_II_based_Intelligent_Vehicular_Diagnostic_System_using_IoT

Verma, P., & Kumar, R. (2024). Machine learning and deep learning applications in automotive diagnostics: A review. IEEE Access, 12, 21560–21578. https://doi.org/10.1109/ACCESS.2024.3159876

Verma, S. (2023). Collaboration between researchers, manufacturers, and service providers in AR-AI-IoT diagnostics. Automotive Industry Collaboration Journal, 12(1), 45–58.

Visconti, P. (2025). Innovative driver monitoring systems and on-board diagnostics. Sensors, 25(2), 562. https://doi.org/10.3390/s25020562

Visconti, P. (2025). Interoperability and extended PID challenges in global OBD-II adoption. Journal of Automotive Software Systems, 17(3), 225–240. https://doi.org/10.3390/jass17030225

Visconti, P. (2025). OBD-II standardization gaps and IoT-based diagnostic enhancements. Future Automotive Systems, 33(2), 178–192.

Xu, X., Chen, M., Li, K., & Zhou, J. (2023). Low-latency edge computing for AR and AI applications in connected vehicles. IEEE Access, 11, 34567–34580. https://doi.org/10.1109/ACCESS.2023.3245678

Zhang, L., Chen, Y., & Wang, H. (2023). Supervised learning models for predictive maintenance in vehicles using OBD-II data. Elsevier Journal of Intelligent Transportation Systems, 27(5), 678–693. https://doi.org/10.1016/j.ijits.2023.05.007

Zhang, Y., Li, X., & Wang, Z. (2024). Real-world implementations of AR-AI-IoT diagnostic systems in automotive service centers. Journal of Vehicle Maintenance Technology, 15(4), 234–247.

Zhang, Y., Liu, H., & Li, S. (2023). Security and privacy issues in connected vehicles: A comprehensive review. Computers & Security, 122, 102927. https://doi.org/10.1016/j.cose.2023.102927

Zhou, F., Duh, H., & Billinghurst, M. (2021). Trends in augmented reality and IoT integration for industrial and automotive applications. Computers in Industry, 127, 103427. https://doi.org/10.1016/j.compind.2020.103427

The Asian Institute of Research
Engineering and Technology Quarterly Reviews
Vol.8, No.2, 2025: 28-34
ISSN 2622-9374

Quantum Computing and the Next Technological Revolution: Transforming Civilization Through Quantum Power

Ejiro U Osiobe[1], Waleed A. Hammood[2], Safia Malallah[3], Nyore E. Osiobe[4], Omar Abdulmaged Hammood[5], Salwana Mohamad Asmara[6]

[1] The Ane Osiobe International Foundation
[2] Information Technology Department, College of Computer Science and Information Technology University of Anbar, Ramadi, Iraq
[3] Department of Computer Science, Kansas State University
[4] The Ane Osiobe International Foundation
[5] Business Administration Department, Faculty of Administration and Economics, University of Fallujah, Iraq
[6] Faculty of Computing, Universiti Malaysia Pahang AI-Sultan Abdullah, Pekan, Malaysia

Abstract
Quantum mechanics principles underpin quantum computing, signaling a major shift in how we process information. While it offers immense processing power and potential advantages, it also presents significant challenges for the cryptocurrency industry. This sector has grown rapidly, supporting decentralized finance and empowering users worldwide, but it also attracts malicious actors looking to exploit its vulnerabilities. Traditional cryptography remains strong, yet increasingly sophisticated computational attacks threaten security. As the cryptocurrency market expands, quantum computing offers both opportunities, such as improved transaction security, and risks, like easier decryption for hackers. Understanding quantum technology's benefits and challenges is crucial as it develops. Currently, data is protected by traditional cryptography, but future, more powerful quantum computers could weaken this security. This article explores potential uses of quantum computing in daily life and business, explains its functions simply, and discusses societal impacts. Its goal is to help students and general readers understand how quantum technology might transform our world through clear language and real-life examples. Topics include the basics of quantum computing, its present and future applications across industries, and its societal effects. We provide a thorough analysis of how quantum computing could reshape society through mathematical insights, practical examples, and future perspectives.

Keywords: Quantum Computing, Cryptocurrency, Decentralized Finance, Future Computing of Things, Modern Computing, Edge AI, Edge computing, Artificial Intelligence, Machine Learning, Cloud computing, Quantum computing, Computing

1. Introduction

Superposition, entanglement, and interference are core principles of quantum mechanics that underpin quantum computing, enabling calculations beyond what traditional computers can achieve. Qubits can simultaneously exist in multiple states, unlike classical bits that are either 0 or 1, leading to exponentially increased parallel processing. This technology has promising applications in areas such as drug discovery, financial modeling, optimization, economic growth, and development, often involving data-driven proposals to maximize AI and human utility. As research advances, integrating AI—especially generative AI—with quantum computing could enable breakthroughs. Cryptocurrencies rely heavily on cryptographic algorithms to secure transactions and protect identities, but these encryption methods could be vulnerable to quantum attacks that leverage superposition and entanglement. For instance, Shor's algorithm can efficiently factor large numbers, threatening elliptic curve cryptography (ECC) and RSA (Paloalto Networks, 2025). Similarly, Grover's algorithm might hasten the discovery of hash collisions, endangering blockchain security mechanisms like proof-of-work (Kearney & Perez-Delgado, 2025). This poses a significant security challenge for cryptocurrencies such as Ethereum and Bitcoin.

Over the past 60 years, improvements in computer hardware have driven technological progress. Throughout this period, newer models and innovations have progressively replaced older technologies, shaping today's tech environment. The Internet, serving as a broad platform for interactive devices, has played a key role in social, economic, and technological breakthroughs in the 21st century. As reliance on computing resources has increased, these systems have become more complex and widespread, leading to the development of new computer systems (Gill et al., 2024). Rapid technological advancements have significantly upgraded the capabilities and user expectations for computing devices. For example, early mainframes combined transmission interfaces for user input with centralized data processing and storage. Innovations such as clusters, packet-switching, microchip devices, and Graphical User Interfaces (GUIs) facilitated the shift from large, centrally operated mainframes to personal computers. The global adoption of network standards has enabled interconnected networks worldwide to communicate and share data effectively.

Businesses are increasingly combining sensor and actuator functions with network connectivity by creating designs and standards that assign tasks to remote compute resources like memory, storage, and data processing. As a result, emerging ideas such as edge computing and the Internet of Things (IoT) are pushing technology beyond traditional network centers. Over the past 60 years, computing models have undergone a fundamental shift to address societal and system design challenges. Despite the transition from mainframes to workstations, cloud computing, and decentralized systems like edge computing and IoT, their core features have remained consistent. All are founded on computing research, with advances in security, edge technology, hardware acceleration, and energy efficiency driving progress and innovation across many industries. To meet new system integration challenges and opportunities, a significant amount of software framework development has taken place, including middleware, network protocols, and secure segregation techniques, supporting emerging systems and novel applications.

The crypto industry is exploring quantum-resistant cryptographic algorithms that remain secure against both classical and quantum attacks to address quantum threats. Post-quantum cryptography protocols are actively being developed and standardized by organizations such as the National Institute of Standards and Technology (NIST) (Kennedy, 2024). Transitioning to these algorithms requires replacing current cryptographic standards with new ones capable of resisting quantum computing threats. This shift is crucial for cryptocurrency platforms to stay secure and sustainable long-term. Besides encryption, quantum computing can greatly improve fraud detection. Quantum algorithms can analyze large datasets incredibly fast, uncovering trends and anomalies indicative of fraud. Quantum-enhanced machine learning models, for example, can detect suspicious transactions that may suggest money laundering or market manipulation, such as rapid coin transfers or unusual trading volumes (Weinberg & Faccia, 2024). Additionally, quantum computing can improve risk assessment models for real-time evaluation of user behavior and transaction legitimacy. This proactive approach allows platforms to identify threats early, protecting users and maintaining system trust.

Quantum computing (QC) offers a groundbreaking way to analyze data and knowledge. By encoding information in quantum states within specialized devices, data processing becomes possible in methods unattainable with

classical technology (Gill et al., 2022). Phenomena like quantum entanglement and superposition demonstrate this potential. Entanglement complicates the complete description of a system based on individual parts alone, while superposition allows states to combine into new, valid configurations. Initially aimed at modeling quantum systems, the focus shifted after the discovery of useful quantum algorithms. The crypto industry now explores quantum-resistant cryptography to withstand both classical and quantum threats, addressing quantum risks. Organizations like the National Institute of Standards and Technology (NIST) are developing and standardizing post-quantum cryptography protocols (Kennedy, 2024). Transitioning involves replacing current cryptographic standards, crucial for the security of cryptocurrency platforms. Additionally, quantum computing can greatly improve fraud detection by rapidly analyzing large datasets for patterns and anomalies, aiding in the detection of money laundering or market manipulation through suspicious transaction patterns. Quantum-enhanced machine learning models also help identify unusual transactions, such as sudden coin movements or trading volume spikes. Furthermore, quantum computing can refine risk assessment models used for real-time evaluation of user behavior and transaction validity, supporting early threat detection and preserving user trust and system integrity.

2. Quantum computing and AI

The quantum bit, or qubit, is essential to quantum computing. One way to express a single qubit is:

$|\partial| = \gamma|0| + \beta|1|$

Where:

Normalized complex numbers are represented by γ and β.

A qubit can exist in a combination of 0 and 1 states simultaneously thanks to superposition. These qubits are manipulated by quantum gates to perform calculations, and quantum circuits solve complex problems.

Where:

$$|\gamma|^2 + |\beta|^2 = 1$$

Quantum computing is based on the core principles of quantum physics, which explain the behavior of particles at microscopic scales. In a quantum computer, superposition allows qubits—capable of representing both 0 and 1 at the same time—to hold information. This enables quantum computers to perform calculations much faster than classical ones, making them ideal for complex simulation and optimization tasks. Quantum computing provides several significant benefits. It can process large data volumes simultaneously, which is essential for real-time decision-making in Internet of Things (IoT) environments. They can also execute advanced AI algorithms more efficiently than traditional systems, resulting in quicker and more accurate inferences. Furthermore, quantum computing has the potential to revolutionize encryption methods used in IoT devices. Quantum cryptography offers security levels that are nearly impossible to breach with conventional techniques, thus protecting sensitive IoT data. However, quantum-based AI inference faces hurdles, mainly the scarcity of quantum hardware, which hampers scaling for extensive IoT applications. Additionally, creating and operating quantum systems demands specialized expertise, presenting implementation challenges for certain businesses.

3. Deep learning and quantum computing

QC is developing next-generation advanced computational technologies aimed at tackling global challenges. This rapidly expanding field, gaining recognition within the scientific community, leverages quantum mechanics principles to solve complex problems in optimization and machine learning. Quantum computers have enabled the development of quantum algorithms that, for certain problems, can deliver exponential speedups compared to classical methods. However, QC faces limitations due to its still-evolving technology. Combining traditional and quantum computing to create hybrid pattern recognition algorithms offers a practical solution for defect analysis and diagnosis. Besides significant performance improvements over classical computers, quantum computing presents innovative approaches to difficult problems. For instance, Grover's quantum search algorithm can find an item in a large database in the square root of the database size, and Shor's algorithm can factor numbers exponentially faster than classical methods. Quantum advantages are anticipated in fields such as quantum chemistry, machine learning, encryption, and optimization. Recent progress in quantum algorithms and hardware allows quantum computers to handle complex energy system optimization tasks, including process integration and superstructure optimization, which are crucial for designing sustainable energy solutions. These problems' high complexity usually requires traditional optimization solvers, often computationally expensive and without

guaranteed solutions. Large-scale renewable energy system optimization demands substantial computing resources. Developing hybrid QC-based deep learning architectures for effective defect detection (Ajagekar & You, 2019) involves several challenges: building defect diagnostic systems that combine decision and classification techniques with feature extraction, creating fast training methods using both QC and classical computers for better parameter estimation, addressing limited data diversity that affects fault diagnosis accuracy, and ensuring scalability to process large datasets without losing performance.

4. Basics of quantum computing

Quantum computing, defined as computing based on quantum mechanics principles, is poised to be the next major development in technology. Over the last fifty years, Moore's law has largely held, with computing power doubling roughly every two years as transistor sizes shrink on integrated circuits. Today's most advanced transistors are just a few atoms thick, yet quantum effects start to impact their behavior as dimensions decrease (Ajagekar & You, 2021). The key component of quantum computing is the qubit, similar to the classical bit—the basic unit of data. Unlike a classical bit, which is either 0 or 1, a qubit can exist in a superposition of states $|0\rangle$ and $|1\rangle$, called the computational basis states.

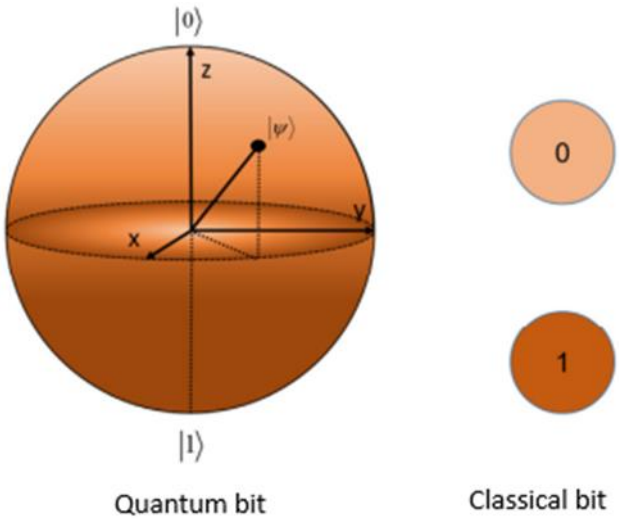

Figure 1: Fundamental units of computing

A key feature distinguishing qubits from classical bits is entanglement. This phenomenon enables correlations between two qubits' independently random behaviors. The properties of superposition and entanglement are exploited in quantum computers to achieve high computational power. Advances in technology have made certain quantum computing architectures feasible. Below is a brief overview of the functions and applications of various quantum computing technologies.

5. Current Applications and Outlooks

Numerous efforts are already underway to incorporate quantum computing into cryptocurrency security systems. For instance, the European bank Intesa Sanpaolo is exploring quantum machine learning techniques to improve its fraud detection methods, aiming for more accurate and faster identification of suspicious activity. Additionally, the AWS and Deloitte partnership: Using Amazon Bracket, Deloitte Italy and AWS have developed a fraud detection system based on quantum neural networks (SEC, 2025). This system demonstrates how quantum computing can be used to detect anomalies in digital payments, including cryptocurrency transactions (Marini et al., 2024).

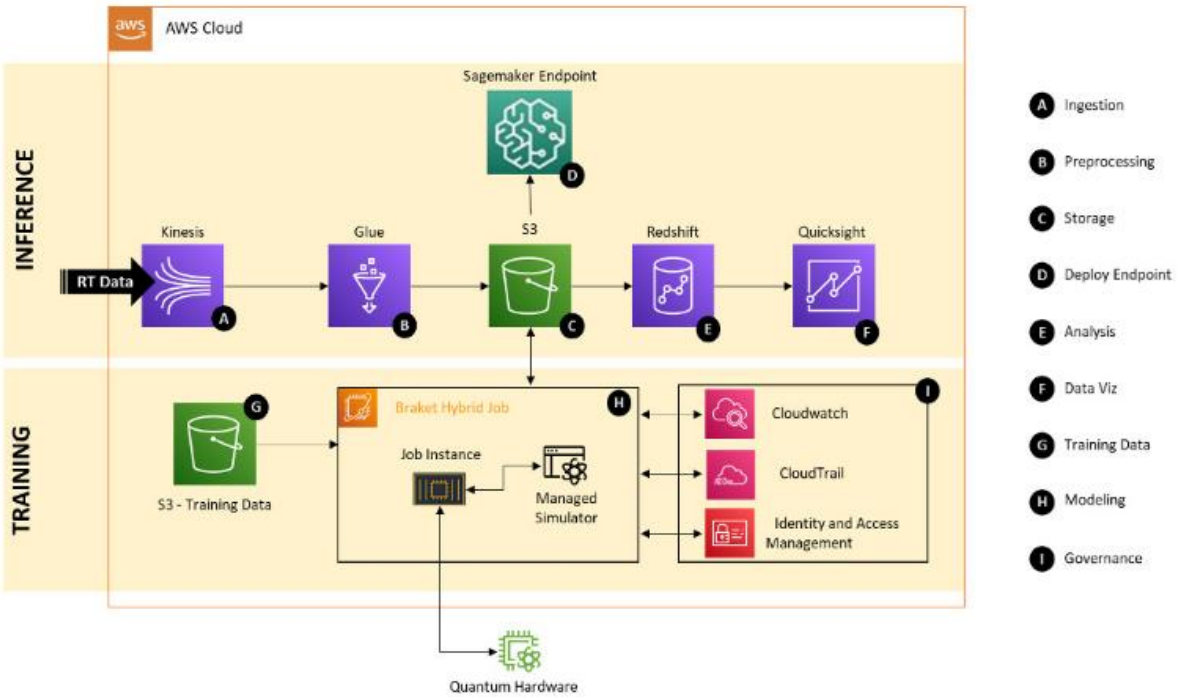

Figure 2: Marini et al, 2024 Architecture Solution of a Neural Network-Based Fraud Detection

The diagram below illustrates the solution architecture for deploying a neural network-based fraud detection system using AWS services. The approach employs a hybrid quantum neural network, built with the Keras library, while PennyLane handles the quantum component (Marini et al., 2024).

6. Predictions for each industry

Quantum computing, by simulating complex molecular interactions and structures, could revolutionize drug discovery in healthcare. Researchers are developing hybrid quantum systems to overcome challenges like calculating Gibbs free energy profiles for prodrug activation and modeling covalent bonds. As Li et al. (2024) mention, these innovations aim to accelerate new therapies and personalized medicine. Additionally, quantum computing promises to improve risk assessment and portfolio management in finance by processing complex models more efficiently than traditional methods, resulting in faster insights and better predictions. In logistics, hybrid approaches combining gate-based methods and quantum annealing address complex routing problems, such as drone navigation, by integrating clustering with real-world constraints (Osaba et al., 2025). The synergy of AI and quantum computing opens new horizons: quantum-enhanced AI can analyze large datasets faster, improving predictions. Researchers at IonQ show how quantum-enhanced generative adversarial networks (QGANs) can enhance material properties. For environmental data, quantum computing could significantly improve climate models, leading to more accurate forecasts and better climate change mitigation. When combined with AI, it further strengthens the analysis of complex environmental systems. Soller et al. (2025) predict the quantum industry might reach a valuation between $28 billion and $72 billion by 2035, transforming sectors like computing, communication, and sensing. This growth underscores the profound societal and industrial impact quantum technologies are expected to have, with anticipated integration into platforms like cryptocurrency systems by 2035.

Standardize quantum-resistant protocols to safeguard transactions across all platforms as post-quantum cryptography algorithms grow in popularity. Deploy advanced fraud detection systems enabled by quantum analytics for real-time prevention, reducing losses and enhancing user trust. Collaborate with governments and regulators to develop regulatory frameworks that establish standards and guidelines for quantum-safe cryptocurrencies, promoting a secure and compliant ecosystem. As quantum computers become commercially available soon, their applications will expand into logistics, healthcare, and finance. Integrating AI with quantum computing will accelerate machine learning, enabling more detailed data analysis and better decision-making.

Quantum computing also aims to support environmental initiatives by improving resource management and climate modeling. Additionally, the industry is expected to generate significant economic growth through innovation and job creation. Quantum-powered precision medicine will facilitate highly personalized treatments tailored to each patient's genetic profile. Advanced quantum models predicting disease progression and susceptibility will aid early detection, leading to more effective interventions. Quantum computing will enable real-time market analysis, rapid trading decisions, and transform financial markets. Quantum-based fraud detection algorithms will identify illegal activities across extensive financial networks. Autonomous logistics, such as self-driving delivery trucks, will become more feasible with quantum computing. Furthermore, quantum networks will improve global supply chain management by increasing responsiveness and resilience.

The development of Artificial General Intelligence (AGI) will heavily depend on quantum computing, which provides the vital computational power needed for advanced learning and reasoning. AI systems integrated with quantum technology will become more adaptable and capable of solving complex problems. Educational institutions will incorporate quantum computing topics into their curricula, nurturing a new generation of quantum technology experts. Moreover, immersive quantum simulations will enable students to better interact with and comprehend complex systems. Smart factories will leverage quantum computing to create self-optimizing manufacturing processes. Advanced robotics equipped with quantum technology will establish more flexible and efficient production lines. The emergence of innovative quantum materials aimed at enhancing energy storage—known as "Quantum-Enhanced Energy Storage"—is poised to revolutionize the energy sector. Additionally, quantum computing will support the development of global energy networks that efficiently manage supply and demand across regions. In agriculture, quantum computing will facilitate precision farming, increasing yields while conserving resources.

Advancements in quantum technologies will drive the development of climate-resilient crops that can withstand environmental changes. Autonomous vehicles, such as drones and self-driving cars, will gain improved capabilities through quantum tech. Quantum networks will enable seamless integration into transportation systems, increasing efficiency. The telecom industry will see the emergence of quantum internet, offering ultra-secure data transfer and global connectivity. Implementing quantum-resistant cryptography will strengthen digital security. Moreover, quantum computing will facilitate real-time detection and response to cyber threats. In entertainment, it will boost immersive experiences by supporting more engaging virtual and augmented reality environments. Generating dynamic, user-interactive content will become easier with quantum models. Retailers will introduce adaptive stores that instantly respond to customer needs, and quantum-enabled tracking will enhance supply chain transparency, improving both efficiency and trust. In construction, quantum tech will support 自动化 building processes and eco-friendly design. Aerospace will benefit from quantum navigation systems for precise spatial positioning and better analysis of large datasets for space exploration.

7. Conclusion

Quantum computing encounters challenges such as qubit coherence, high error rates, and the necessity for cryogenic temperatures. As the field progresses, ethical concerns like data security, privacy, and automation of jobs also come to the forefront. Despite these hurdles, quantum computing is moving from theoretical research to practical use, revolutionizing various industries. Ideas once considered science fiction are now becoming reality, especially with the integration of quantum technology with AI and other innovations. Although the technology presents specific difficulties for cryptocurrencies, it also opens up opportunities to enhance security and combat fraud. By implementing quantum-resistant solutions and leveraging advanced quantum analytics, the crypto industry can safeguard its future and create a trustworthy, resilient environment for users.

Author Contributions: All authors contributed to this research.

Funding: Not applicable.

Conflict of Interest: The authors declare no conflict of interest.

Informed Consent Statement/Ethics Approval: Not applicable.

Declaration of Generative AI and AI-assisted Technologies: This study has not used any generative AI tools or technologies in the preparation of this manuscript.

References

Ajagekar, A., & You, F. (2019). Quantum computing for energy systems optimization: Challenges and opportunities. *Energy*, 76-89.

Ajagekar, A., & You, F. (2021). Quantum computing based hybrid deep learning for fault diagnosis in electrical power systems. *Applied Energy*, 117628.

Gill, S. S., Kumar, A., Singh, H., Singh, M., Kaur, K., Usman, M., & Buyya, R. (2022). Quantum computing: A taxonomy, systematic review and future directions. *Software; Practice and Experience*, 66 - 114.

Gill, S. S., Wu, H., Patros, P., Ottaviani, C., Arora, P., Pujol, V. C., . . . Qadir, J. e. (2024). Modern computing: Vision and challenges. *Telematic and Informatic Reports*, 100-116.

Hammood, W. A., Asmara, S. M., Rosli, M. M., Ghdhban, I. I., & Osiobe, E. U. (2025). Sensitivity Analysis of Electromechanical Impedance Signals for Early Detection of Debonding in Sandwich Face Layers: A Case Study Using SHM Data. *Mesopotamian Journal of Civil Engineering* , 1-19.

Kearney, J. J., & Perez-Delgado, C. A. (2021). Vulnerability of blockchain technologies to quantum attacks. *Array, 10*, 1-10.

Kennedy, A. (2024, 12 30). *Bank Policy Institute*. Retrieved from Quantum Computing: The Urgent Need to Transition to Quantum-Resistant Cryptography: https://bpi.com/quantum-computing-the-urgent-need-to-transition-to-quantum-resistant-cryptography/?utm_source=chatgpt.com

Li, W., Yin, Z., Li, X., Ma, D., Yi, S., Zhang, Z., . . . Zhang, S. (2024). A Hybrid Quantum Computing Pipeline for Real World Drug Discovery.

Marini, F., Capozi, M., Muthu, K., & Singh, K. (2024, 7 17). *How Deloitte Italy built a digital payments fraud detection solution using quantum machine learning and Amazon Braket*. Retrieved from Amazon Web Services (AWS)-Artificial Intelligence: https://aws.amazon.com/blogs/machine-learning/how-deloitte-italy-built-a-digital-payments-fraud-detection-solution-using-quantum-machine-learning-and-amazon-braket/?utm_source=chatgpt.com

Osaba, E., Miranda-Rodrigue, P., Oikonomakis, A., Petric, M., Ruiz, A., Bock, S., & Kourtis, M.-A. (2025). Solving Drone Routing Problems with Quantum Computing: A Hybrid Approach Combining Quantum Annealing and Gate-Based Paradigms.

Osiobe, E. U. (2025). *An Economic Overview of the Nigerian Economy.*

Osiobe, E. U. (2025). *Educating Our Girls.*

Osiobe, E. U., Hammood, W. A., Malallah, S., Osiobe, N. E., Hammood, O. A., & Asmara, S. M. (2025). Quantum Computing: An Overview of its Potential to Revolutionize Civilization. *Missouri Iowa Nebraska Kansas Women in Computing.* Lenexa: MINK-WIC.

Osiobe, E. U., Malallah, S., & Osiobe, N. E. (2024). Enhancing Data Visualization Accessibility: A Case for Equity and Inclusion. *Engineering and Technology Quarterly Reviews*, 24-32.

Paloalto Networks. (2025). *What Is Quantum Computing's Threat to Cybersecurity?* Retrieved 6 19, 2025, from https://www.paloaltonetworks.com/cyberpedia/what-is-quantum-computings-threat-to-cybersecurity?utm_source=chatgpt.com

Soller, H., Gschwendtner, M., Shabani, S., & Svejstrup, W. (2025, 9 15). *The Year of Quantum: From concept to reality in 2025*. Retrieved from McKinsey & Company: https://www.mckinsey.com/capabilities/mckinsey-digital/our-insights/the-year-of-quantum-from-concept-to-reality-in-2025?utm_source=chatgpt.com

U.S. Securities and Exchange Commission (SEC). (2025, 8 13). *The SEC Launches "Project Crypto"*. Retrieved from https://www.sec.gov/about/sec-launches-project-crypto and https://www.sec.gov/files/cft-written-input-daniel-bruno-corvelo-costa-090325.pdf?utm_source=chatgpt.com

Weinberg, A. I., & Faccia, A. (2024). Quantum Algorithms: A New Frontier in Financial Crime Prevention.

ASIAN INSTITUTE OF RESEARCH
Connecting Scholars Worldwide

The Asian Institute of Research
Engineering and Technology Quarterly Reviews
Vol.8, No.2, 2025: 35-45
ISSN 2622-9374

Structural Health Monitoring of Buildings Using Computer Vision: A State-of-the-Art Review

Horatiu-Alin Mociran[1], Adina-Victorița Lăpuște[2]

[1,2] Faculty of Civil Engineering, Technical University of Cluj-Napoca, Cluj-Napoca, Romania

Correspondence: Horatiu-Alin Mociran, Faculty of Civil Engineering, Technical University of Cluj-Napoca, Cluj-Napoca, St. Memorandumului 28, Romania. E-mail: horatiu.mociran@mecon.utcluj.ro

Abstract
Structural Health Monitoring (SHM) is essential for building safety, durability, and functionality. Buildings, as key components of the built environment, suffer from cracking, spalling, corrosion, and moisture damage. Traditional SHM approaches like vibration-based measurements, non-destructive testing (NDT), and manual inspections are reliable. However, they are expensive, slow, and difficult to use at scale. Recent developments in computer vision (CV), powered by advances in machine learning (ML) and deep learning (DL), have enabled modern, automated, and contactless inspection systems capable of detecting structural defects with high precision. This paper reviews the state of the art in computer vision applications for SHM of buildings. It focuses on the evolution of image processing, ML and DL architectures, and new 3D and multimodal systems. The paper categorizes common building defects, lists datasets for algorithm training and validation, and gives examples from recent studies. Finally, the review identifies current obstacles and suggests future research directions. It focuses on integration with drones, Building Information Modelling (BIM), the Internet of Things (IoT), and Digital Twin technologies.

Keywords: Structural Health Monitoring, Computer Vision, Deep Learning, Defect Detection, Buildings, Civil Engineering

1. Introduction

Ensuring the safety and long-term performance of civil engineering structures is one of the fundamental goals of structural engineering practice. Among these structures, buildings represent the backbone of the built environment, accommodating residential, commercial, educational, and industrial activities. Preserving their integrity and reliability throughout their service life is therefore a matter of public safety, economic value, and social well-being.

Structural Health Monitoring (SHM) has become a multidisciplinary approach dedicated to assessing the condition of structures, identifying early signs of deterioration, and supporting decisions regarding maintenance and rehabilitation. Its ultimate objective is to extend the service life of structures, reduce life-cycle costs, and improve their resilience against natural or anthropogenic hazards (Farrar & Worden, 2012).

Conventional SHM practices rely heavily on non-destructive testing (NDT) techniques such as ultrasonic pulse velocity, infrared thermography, rebound hammer testing, and strain gauge measurements, often complemented by manual visual inspections. While these methods are well established, they also face inherent limitations: manual inspections are time-consuming and subjective, whereas sensor-based systems require extensive setup, calibration, and maintenance, which increase operational costs.

In recent years, the convergence of computer vision (CV), machine learning (ML), and deep learning (DL) has triggered a paradigm shift in how structural health can be monitored. With the availability of high-resolution cameras, affordable unmanned aerial vehicles (UAVs), and increasingly powerful computational tools, vision-based systems have made it possible to perform scalable, automated, and non-contact inspections. These systems are particularly suitable for buildings, where most degradation processes—such as cracks or spalling—are visually perceptible and can be effectively analysed using digital imagery (Spencer et al., 2025; Zhuang et al., 2025).

The present paper aims to provide a comprehensive synthesis of computer vision applications in building SHM. The main contributions are as follows:

- Methodological overview: A detailed summary of computer vision approaches ranging from traditional image processing to deep learning and multimodal frameworks used for defect detection.
- Application-oriented review: An examination of practical case studies focusing on typical building defects such as cracks, spalling, corrosion, and moisture damage.
- Research perspectives: A discussion of current challenges and future directions, including integration with BIM, IoT, and Digital Twin environments.

2. Fundamentals of Structural Health Monitoring

2.1 Definition and Objectives

It is both conventional and expedient to divide the Method section into labeled subsections. These usually include a section with descriptions of the participants or subjects and a section describing the procedures used in the study. The latter section often includes description of (a) any experimental manipulations or interventions used and how they were delivered-for example, any mechanical apparatus used to deliver them; (b) sampling procedures and sample size and precision; (c) measurement approaches (including the psychometric properties of the instruments used); and (d) the research design. If the design of the study is complex or the stimuli require detailed description, additional subsections or subheadings to divide the subsections may be warranted to help readers find specific information.

Include in these subsections the information essential to comprehend and replicate the study. Insufficient detail leaves the reader with questions; too much detail burdens the reader with irrelevant information. Consider using appendices and/or a supplemental website for more detailed information.

Structural Health Monitoring (SHM) refers to the continuous or periodic observation of a structure through the acquisition and interpretation of data obtained from sensors, measurements, or visual inputs. Its purpose is to assess the current condition of a structure, detect potential damage, and predict its future performance. The concept of SHM emerged in the late 20th century as an evolution of traditional Non-Destructive Evaluation (NDE), shifting the focus from localized inspections toward global and continuous assessments (Sohn et al., 2001; Farrar & Worden, 2007).

In the case of buildings, SHM serves several essential objectives:

- Safety: Detecting early signs of damage before structural integrity is compromised.
- Serviceability: Ensuring that the building continues to perform its intended function effectively.
- Lifecycle management: Supporting preventive maintenance and timely repairs to extend service life.
- Post-event assessment: Providing rapid evaluations following earthquakes, fires, or extreme weather

conditions.

An effective SHM system thus provides engineers and facility managers with actionable information that enables data-driven decision-making and enhances the reliability of the built environment throughout its life cycle.

2.2 Traditional SHM Methods

Before the emergence of vision-based approaches, SHM systems relied primarily on three categories of methods: vibration-based measurements, non-destructive testing (NDT), and manual inspections.

Vibration-Based Methods - These techniques are founded on the principle that structural damage modifies the dynamic properties of a system—such as its natural frequencies, damping ratios, or mode shapes (Doebling et al., 1996). Accelerometers and strain gauges are typically employed to record such variations, especially in tall buildings or after seismic events. Advantages: sensitive to global damage and useful for dynamic behaviour assessment. Limitations: require dense sensor networks, complex modal analysis, and are less effective for localized surface-level defects.

Non-Destructive Testing (NDT) - Techniques including ultrasonic pulse velocity, infrared thermography, and rebound hammer testing are widely applied for localized inspections and subsurface assessment. Advantages: high precision in identifying internal or material-level damage. Limitations: labour-intensive, dependent on specialized equipment, and difficult to scale for large areas.

Manual Visual Inspection - Still the most common method in practice, manual inspection relies on the experience of engineers or inspectors who visually examine accessible parts of the structure. Advantages: straightforward, inexpensive, and does not require complex instrumentation. Limitations: subjective, time-consuming, and limited by accessibility and safety conditions.

While these traditional techniques remain valuable, their use on a large scale is constrained by high operational costs, potential human bias, and limited scalability (Balageas et al., 2006). The increasing complexity and ageing of urban infrastructure have made the need for more automated and efficient monitoring approaches evident.

2.3 Computer Vision vs. Conventional Methods

Over the last decade, computer vision (CV) has emerged as a promising alternative and complement to traditional SHM methods. Unlike sensor-based systems that depend on physical contact, CV relies on visual data—images or videos—acquired using cameras placed on tripods, handheld devices, or unmanned aerial vehicles (UAVs).

Main advantages of CV-based SHM include: non-contact monitoring; cost efficiency as cameras and UAVs become affordable; scalability for inspecting large façades or multiple structures; automation through ML/DL algorithms; and integration potential with BIM and Digital Twin platforms. Limitations include sensitivity to lighting and environmental factors, dependence on image quality, the need for large annotated datasets, and the difficulty of detecting subsurface defects without complementary NDT methods.

Despite these drawbacks, numerous studies indicate that CV-based techniques are maturing rapidly. In many cases, they now outperform conventional methods in terms of efficiency, automation, and scalability (Hoskere et al., 2018; Dong & Catbas, 2018). Hybrid frameworks that combine sensor data and vision analytics are also emerging as a balanced approach for comprehensive SHM (Mardanshahi et al., 2025).

2.4 Summary

The evolution of SHM represents a shift from localized, sensor-dependent evaluations toward image-based and data-driven methodologies. Traditional methods continue to play an important role, especially for subsurface defect analysis. However, computer vision provides major advantages in scalability, automation, and cost

reduction. Given that most building defects—such as cracks, corrosion, or spalling—manifest on visible surfaces, vision-based systems are naturally suited to this domain.

3. Computer Vision Techniques for SHM

Computer Vision (CV) has become an increasingly important tool in Structural Health Monitoring (SHM) because it can extract relevant information from visual data and automate structural defects identification. Over the past two decades, CV techniques have evolved from classical image processing to advanced machine learning (ML) and deep learning (DL) methods, bringing substantial improvements in accuracy, robustness, and scalability.

3.1 Image Processing Techniques

Early vision-based SHM systems relied mainly on traditional image processing algorithms designed to enhance visible defects—such as cracks, spalling, or discoloration—by analysing variations in pixel intensity and texture. Common approaches include edge detection (e.g., Canny, Sobel), thresholding (e.g., Otsu), morphological operations (erosion, dilation, skeletonization), and texture analysis (GLCM). These methods are efficient and easy to implement, but are sensitive to lighting variations, surface textures, and noise. For instance, stains or paint patterns may be misclassified as cracks. Parrany et al. (2022) showed that with careful tuning, classical methods can still perform well under variable lighting. Today, image processing is often used as a preprocessing stage rather than a standalone detector.

3.2 Machine Learning Approaches

As labelled datasets became more available, machine learning (ML) methods emerged as a data-driven alternative to handcrafted rules. Algorithms such as Support Vector Machines (SVM), k-Nearest Neighbours (k-NN), and ensemble methods like Decision Trees and Random Forests classify patterns associated with defects using engineered features (e.g., HOG, LBP, wavelets). ML models are more flexible than classical image processing but depend strongly on feature quality and data diversity. Jahanshahi & Masri (2012) demonstrated an SVM-based system for crack detection in reinforced concrete with robust results in practical settings.

3.3 Deep Learning Approaches

Deep Learning (DL) has transformed CV applications in SHM by learning hierarchical features directly from raw images. Major architectures include classification networks (AlexNet, VGG, ResNet), object detection frameworks (Faster R-CNN, YOLO, SSD), segmentation models (U-Net, SegNet, Mask R-CNN), and transformer-based models (Vision Transformers and hybrid CNN–Transformer designs). DL offers high accuracy and robustness but requires large annotated datasets and considerable computation, and may struggle to generalize to unseen conditions (Zhang et al., 2018). Cha et al. (2017) achieved >98% crack detection accuracy using CNNs; Yasmin et al. (2023) demonstrated effective spalling detection via deep segmentation. Reviews by Cha et al. (2024) and Gao et al. (2023) underline DL's dominant role in current SHM research.

3.4 3D Vision and Multi-Modal Approaches

Beyond 2D imagery, 3D vision and multimodal systems combine visual, geometric, and thermal information for richer assessment. Photogrammetry and Structure-from-Motion reconstruct 3D façade models onto which defects can be mapped. LiDAR–CV integration enables accurate geometry and spatial localization (Tang et al., 2010; Olsen et al., 2010). Depth sensors (e.g., RGB-D) assist in detecting spalling and surface deformation, while RGB–thermal fusion supports moisture and subsurface defect identification. These benefits come with higher equipment costs and more complex data processing pipelines.

3.5 Summary

Computer vision for SHM has progressed from pixel-based processing to deep learning and multimodal 3D frameworks. While classical processing remains valuable for enhancement and preprocessing, DL currently leads

in automation and precision. Integrating LiDAR, 3D reconstruction, and thermal imaging paves the way for hybrid monitoring systems that merge visual, geometric, and physical data.

4. Applications in Buildings

The adoption of CV for SHM in buildings has accelerated due to the prevalence of surface-visible defects and the practicality of image-based methods. Yet, challenges such as variable textures, illumination, and limited access—particularly for high-rise façades—persist. This section reviews typical building defects and representative case studies.

4.1 Typical Defects in Buildings

4.1.1 Cracks in Concrete and Masonry

Cracks arise from shrinkage, thermal effects, settlement, overloading, or seismic actions. Although fine cracks may be superficial, their propagation can affect serviceability and safety. Detection approaches include classical edge-based and thresholding methods (Yamaguchi & Hashimoto, 2010), DL models (e.g., CNNs) with accuracies above 95% (Cha et al., 2017), and emerging Vision Transformers that improve robustness to lighting and noise.

4.1.2 Spalling of Concrete

Spalling involves the flaking or detachment of concrete cover, often exposing reinforcement and accelerating corrosion. DL-based segmentation (U-Net, Mask R-CNN) on RGB images is widely used (Yasmin et al., 2019). Combining RGB with depth or 3D photogrammetry improves quantification of depth and extent. UAV imaging is practical for upper façades and difficult-to-reach areas.

4.1.3 Corrosion of Reinforcement and Metallic Components

Corrosion reduces the cross-sectional area of steel elements, leading to capacity loss. Colour-based segmentation using hue/saturation and DL models trained on corrosion datasets have shown strong performance (Gao & Mosalam, 2018). Infrared–RGB fusion can reveal corrosion beneath coatings in some scenarios.

4.1.4 Moisture and Water-Induced Damage

Moisture ingress leads to staining, efflorescence, biological growth, and coating delamination. Thermal infrared combined with CV detects temperature anomalies linked to moisture; RGB methods capture discoloration, and CNNs improve robustness. Linking moisture maps with BIM facilitates preventive maintenance planning.

4.2 Case Studies from Literature

4.2.1 UAV-Based High-Rise Façade Inspection

Dorafshan et al. (2018) compared edge-based crack detection with CNNs on UAV imagery, finding higher accuracy and faster inspection using deep learning—improving safety and efficiency in façade assessments.

4.2.2 Deep Learning for Crack Detection in Walls

Cha et al. (2017) developed a CNN-based framework for detecting cracks on concrete surfaces, achieving accuracy above 98% and demonstrating feasibility for real inspections.

4.2.3 UAV Inspection with Infrared and Visual Imaging

UAVs equipped with RGB and infrared cameras effectively assess building envelopes. Thermal imagery identifies insulation defects and moisture ingress, while RGB supports detailed crack analysis (Fox et al., 2016; Hoskere et al., 2018).

4.2.4 Crack Mapping Using Fully Convolutional Networks (FCNs)

Dung & Anh (2019) proposed an FCN for pixel-level crack segmentation, enabling quantitative evaluation and monitoring of crack evolution.

4.2.5 Spalling Detection in Reinforced Concrete Buildings

Yasmin et al. (2023) applied deep segmentation for spalling detection and, by incorporating depth information, estimated severity as well as extent.

4.2.6 Transfer Learning for Corrosion Recognition

Gao & Mosalam (2018) used deep transfer learning to recognize corrosion in reinforced concrete, showing that pre-trained CNNs can perform well even with limited training data.

4.2.7 BIM-Integrated Computer Vision for Maintenance

Brilakis et al. (2010) integrated CV-based defect detection with BIM, mapping defects onto 3D models to support predictive maintenance. Recent work extends this toward Digital Twin frameworks (Xu et al., 2023).

4.2.8 Hybrid Thermal and RGB Imaging for Moisture Detection

Fox et al. (2016) combined thermal and RGB imaging to detect moisture-induced deterioration, providing early warning of insulation failures and potential mould growth.

4.2.9 Post-Earthquake Building Assessment

Zhuang et al. (2025) developed a deep learning framework for post-earthquake damage classification with 96.1% accuracy, using Grad-CAM for interpretability and prioritization in emergency response.

4.3 Summary

CV applications in building SHM span cracks, spalling, corrosion, and moisture-related defects. Field studies, including UAV-based inspections, confirm gains in efficiency and safety. Persistent challenges include environmental variability, dataset standardization, and multimodal integration. Addressing these is key to robust, scalable, automated monitoring.

5. Datasets and Benchmarks

The performance and reliability of CV techniques for SHM depend on dataset quality and diversity. Large, well-annotated datasets are essential for robust ML/DL models capable of handling varied materials, defect types, and conditions.

5.1 Importance of Datasets in CV – based SHM

DL algorithms rely on large labelled datasets to achieve generalizable performance. Ideal SHM datasets include multiple defect categories (cracks, spalling, corrosion, moisture), various materials (concrete, masonry, steel), and diverse environmental conditions. Without such diversity, models overfit and fail in new scenarios (Zhang et al., 2018; Özgenel, 2018). Dataset creation is hindered by manual annotation effort, class imbalance, and limited diversity.

5.2 Publicly Available Datasets

5.2.1 CrackForest Dataset (CFD)

Originally for road surfaces, CrackForest (Shi et al., 2016) includes 118 annotated concrete images with pixel-level crack labels and is widely reused for building studies.

5.2.2 SDNET2018

SDNET2018 (Dorafshan et al., 2018) provides over 56,000 images of decks, walls, and pavements under diverse conditions. Though bridge-oriented, its vertical imagery suits façade inspection.

5.2.3 Concrete Crack Dataset (Özgenel, 2018)

Comprising 40,000 cropped patches labelled as crack/non-crack, this dataset is common for binary CNN training, though it lacks pixel-level annotations for segmentation.

5.2.4 Masonry Crack Dataset (MCD)

MCD (Dung & Anh, 2019) targets masonry walls and heritage buildings with labelled cracked and intact regions—useful beyond concrete, albeit smaller in scale.

5.2.5 Additional Specialized Datasets

Thermal datasets (moisture, subsurface defects) are often proprietary. Small corrosion datasets (e.g., Gao & Mosalam, 2018) support transfer learning. Spalling datasets exist but lack a standard public benchmark.

5.3 Benchmarking Practices

Common metrics: Accuracy and F1-score (classification), IoU (segmentation/localization), Precision–Recall (class imbalance), and FPS (real-time/UAV contexts). Comparisons across studies are difficult due to differing datasets, preprocessing, and protocols; the field lacks ImageNet-like standardized benchmarks (Hoskere et al., 2018).

5.4 Limitations of Current Datasets

Key limitations: small scale and narrow scope (focus on cracks), limited diversity (materials, lighting, weather), inconsistent annotation formats, and restricted access to industry data. These hinder generalization and slow progress toward deployable SHM systems.

5.5 Summary

Public datasets such as CrackForest, SDNET2018, and Özgenel's collection have shaped SHM research, but broader, multi-defect, multimodal datasets are needed. Standardized benchmarks and open challenges would accelerate progress and improve reproducibility.

6. Challenges and Future Directions

CV enables efficient, automated, non-contact SHM for buildings, yet adoption in practice is limited by environmental sensitivity, data scarcity, generalization issues, and computational demands. Concurrently, advances in AI, sensing, and digital construction create new opportunities.

6.1 Current Challenges

6.1.1 Environmental Sensitivity

Algorithms are sensitive to lighting, shadows, textures, and weather. Crack detection suffers under uneven illumination or stain-like backgrounds, limiting robustness (Chen et al., 2017).

6.1.2 Data Limitations

Large, diverse labelled data are scarce for buildings; popular datasets emphasize cracks. Models trained on one dataset often generalize poorly due to bias (Dong & Catbas, 2018).

6.1.3 Generalization and Transferability

Performance drops when moving from lab to field because of changing textures and lighting. Transfer learning and domain adaptation help but remain underexplored in SHM (Gao & Mosalam, 2018).

6.1.4 Integration with Structural Engineering Knowledge

Many CV systems lack explicit links between visual detections and structural significance (e.g., load paths, safety margins). Tighter coupling with mechanics would improve interpretability and usefulness (Hoskere et al., 2018).

6.1.5 Computational Demands and Real-Time Operation

Training and inference are resource-intensive, challenging real-time UAV deployments. Lightweight, energy-efficient models for edge devices are an active research area.

6.2 Integration with Emerging Technologies

6.2.1 Unmanned Aerial Vehicles (UAVs)

UAVs provide rapid, safe access to façades, roofs, and hard-to-reach zones. With RGB/IR/depth sensors, they capture high-resolution data at scale; paired with CV, they enable automated, repeatable monitoring (Dorafshan et al., 2018).

6.2.2 Internet of Things (IoT) and Wireless Sensor Networks

Hybrid SHM merges visual data with strain, vibration, and humidity sensing via IoT platforms, enabling richer diagnostics and multi-sensor fusion (Seo et al., 2015).

6.2.3 Building Information Modeling (BIM) and Digital Twins

CV detections can be mapped onto BIM for spatial records and maintenance planning. Digital Twins link physical assets to virtual models for real-time visualization, simulation, and prediction (Brilakis et al., 2010; Torzoni et al., 2024; Sun et al., 2025).

6.2.4 Augmented and Virtual Reality (AR/VR)

AR/VR enhances on-site decision-making by overlaying defect information on real scenes, enabling access to historical records and facilitating repair simulations.

6.3 Research Gaps and Future Trends

Promising directions include: large, multi-defect open datasets; compact models for edge/UAV deployment; self-supervised and semi-supervised learning to reduce labelling needs; explainable AI to link visual cues with

structural behaviour; integration with lifecycle asset management; and advanced transformer-based architectures (Hu et al., 2025) for context-aware analysis.

6.4 Summary

Despite clear benefits, CV-based SHM faces barriers related to data, environment, and computation. Progress will rely on tighter integration with UAVs, IoT, BIM, and Digital Twins, along with explainable, lightweight AI models. These advances will shift practice from reactive inspection to proactive, predictive maintenance.

7. Conclusions

Structural Health Monitoring (SHM) plays a vital role in ensuring the safety, functionality, and durability of buildings throughout their service life. Traditional inspection methods—such as manual surveys, non-destructive testing (NDT), and sensor-based systems—have served the profession effectively for decades, yet their limitations in cost, scalability, and subjectivity motivate more automated solutions. Computer vision (CV) enables non-contact, efficient, and scalable monitoring.

This review summarized computer vision–based SHM approaches for buildings, covering foundational concepts, methods from classical image processing to deep learning and multimodal 3D systems, applications to typical defects, datasets and benchmarking practices, and key challenges with future directions. DL models—especially CNNs and segmentation networks—currently offer the most accurate detection and quantification of surface defects. Field studies confirm the maturity and feasibility of CV-based inspections.

While public datasets such as CrackForest, SDNET2018, and Özgenel's collection have accelerated progress, broader, standardized multi-defect datasets are needed for fair comparison and reproducibility. Future development will likely be shaped by integration with UAVs, IoT, BIM, and Digital Twins, together with advances in explainable, lightweight AI.

By leveraging modern AI, multimodal sensing, and digital construction workflows, CV-based SHM can deliver accurate, real-time, and cost-efficient assessments—supporting a shift from reactive inspection to proactive, predictive maintenance. This review aims to serve researchers and practitioners as a concise reference and to encourage scalable frameworks for smart, resilient, and sustainable cities.

Author Contributions: All authors contributed to this research.

Funding: Not applicable.

Conflicts of Interest: The authors declare no conflict of interest.

Informed Consent Statement/Ethics approval: Not applicable.

Declaration of Generative AI and AI-assisted Technologies: The authors declare that ChatGPT (OpenAI, GPT-5 model) was used to assist in language refinement and editing of the manuscript. The use of this tool was limited to improving clarity, coherence, and consistency of expression. The authors reviewed and approved all content prior to submission and take full responsibility for the scientific integrity and accuracy of the manuscript.

References

Balageas, D., Fritzen, C. P., & Güemes, A. (2006). *Structural health monitoring*. John Wiley & Sons.

Brilakis, I., Lourakis, M., Sacks, R., Savarese, S., Christodoulou, S., Teizer, J., & Makhmalbaf, A. (2010). Toward automated generation of parametric BIMs based on hybrid video and laser scanning data. Advanced Engineering Informatics, 24(4), 456–465. https://doi.org/10.1016/j.aei.2010.06.006.

Cha, Y. J., Ali, R., Lewis, J., Büyüköztürk, O. (2024). Deep learning-based structural health monitoring. Automation in Construction, 161, 105328. https://doi.org/10.1016/j.autcon.2024.105328.

Cha, Y. J., Choi, W., & Büyüköztürk, O. (2017). Deep learning-based crack detection using convolutional neural networks. Computer-Aided Civil and Infrastructure Engineering, 32(5), 361–378. https://doi.org/10.1111/mice.12263.

Chen, F. C., Jahanshahi, M. R., Wu, R. T., & Joffre, C. (2017). A texture-based video processing methodology using Bayesian data fusion for autonomous crack detection on metallic surfaces. Computer-Aided Civil and Infrastructure Engineering, 32(4), 271–287. https://doi.org/10.1111/mice.12256.

Doebling, S. W., Farrar, C. R., Prime, M. B., & Shevitz, D. W. (1996). *Damage identification and health monitoring of structural and mechanical systems from changes in their vibration characteristics: A literature review*. Los Alamos National Laboratory Report LA-13070-MS. https://doi.org/10.2172/249299.

Dong, C. Z., & Catbas, F. N. (2020). A review of computer vision–based structural health monitoring at local and global levels. Structural Health Monitoring, 20(2). https://doi.org/10.1177/1475921720935585.

Dorafshan, S., Thomas, R. J., & Maguire, M. (2018). SDNET2018: An annotated image dataset for non-contact concrete crack detection using deep convolutional neural networks. Data in Brief, 21, 1664–1668. https://doi.org/10.1016/j.dib.2018.11.015.

Dorafshan, S., Thomas, R. J., & Maguire, M. (2018). Comparison of deep convolutional neural networks and edge detectors for image-based crack detection in concrete. Construction and Building Materials, 186, 1031–1045. https://doi.org/10.1016/j.conbuildmat.2018.08.011.

Dung, C. V., & Anh, L. D. (2019). Autonomous concrete crack detection using deep fully convolutional neural networks. Automation in Construction, 99, 52–58. https://doi.org/10.1016/j.autcon.2018.11.028.

Farrar, C. R., & Worden, K. (2007). An introduction to structural health monitoring. Philosophical Transactions of the Royal Society A, 365(1851), 303–315. https://doi.org/10.1098/rsta.2006.1928.

Farrar, C. R., & Worden, K. (2012). *Structural health monitoring: A machine learning perspective*. John Wiley & Sons.

Fox, M., Goodhew, S., & De Wilde, P. (2016). Building defect detection: External versus internal thermography. Building and Environment, 105, 317–331. https://doi.org/10.1016/j.buildenv.2016.06.011.

Gao, Y., & Mosalam, K. M. (2018). Deep transfer learning for image-based structural damage recognition. Computer-Aided Civil and Infrastructure Engineering, 33(9), 748–768. https://doi.org/10.1111/mice.12363.

Gao, Y., Xu, W., Yang, J., Qian, H., Mosalam, K. M. (2023). Multiattribute multitask transformer framework for vision-based structural health monitoring. Computer-Aided Civil and Infrastructure Engineering, 38(12), 1578–1596. https://doi.org/10.1111/mice.13067.

Hoskere, V., Narazaki, Y., Hoang, T. A., & Spencer, B. F. (2018). *Vision-based structural inspection using Multiscale Deep Convolutional Neural Networks*. 3rd Huixian International Forum on Earthquake Engineering for Young Researchers, University of Illinois, Urbana-Champaign. https://doi.org/10.48550/arXiv.1805.01055.

Hu, D., Lin, Y., Li, S., Wu, J., & Ma, H. (2025). Hierarchical attention transformer-based sensor anomaly detection in structural health monitoring. Sensors, 25(16), 4959. https://doi.org/10.3390/s25164959.

Jahanshahi, M. R., & Masri, S. F. (2012). Adaptive vision-based crack detection using 3D scene reconstruction for condition assessment of structures. Automation in Construction, 22, 567–576. https://doi.org/10.1016/j.autcon.2011.11.018.

Mardanshahi, A., Sreekumar, A., Yang, X., Barman, S. K., & Chronopoulos, D. (2025). Sensing Techniques for Structural Health Monitoring: A State-of-the-Art Review on Performance Criteria and New-Generation Technologies. Sensors, 25(5), 1424. https://doi.org/10.3390/s25051424.

Olsen, M. J., Kuester, F., Chang, B. J., & Hutchinson, T. C. (2010). Terrestrial laser scanning-based structural damage assessment. Journal of Computing in Civil Engineering, 24(3), 264–272. https://doi.org/10.1061/(ASCE)CP.1943-5487.0000028.

Özgenel, Ç. F. (2018). *Concrete crack images for classification. Mendeley Data*, V1. https://doi.org/10.17632/5y9wdsg2zt.1.

Park, J. S., Joohyun, A., & Park, H. S. (2023). Computer Vision-based Structural Health Monitoring: A Review. International Journal of High-Rise Buildings, 12(4), 321–333. https://doi.org/10.21022/IJHRB.2023.12.4.321.

Parrany, R., Yazdani, N., & Dey, S. (2022). A new image processing strategy for surface crack identification in building structures under non-uniform illumination. IET Image Processing, 16(2), 407–415. https://doi.org/10.1049/ipr2.12357.

Pan, X., Yang, T. T. Y., Li, J., Ventura, C., Málaga-Chuquitaype, C., Li, C., Su, R. K. L., & Brzev, S. (2025). A review of recent advances in data-driven computer vision methods for structural damage evaluation: algorithms, applications, challenges, and future opportunities. Archives of Computational Methods in Engineering. https://doi.org/10.1007/s11831-025-10279-8.

Seo, J., Han, S., Lee, S., & Kim, H. (2015). Computer vision techniques for construction safety and health monitoring. Advanced Engineering Informatics, 29(2), 239–251. https://doi.org/10.1016/j.aei.2015.02.001.

Shi, Y., Cui, L., Qi, Z., Meng, F., & Chen, Z. (2016). Automatic road crack detection using random structured forests. IEEE Transactions on Intelligent Transportation Systems, 17(12), 3434–3445. https://doi.org/10.1109/TITS.2016.2552248.

Sohn, H., Farrar, C. R., Hemez, F. M., & Czarnecki, J. J. (2001). *A review of structural health monitoring literature: 1996–2001*. Los Alamos National Laboratory Report LA-UR-02-2095.

Spencer Jr., B. F., Sim, S. H., Kim, R. E., & Yoon, H. (2025). Advances in artificial intelligence for structural health monitoring: A comprehensive review. KSCE Journal of Civil Engineering, 29(3), 100203. https://doi.org/10.1016/j.kscej.2025.100203.

Sun, Z., Jayasinghe, S., Sidiq, A., Shahrivar, F., Mahmoodian, M., & Setunge, S. (2025). Approach towards the development of digital twin for structural health monitoring of civil infrastructure: A comprehensive review. Sensors, 25(1), 59. https://doi.org/10.3390/s25010059.

Tang, P., Huber, D., Akinci, B., Lipman, R., & Lytle, A. (2010). Automatic reconstruction of as-built building information models from laser-scanned point clouds: A review of related techniques. Automation in Construction, 19(7), 829–843. https://doi.org/10.1016/j.autcon.2010.06.007.

Torzoni, M., Tezzele, M., Mariani, S., Manzoni, A., & Willcox, K. E. (2024). A digital twin framework for civil engineering structures. Computer Methods in Applied Mechanics and Engineering, 418(Part B), 116584. https://doi.org/10.1016/j.cma.2023.116584.

Xu, J., Shu, X., Qiao, P., Li, S., & Xu, J. (2023). Developing a digital twin model for monitoring building structural health by combining a building information model and a real-scene 3D model. Measurement, 217, 112955. https://doi.org/10.1016/j.measurement.2023.112955.

Yamaguchi, T., & Hashimoto, S. (2010). Fast crack detection method for large-size concrete surface images using percolation-based image processing. Machine Vision and Applications, 21, 797–809. https://doi.org/10.1007/s00138-009-0189-8.

Yasmin, T., La, D., La, K., Nguyen, M. T., & La, H. M. (2023). Concrete spalling detection system based on semantic segmentation using deep architectures. Computers & Structures, 300. https://doi.org/10.1016/j.compstruc.2024.107398.

Zhang, A., Wang, K. C. P., Fei, Y., Liu, Y., Tao, S., Chen, C., Li, J. Q., & Li, B. (2018). Deep Learning–Based Fully Automated Pavement Crack Detection on 3D Asphalt Surfaces with an Improved CrackNet. Journal of Computing in Civil Engineering, 32(5). https://doi.org/10.1061/(ASCE)CP.1943-5487.0000775.

The Asian Institute of Research
Engineering and Technology Quarterly Reviews
Vol.8, No.2, 2025: 46-57
ISSN 2622-9374

PoA-PBFT Blockchain Architecture Design for Authentication and Identity Protection in Electronic Passports

Priati Assiroj[1], Baluh B. Hertantyo[1], Besse Hartati[1], Sirojul Alam[2]

[1] Immigration Technology Management, Politeknik Pengayoman Indonesia, Tangerang, Indonesia
[2] Certificate Authority Department, PERURI Indonesia, Jakkarta, Indonesia

Correspondence: Priati Assiroj, Immigration Technology Management, Politeknik Pengayoman Indonesia, Tangerang, Indonesia. Tel: -. E-mail: priati.assiroj@poltekim.ac.id

Abstract
Centralized e-passport infrastructures remain vulnerable to forgery, data manipulation, and single points of failure, undermining both national and international identity management systems' integrity and transparency. These limitations restrict real-time cross-agency verification and create dependencies on centralized authorities. This study introduces a permissioned blockchain model designed to enable decentralized trust, institutional accountability, and fault-tolerant verification to overcome these challenges. The proposed framework integrates certified government entities, such as the Ministry of Immigration and Corrections and the Directorate General of Immigration, within a secure validation network governed by a National Certificate Authority (CA). This paper proposes a hybrid blockchain architecture that combines PoA for institutional legitimacy with PBFT for deterministic consensus and data immutability. All passport-related transactions, including issuance, renewal, and revocation are validated through smart contracts and recorded in a distributed ledger, ensuring secure, transparent, and interoperable data exchange compliant with ICAO standards. The model demonstrates that blockchain can be feasibly applied to national e-passport infrastructures, thereby establishing a digital identity ecosystem that is tamper-resistant and auditable. Future work includes implementing a prototype using Hyperledger Fabric to evaluate latency, throughput, and consensus efficiency.

Keywords: Blockchain, E-Passport, Proof-Of-Authority, Practical Byzantine Fault Tolerance

1. Introduction

The rapid digitalization of personal identification and cross-border travel management has introduced new challenges in maintaining the authenticity, privacy, and security of sensitive identity data. The electronic passport (e-passport), which embeds a microprocessor chip storing biometric and demographic information, has become a cornerstone of modern border control. However, despite its adoption by more than 150 countries, current e-

passport infrastructures remain dependent on centralized verification authorities, introducing single points of failure, privacy vulnerabilities, and limited transparency across international borders. Such structural weaknesses expose the system to forgery, data manipulation, and insider abuse, ultimately threatening national security and citizen trust (Jahan et al., 2023) (Diego & Gutierrez-aguero, 2025) (KOCAOĞULLAR et al., 2025). Traditional certificate-based identity management systems ensure authenticity during issuance but rely on hierarchical trust structures and periodic synchronization through the International Civil Aviation Organization (ICAO) Public Key Directory (PKD) (KOCAOĞULLAR et al., 2025). This centralized model impedes real-time interagency verification and increases operational latency. In cases where digital certificates are revoked or compromised, downstream verifiers may not immediately detect the change, allowing potentially fraudulent documents to remain active. Recent research highlights the scalability limitations of centralized verification systems and recommends hybrid trust frameworks that integrate distributed validation mechanisms for greater resilience (Butera et al., 2023) (Kuperberg, 2020).

Blockchain technology has emerged as a promising solution for identity protection and authentication by decentralizing trust and enhancing transparency. As a distributed ledger collectively maintained by authorized nodes, the blockchain guarantees immutability, integrity, and traceability for every recorded transaction (Vinoth Kumar et al., 2024) (Ricci et al., 2021) (Papatheodorou et al., 2025). In identity management contexts, it enables multiple government and border-control entities to securely share verified data without relinquishing sovereignty or administrative control. Furthermore, blockchain's transparent auditability supports compliance with accountability and privacy regulations while preventing unauthorized data manipulation. However, the selection of consensus mechanisms determines the efficiency and reliability of blockchain-based identity systems. Public blockchains, such as Bitcoin and Ethereum, which employ Proof of Work (PoW) or Proof of Stake (PoS), are energy-intensive and rely on anonymous validators—properties unsuitable for regulated identity frameworks. Consequently, research has shifted toward permissioned consensus protocols such as Proof of Authority (PoA) and Practical Byzantine Fault Tolerance (PBFT), which enable deterministic, low-latency consensus among known institutional nodes (Kuperberg, 2020) (Ricci et al., 2021) (KOCAOĞULLAR et al., 2025).

Figure 1 illustrates the proposed blockchain-based e-passport system's conceptual model. Each authorized institution—represented by a validator node from the Ministry of Immigration and Corrections or the Directorate General of Immigration—interacts through smart contracts to record and verify passport-related transactions on a shared distributed ledger. This permissioned and auditable structure establishes a foundation for secure, transparent, and interoperable digital identity management at both national and international levels.

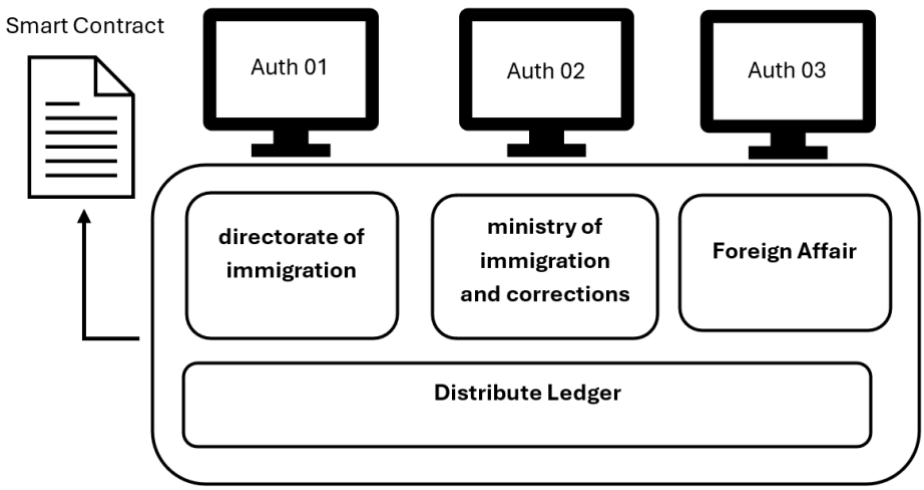

Figure 1: Conceptual model of proposed blockchain based e-passport system

Proof-of-Authority (PoA) relies on validator reputation and certified digital identities, making it suitable for governmental or inter-agency entities' consortium blockchains (Kuperberg, 2020) (Ricci et al., 2021). However,

pure PoA assume that all validators are permanently honest and online, thereby providing limited fault tolerance. In contrast, Practical Byzantine Fault Tolerance (PBFT) employs a multi-phase message exchange process—pre-prepare, prepare, and commit—to maintain ledger consistency even when up to one-third of nodes are faulty or malicious (Medina et al., 2021). Integrating both mechanisms into a single hybrid PoA-PBFT framework provides an optimal balance between performance, determinism, and resilience (Jahan et al., 2023) (Papatheodorou et al., 2025). Several recent studies have reinforced the potential of blockchain in e-governance and identity verification. Hasan et al. (Hasan et al., 2020) introduced a blockchain-based digital medical-passport framework to authenticate COVID-19 immunity credentials, enabling secure validation across institutional boundaries. Ricci et al. (Ricci et al., 2021) presented a systematic review of blockchain-enabled contact tracing and vaccine-distribution systems, emphasizing scalability and data integrity. Butera et al. (Butera et al., 2023) explored NFT-based origin verification for second-hand assets, demonstrating how ownership can be tracked using immutable digital proofs. Kuperberg (Kuperberg, 2020) provided a comprehensive survey of blockchain-driven identity management models, outlining organizational and technological challenges in enterprise and governmental contexts. Collectively, these works demonstrate the capacity of blockchain to prevent tampering, enhance transparency, and automate trust verification.

Nevertheless, the application of blockchain to e-passport authentication remains underexplored (KOCAOĞULLAR et al., 2025). Existing systems primarily address medical financial or supply-chain credentials rather than government-issued travel documents. Integrating blockchain with International Civil Aviation Organization (ICAO)-compliant infrastructures—while preserving interoperability, scalability, and legal validity—requires further architectural investigation. The absence of a standardized multi-authority framework for e-passport validation motivates the design of a secure, transparent, and auditable blockchain-based model (Terkes et al., 2024).

Therefore, this study proposes a hybrid PoA–PBFT blockchain architecture for e-passport authentication and identity protection in Indonesia. The framework leverages PoA's efficiency and PBFT's fault tolerance to form a permissioned, multi-agency network involving the Ministry of Immigration and Corrections and the Directorate General of Immigration as validator nodes. Each node receives a cryptographic certificate issued by a national certificate authority (CA), enabling secure block creation and consensus participation. Every passport issuance, renewal, or revocation is immutably recorded, and real-time verification occurs at border gates or embassies through smart contracts (Papatheodorou et al., 2025). The proposed model mitigates forgery, eliminates single points of failure, and enhances transparency in alignment with ICAO standards by decentralizing validation among certified institutions. The contributions of this study are threefold. First, a hybrid PoA–PBFT consensus framework optimized for sovereign identity systems is introduced, ensuring deterministic finality and institutional accountability. Second, it presents an architectural blueprint for integrating blockchain into existing electronic-passport infrastructures, enabling decentralized validation among trusted government authorities. Third, it evaluates expected security, efficiency, and interoperability gains, emphasizing compliance with international identity management standards (Papatheodorou et al., 2025) (KOCAOĞULLAR et al., 2025). Overall, this research establishes a foundational model for implementing and testing permissioned blockchain networks in national digital-identity ecosystems—advancing toward a transparent, tamper-resistant, and interoperable e-governance paradigm.

2. Method

The efficiency, scalability, and trustworthiness of any blockchain-based identity system primarily depend on its consensus mechanism—the protocol that enables distributed nodes to agree on the validity of transactions and blocks. The ideal consensus framework for an e-passport authentication system must ensure deterministic finality, low latency, verifiable authority, and resilience against partial node failures. To achieve this, the proposed framework adopts a hybrid PoA and PBFT mechanism, combining institutional legitimacy with Byzantine fault resilience (Jahan et al., 2023) (Kuperberg, 2020) (Papatheodorou et al., 2025).

2.1 Proof-of-Authority (PoA) Overview

Proof-of-Authority (PoA) is a permissioned consensus protocol in which, rather than anonymous participants, validators are pre-approved, identifiable, and institutionally accountable entities. Each validator node represents a recognized government organization operating under a legally verifiable identity, such as the Ministry of Immigration and Corrections or the Directorate General of Immigration. Unlike open blockchain models, such as Proof-of-Work (PoW) or Proof-of-Stake (PoS), PoA does not depend on computational competition or financial stake. Instead, it relies on the credibility and authenticity of the validator identities, each of which is verified through cryptographic certification issued by a trusted national certificate authority (CA). This approach establishes a trust-anchored yet decentralized governance model in which the number of validators is limited but transparent and auditable. PoA offers the following intrinsic advantages that make it suitable for sovereign identity systems and inter-agency data-sharing frameworks:

2.1.1 High throughput and low latency.

Block production is deterministic and sequentially assigned among authorized validators, eliminating the probabilistic delays typical in mining-based systems.

2.1.2 Energy efficiency and sustainability.

Consensus is achieved through digital signature verification instead of computationally intensive puzzles, making it viable for government-scale deployments.

2.1.3 Institutional accountability.

Every block proposal and validation is cryptographically signed and traceable to a specific government authority, ensuring legal responsibility for all ledger operations.

In the context of the proposed blockchain-based e-passport architecture, the PoA layer functions as the primary access-control layer that governs validator participation. Only government institutions with valid CA-issued certificates are permitted to propose or validate transactions such as passport issuance, renewal, or revocation. The CA acts as the root of trust, validating institutional credentials, issuing digital keys, and managing validator lifecycle policies. This structure ensures legal auditability and operational transparency while maintaining each participating agency's sovereignty. It guarantees that all blockchain activities are technically verifiable and administratively attributable, aligning with national governance mandates and ICAO standards for cross-border identity validation (KOCAOĞULLAR et al., 2025). Consequently, PoA establishes a secure and controlled foundation on which the PBFT consensus mechanism can operate efficiently, ensuring that only trusted entities participate in subsequent block validation and message-exchange processes.

2.2 Practical Byzantine Fault Tolerance Overview

Practical Byzantine Fault Tolerance (PBFT) is a deterministic consensus algorithm designed to ensure consistency and reliability within distributed systems, even when certain nodes behave arbitrarily or maliciously—known as Byzantine faults. Such faults may result from hardware failures, software errors, or external adversarial compromise. Initially proposed by Castro and Liskov, PBFT has become one of the most widely implemented consensus mechanisms in permissioned blockchain environments, particularly in enterprise and government networks where validator identities are authenticated and authorized (Kuperberg, 2020) (Medina et al., 2021). Unlike probabilistic consensus models, such as Proof-of-Work (PoW) or Proof-of-Stake (PoS), PBFT guarantees final and irreversible agreement through multiphase message exchange among known validators. This deterministic approach ensures that all honest nodes reach agreement on the same transaction order, provided that no more than f nodes are faulty within a network of $3f + 1$ total nodes. This reliability makes PBFT particularly suitable for national e-passport infrastructures, where integrity, non-repudiation, and auditability are essential (Ricci et al., 2021) (Terkes et al., 2024).

In the proposed hybrid PoA–PBFT architecture, each validator node—representing a certified government authority, such as the Ministry of Immigration and Corrections or the Directorate General of Immigration—engages in structured communication rounds to validate every passport-related transaction. PBFT operates through five sequential phases:

2.2.1 Request Phase.

The PBFT process begins when a client node—such as a border control system or embassy terminal—submits a digitally signed transaction request to the primary node, ensuring authenticity and integrity. In the Pre-Prepare phase, the primary verifies the signature, checks for duplicates, and assigns a valid unique sequence number before forwarding the proposal to replica nodes. This stage ensures non-repudiation, as each transaction is traceable to an authenticated source, forming the trust foundation that only legitimate, verifiable passport operations enter the blockchain network.

2.2.2 Pre-Prepare Phase.

In the pre-prepare phase, a designated primary node—also referred to as the leader—initiates the consensus process by proposing a new block that contains one or more verified transactions. In this research context, each transaction may correspond to an e-passport event, such as issuance, renewal, or revocation. The primary node aggregates these transactions into a candidate block, attaches its digital signature and a sequence number, and broadcasts a pre-prepare message to all replica nodes. This message acts as the official proposal for the current round of consensus. This phase ensures that all validators are aware of an identical block proposal and are synchronized in the same view of the system state before validation begins. At this stage, no voting or decision occurs; it is purely a dissemination step that sets the baseline for subsequent agreement.

2.2.3 Prepare Phase.

Each replica node independently verifies the block's validity by checking its cryptographic hash, each transaction's integrity, and the leader's signature authenticity upon receiving the pre-prepare message. If the verification is successful, the node broadcasts a message to all other replicas, signalling its preliminary approval of the proposal. Then, every validator collects prepare messages from its peers. The process continues until the node receives confirmations from at least $2f + 1$ distinct nodes, where "f" denotes the system's maximum number of faulty or malicious nodes. This threshold guarantees that a sufficient majority of honest validators have inspected and agreed on the same block proposal. The outcome of this phase is the formation of a qualified majority agreement—a consensus that the proposed block is valid and ready to be committed if further votes corroborate it.

2.2.4 Commit Phase.

The commit phase finalizes the consensus decision. After obtaining a quorum of prepared messages, each node broadcasts a commit message to the network, confirming its intent to append the validated block to the ledger. Once a node collects $2f + 1$ matching commit messages, it determines that a supermajority consensus has been achieved, and the block is irreversibly confirmed. The node then appends the block to its copy of the local distributed ledger, ensuring that all honest participants maintain an identical and synchronized state. This stage marks the transition from provisional agreement to deterministic finality—a state in which the block cannot be altered or replaced without the majority's cooperation. In the context of an e-passport system, each passport issuance or verification record becomes immutable, auditable, and cryptographically verifiable across all nodes of government authority.

2.2.5 Reply Phase.

Once a validator node receives at least 2f + 1 matching prepare messages, it moves into the commit phase, broadcasting to peers signed confirmations that the block is valid. When 2f + 1 commit messages are collected, the block is permanently appended to every ledger, ensuring a consistent, immutable e-passport record. Finally, during the reply phase, validators notify the client (e.g., border or embassy system) that the transaction is finalized across the network, confirming deterministic consensus and eliminating the risk of forks or conflicting records. Figure 2 shows the PBFT consensus flow in the proposed architecture. Each authorized node exchanges digitally signed messages through three communication rounds, and the system commits the transaction to the distributed ledger only when at least two-thirds of nodes confirm the block's validity. The deterministic finality achieved through PBFT eliminates the possibility of forks or conflicting passport records, thereby guaranteeing that all nodes maintain a consistent, tamper-proof copy of the e-passport ledger.

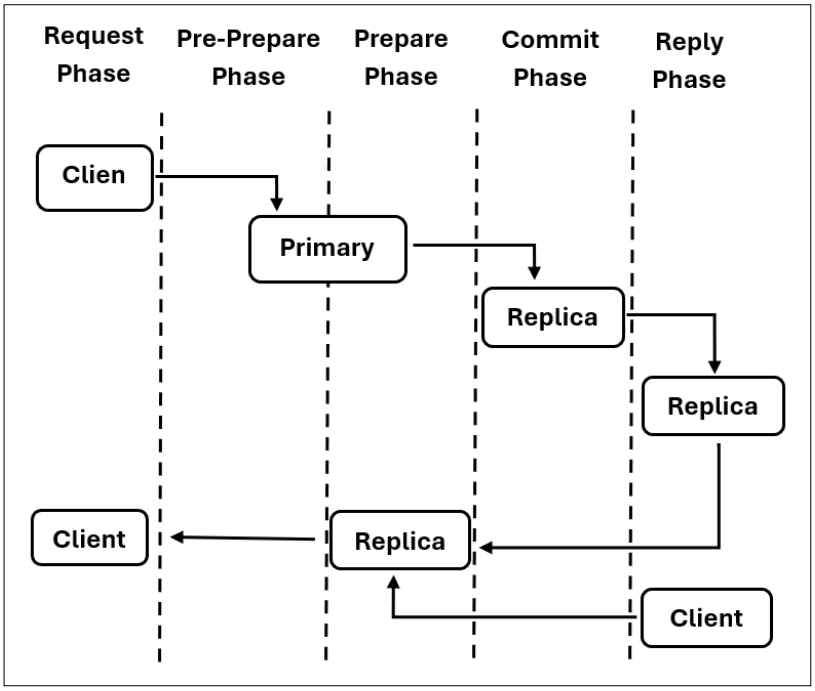

Figure 2: PBFT consensus flow on the proposed architecture

The process begins when a client node (such as a border control terminal or embassy system) sends a digitally signed request to the primary node, initiating the Request Phase. The primary node validates the request and broadcasts a proposal to the replica nodes during the Pre-Prepare Phase. Each replica then verifies the proposal and exchanges Prepare messages with its peers to confirm the transaction's validity. Once at least 2f + 1 nodes agree, the system enters the commit phase, in which all replicas append the verified block to their local ledgers. Finally, in the Reply Phase, replicas send confirmation messages back to the client, ensuring that all nodes maintain a synchronized and immutable record of the passport transaction across the distributed network.

2.3 Related Works

Several recent studies have investigated the use of blockchain technology for secure identity management and authentication within digital ecosystems. Kuperberg (Kuperberg, 2020) provided a comprehensive survey of blockchain-based identity management frameworks, emphasizing the transition from centralized identity and access management (IAM) models toward decentralized and self-sovereign identity (SSI) architectures. The study highlighted major challenges related to compliance, privacy protection, and the integration of blockchain with certificate-based authentication infrastructures and enterprise trust systems. The findings suggest that blockchain can enhance institutional trust, transparency, and accountability while minimizing the dependency on single centralized authorities.

Jahan et al. (Jahan et al., 2023) proposed a private permissioned blockchain for digital passport management combined with the InterPlanetary File System (IPFS) to achieve secure storage and traceable document verification

in the context of e-government and e-passport applications. Similarly, Hasan et al. (Hasan et al., 2020) introduced a blockchain-based digital medical passport model for verifying COVID-19 immunity certificates, demonstrating cross-institutional authentication without relying on a single national database. Al-Bassam's research further extended this concept by using smart contracts to replace conventional digital certificate authority frameworks, ensuring verifiable and tamper-resistant credential validation for government systems. Collectively, these approaches show that permissioned blockchain networks provide immutability, auditability, and verifiable identity exchange across administrative domains.

Hybrid consensus models have been developed to improve the scalability and fault tolerance of controlled blockchain environments. Butera (Butera et al., 2023) proposed an enhanced proof-of-authority (EA-PoA) model for optimizing the lifetime of wireless sensor networks through energy-aware leader selection and hierarchical clustering. Similarly, Stokkink and Pouwelse combined zero-knowledge proofs with PBFT-based validation to support identity claims in distributed ecosystems that are verifiable and privacy-preserving. These studies confirm that integrating deterministic protocols, such as PBFT, with authority-based validator selection enhances throughput, reliability, and security—key features required in regulated national identity infrastructures.

Recent decentralized identity frameworks, such as Sovrin, uPort, and Hyperledger Indy, emphasize user autonomy and cryptographic verifiability (Papatheodorou et al., 2025). However, their general SSI-based architecture renders them unsuitable for highly regulated government systems that require hierarchical control, legal accountability, and compliance with International Civil Aviation Organization (ICAO) Doc 9303 standards. To bridge this gap, de Diego and Gutiérrez-Aguero (Diego & Gutierrez-aguero, 2025) and Alaraj and Bani-Salameh (Papatheodorou et al., 2025) proposed hybrid blockchain architectures that integrate government-controlled validator networks with public verification layers to ensure interoperability and audit transparency. Based on the reviewed literature, the application of blockchain in e-Passport ecosystems remains an emerging research field. While most studies focus on digital identity or credential verification, few address multi-authority consensus, cross-border validation, or interoperability with traditional Machine Readable Travel Document (MRTD) systems. Therefore, this study proposes a hybrid PoA–PBFT blockchain model designed for national e-Passport infrastructures, combining deterministic PoA with PBFT to achieve operational efficiency, resilience, and full compliance with international security and governance standards (Jahan et al., 2023) (Butera et al., 2023) (KOCAOĞULLAR et al., 2025).

3. Results

The proposed system introduces a hybrid blockchain architecture that integrates the PoA and PBFT consensus mechanisms to ensure secure, verifiable, and tamper-resistant e-passport data management. This framework is designed to support multi-agency collaboration across the Ministry of Immigration and Corrections, the Directorate General of Immigration, and the National Certificate Authority of Indonesia. Its core objective is to overcome the limitations of centralized public key infrastructures by enabling distributed validation, auditable record-keeping, and fault-tolerant consensus among authorized government nodes. Figure 3 conceptually depicts the hybrid consensus process that integrates PoA's deterministic validator selection with PBFT's multi-phase message exchange for block confirmation.

3.1 System Overview

The proposed blockchain-based e-passport architecture establishes a permissioned, multi-authority network to enhance national identity management processes' integrity, traceability, and transparency. At its core, the system replaces the traditional centralized public key infrastructure with a distributed ledger governed by a hybrid PoA–PBFT consensus mechanism. This hybrid model ensures that only verified institutions can participate in block validation while maintaining deterministic finality and FTT across all nodes. Figure 3 shows that the architecture is composed of the following four key components:

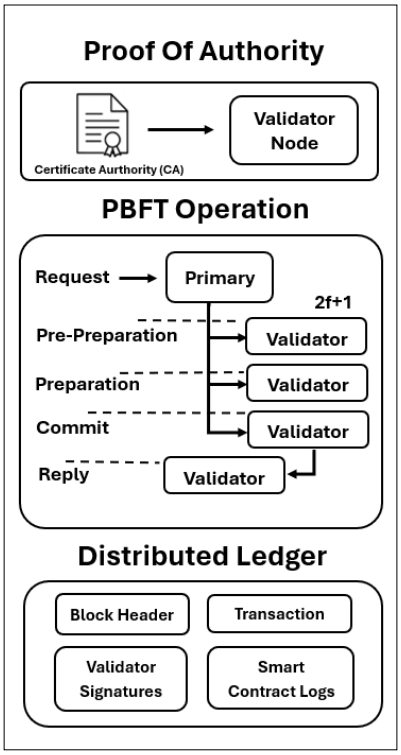

Figure 3: Hybrid PoA-PBFT consensus mechanism

3.1.1 Certificate Authority. CA is responsible for issuing cryptographic credentials to participating institutions;
3.1.2 Validator Nodes. It represents the Ministry of Immigration and Corrections and Directorate General of Immigration;
3.1.3 The PBFT Consensus Layer. It coordinates message exchanges (pre-prepare, prepare, commit, and reply phases) among validator nodes to reach agreement on each transaction; and
3.1.4 The Distributed Ledger. This is where validated e-passport events—such as issuance, renewal, or revocation—are permanently stored in a tamper-proof blockchain.

The Hybrid PoA–PBFT Consensus Mechanism for the E-Passport Blockchain Architecture illustrates the interaction between institutional authorization and distributed consensus to maintain integrity across national identity systems. In this framework, each e-passport transaction begins at the PoA layer, where a national certificate authority authenticates the validator nodes before participating in consensus. Then, the validated nodes engage in the PBFT process, exchanging signed messages across the Request, Pre-Prepare, Prepare, Commit, and Reply phases to reach a deterministic agreement.

Once the block is confirmed by a supermajority of $2f + 1$ validators, the transaction is appended to the distributed ledger, which stores block headers, validator signatures, transaction data, and smart-contract logs. This ensures that every passport issuance, renewal, or revocation is cryptographically verified, immutably recorded, and auditable across all authorized government institutions, thereby reinforcing trust and resilience within the national e-passport ecosystem.

3.2 Architecture Model

The proposed e-passport blockchain framework adopts a hybrid layered architecture that integrates the PoA and PBFT consensus mechanisms to ensure institutional legitimacy, operational resilience, and deterministic transaction finality. As shown in Fig. 3, the system operates within a permissioned environment comprising certified validator nodes representing governmental entities, each authenticated through cryptographic certificates issued by a National Certificate Authority (CA). This configuration guarantees that only trusted and legally

recognized institutions—such as the Ministry of Immigration and Corrections, the Directorate General of Immigration, and the Ministry of Foreign Affairs—participate in the validation and consensus processes. The architecture is logically structured into four functional layers, each contributing distinct responsibilities to the network's overall security and performance: the application, consensus, network, and ledger layers.

At the Application Layer, user-facing entities—such as passport issuance systems, border inspection terminals, and embassy verification nodes—initiate authenticated transactions. Each transaction request (e.g., issuance, renewal, or revocation) is digitally signed using the institution's private key to ensure data origin authenticity and integrity before blockchain submission.

The Consensus Layer governs validation operations and enforces agreement across the participating nodes. The PoA sublayer establishes validator eligibility based on institutional certification, preventing unauthorized access, and ensuring administrative accountability. Upon authentication, the PBFT sublayer manages the multiphase consensus procedure. The primary node aggregates verified transactions into candidate blocks and disseminates pre-prepare messages to all replicas. Each replica independently verifies block integrity and authenticity before exchanging prepare and commit messages. Consensus is achieved when at least $2f + 1$ validators confirm identical block states, providing deterministic finality and fault tolerance against Byzantine failures. This hybridization eliminates probabilistic delays and reduces computational overhead compared to Proof-of-Work (PoW) systems, achieving a low-latency, high-throughput consensus suitable for real-time identity verification.

The network layer enables secure communication among the validator nodes through encrypted and authenticated channels. A partially meshed topology is employed to balance fault resilience and transmission efficiency, ensuring rapid consensus message propagation even under partial node failures. All inter-node communications are digitally signed and timestamped, thereby preventing tampering, message reordering, or replay attacks.

The Ledger Layer provides immutable storage and cryptographic auditability. Each block contains a structured combination of a block header, validated transaction data, validator signatures, and smart contract execution logs. The block header links to its predecessor through a secure hash reference, ensuring temporal consistency and tamper resistance. Embedded smart contracts automate rule enforcement for passport issuance, renewal, and revocation while fine-grained access control between institutions is implemented. Sensitive biometric or personal data are encrypted or hashed to preserve privacy compliance while retaining full audit traceability.

Collectively, this architecture establishes a hierarchical yet decentralized governance model, where PoA defines validator identity and authority, and PBFT enforces deterministic consensus among validated participants. The resulting infrastructure delivers institutional accountability, Byzantine fault tolerance, and transparency of data provenance. The design aligns with the International Civil Aviation Organization (ICAO) Public Key Directory standards while extending its capabilities toward real-time, cross-agency synchronization, and multi-jurisdictional interoperability.

Consequently, the hybrid PoA–PBFT architecture provides a robust technical foundation for next-generation sovereign identity systems. It supports high integrity in e-passport authentication, reduces dependency on centralized validation intermediaries, and enables scalable integration with future e-government services, such as e-visa issuance, border security analytics, and decentralized travel record management.

3.3 Operation Workflow

Figure 3 shows the proposed hybrid PoA–PBFT blockchain architecture's operational workflow for electronic passport authentication. The figure is divided into three major functional sections —PoA, PBFT operation, and distributed ledger— each representing a sequential phase of the validation and recording process.

The PoA section begins the workflow with the Authority Registration phase. Institutional participants, such as the Directorate General of Immigration and the, Ministry of Immigration and Corrections, register as validator nodes. Each node receives a digital certificate issued by the National Certificate Authority (CA), which serves as its immutable credential for participating in block validation. This process ensures that only verified governmental

entities are eligible to join the network, eliminating the possibility of untrusted or anonymous participants. Thus, the PoA layer establishes the system's institutional trust foundation, binding every node's cryptographic identity to its legal authority. The transaction proceeds to the PBFT operation block following registration, which represents the core consensus process. When an authorized operator initiates a passport-related transaction—such as issuance, renewal, or revocation—the request is sent to the primary node. The primary node aggregates verified data and triggers the multi-phase PBFT process, which starts with the request message. Then, a Pre-Prepare message is broadcast to all replica validators, ensuring that each receives an identical validation proposal. Each Validator Node independently examines the cryptographic integrity of the block, verifying the transaction signatures and timestamps. Then, the validates exchange Prepare and Commit messages, ensuring agreement through cross-validation. A consensus is reached when a quorum of 2f+1 matching commit messages is reached, guaranteeing deterministic and fault-tolerant agreement even in the presence of faulty or malicious nodes.

Finally, in the Distributed Ledger section, the validated block is permanently appended to the blockchain. Each block comprises a block header, validator signatures, transaction data, and smart contract logs. The block header contains a hash pointer linking it to the previous block, maintaining the immutability and chronological integrity of the ledger. Validator signatures provide cryptographic proof of consensus, while the transaction field records details of the passport operation. Smart contract logs document the automated validation and policy enforcement actions performed during the process. Together, these components establish an auditable and tamper-resistant ledger that supports transparent verification across all authorized institutions.

4. Discussion

This operational workflow demonstrates how the proposed system harmonizes institutional trust with the Distributed Consensus System (DCS). The PoA layer enforces access control and node legitimacy, whereas the PBFT mechanism ensures synchronization, fault tolerance, and deterministic finality across validator nodes. The system transforms the e-passport into a self-verifiable digital identity asset that can be authenticated in real-time across ministries and border agencies without relying on centralized verification authorities by combining these mechanisms.

The proposed PoA–PBFT blockchain architecture incorporates a multilayer security and governance model that ensures institutional trust, cryptographic integrity, and operational accountability across all participating authorities. As illustrated in Figure 4, the framework integrates three principal domains—governance authentication, consensus operation, and application interoperability—within a unified and verifiable security structure that mirrors real-world governmental hierarchy.

Figure 4 shows that the proposed e-passport blockchain architecture integrates three primary layers: the governance and validation layer, the blockchain network layer, and the application interoperability layer. At the top level, the CA acts as the root of trust, issuing cryptographic certificates that authorize participation in the network. Validator legitimacy is governed by the Proof-of-Authority (PoA) mechanism, ensuring that only certified government entities—such as the Ministry of Immigration and Corrections and the Directorate General of Immigration—are allowed to operate as validator nodes (VA Node01 and VA Node02). This mechanism replaces anonymous participation with institutional accountability, thereby forming the foundation for a secure verification of national identity.

The second layer represents the blockchain network, where the primary node initiates transactions and the PBFT consensus mechanism validates them through structured message exchanges. Each validator node verifies the transaction and confirms agreement once at least 2f + 1 validators reach quorum. The Distributed Ledger permanently stores the validated data, while Smart Contracts automate validation rules, manage access control, and ensure that all e-passport records remain immutable and auditable.

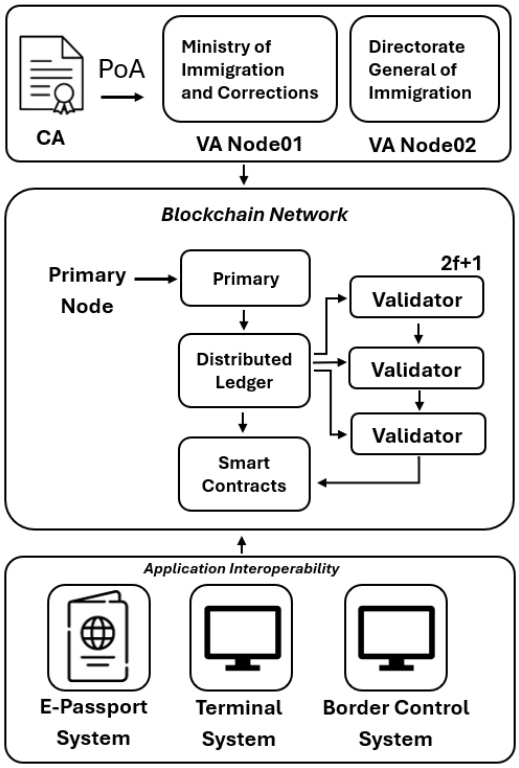

Figure 4: Application interoperability layer

The bottom layer, the Application Interoperability Layer, enables seamless communication between the blockchain network and government application systems. This layer connects the E-Passport Issuance System, Embassy or Terminal Systems, and Border Control Systems, allowing real-time travel document authentication and verification across national and diplomatic authorities. Through this integration, the system achieves secure, interoperable, and verifiable e-passport management while maintaining compliance with international standards, such as ICAO Doc 9303 (Edition, 2021).

This paper proposes a hybrid PoA and PBFT blockchain architecture for securing the authentication and verification processes in national e-passport systems. The model integrates the institutional legitimacy of PoA with the deterministic fault tolerance of PBFT, creating a permissioned blockchain framework capable of ensuring data integrity, immutability, and real-time interoperability among government agencies. The design eliminates single points of failure, enhances transparency, and enables automated validation through smart contracts, making it suitable for large-scale e-governance applications. The findings demonstrate that the proposed blockchain model can be feasibly implemented within Indonesia's e-passport infrastructure and can be extended to support cross-border authentication in compliance with the International Conference on Authentication and Privacy (ICAO) standards. The hybrid PoA–PBFT mechanism provides a practical balance between governance control and distributed trust, offering a secure foundation for sovereign digital identity systems. Future work will focus on developing a prototype implementation using Hyperledger Fabric to evaluate system performance, including consensus latency, throughput, and network resilience under operational conditions.

Author Contributions: All authors contributed to this research.

Funding: This research was funded by Politeknik Pengayoman Indonesia, The Ministry of Law of The Republic of Indonesia.

Conflicts of Interest: The authors declare no conflict of interest.

Informed Consent Statement/Ethics approval: Not applicable.

Declaration of Generative AI and AI-assisted Technologies: AI-based text assistance was used to improve grammar, clarity, translation, and overall readability. All research design, experimental work, analysis, and conclusions were conducted independently, and the AI tool was specifically used as a language support.

References

Butera, A., Gatteschi, V., Member, S., Gabriele, F., Novaro, D., & Vianello, D. (2023). *Blockchain and NFTs-based Trades of Second-hand Vehicles*. 1–18. https://doi.org/10.1109/ACCESS.2023.3284676

Diego, S. D. E., & Gutierrez-aguero, I. (2025). Decentralized Digital Product Passport Building Blocks for Enhancing Supply Chain Sovereignty and Circular Economy Practices. *IEEE Access*, *PP*, 1. https://doi.org/10.1109/ACCESS.2025.3594826

Edition, E. (2021). *ICAO Doc 9303 Part 8: Emergency Travel Documents*.

Hasan, H. R., Salah, K., Member, S., Jayaraman, R., & Ellahham, S. (2020). *Blockchain-Based Solution for COVID-19 Digital Medical Passports and Immunity Certificates*. 222093–222108. https://doi.org/10.1109/ACCESS.2020.3043350

Jahan, N., Reno, S., & Ahmed, M. (2023). Securing E-Passport Management Using Private-Permissioned Blockchain and IPFS. *3rd International Conference on Electrical, Computer and Communication Engineering, ECCE 2023*. https://doi.org/10.1109/ECCE57851.2023.10101496

KOCAOĞULLAR, C., YILDIRIM, K., SAKAOĞULLARI, M. A., & KÜPÇÜ, A. (2025). BasGit: a secure digital ePassport alternative. *Turkish Journal of Electrical Engineering and Computer Sciences*, *33*(5), 631–646. https://doi.org/10.55730/1300-0632.4148

Kuperberg, M. (2020). *Blockchain-based Identity Management : A Survey from the Enterprise and Ecosystem Perspective*. *November*. https://doi.org/10.1109/TEM.2019.2926471

Medina, J., Member, S., Cessa-rojas, R., Member, S., & Umpaichitra, V. (2021). Reducing COVID-19 Cases and Deaths by Applying Blockchain in Vaccination Rollout Management. *IEEE Open Journal of Engineering in Medicine and Biology*, *PP*, 1. https://doi.org/10.1109/OJEMB.2021.3093774

Papatheodorou, N., Hatzivasilis, G., & Papadakis, N. (2025). The YouGovern Secure Blockchain-Based Self-Sovereign Identity (SSI) Management and Access Control. *Applied Sciences (Switzerland)*, *15*(12). https://doi.org/10.3390/app15126437

Ricci, L., Di Francesco Maesa, D., Favenza, A., & Ferro, E. (2021). Blockchains for covid-19 contact tracing and vaccine support: A systematic review. *IEEE Access*, *9*, 37936–37950. https://doi.org/10.1109/ACCESS.2021.3063152

Terkes, M., Demirci, A., Gokalp, E., & Cali, U. (2024). Battery Passport for Second-Life Batteries: Potential Applications and Challenges. *IEEE Access*, *12*, 128424–128467. https://doi.org/10.1109/ACCESS.2024.3450790

Vinoth Kumar, C., Selvaprabhu, P., Baska, N., Vivek Menon, U., Babu Kumaravelu, V., Chinnadurai, S., & Ali, F. (2024). Ethereum Blockchain Framework Enabling Banks to Know Their Customers. *IEEE Access*, *12*, 101356–101365. https://doi.org/10.1109/ACCESS.2024.3427805

ASIAN INSTITUTE OF RESEARCH
Connecting Scholars Worldwide

The Asian Institute of Research
Engineering and Technology Quarterly Reviews
Vol.8, No.2, 2025: 58-75
ISSN 2622-9374

Future-Oriented Simulation-Based Strategies for the Sustainable Development of Batıkent, Ankara

Nadir Nasir Shembesh[1], Halil Semih Eryıldız[2], Demet Irklı Eryıldız[3]

[1,2,3] Department of Architecture, Faculty of Design and Architecture, Istanbul Okan University, İstanbul, Turkey.

Correspondence: Nadir Nasir Shembesh, Department of Architecture, Faculty of Design and Architecture, Istanbul Okan University, İstanbul, Turkey. E-mail: nadir.shembesh.okan@gmail.com

Abstract
The sustainable transformation of existing urban districts requires forward-looking strategies that integrate environmental performance, spatial morphology, and advanced simulation tools. This study explores future-oriented, simulation-based strategies for the sustainable development of Batıkent, Ankara, a large-scale cooperative housing district characterized by diverse building typologies and terrain conditions. Using parametric environmental simulation tools, the research evaluates future development scenarios focusing on topography-sensitive planning, renewable energy integration, and nature-based material solutions. The study examines four representative cooperative areas—3D Dubleks, Harp-İş, Tez-Koop, and Ortadoğulular—under alternative future scenarios, including flat versus sloped terrain conditions, and the integration of solar panels, green walls, and advanced insulation materials. Solar radiation simulations are employed to assess how terrain variation and design interventions influence environmental performance across low-rise, mid-rise, high-rise, and mixed-typology settlements. In addition, before–after visual simulations are used to translate numerical results into spatially interpretable outcomes, supporting design-based decision-making. The results indicate that terrain-responsive configurations generally enhance solar radiation stability and reduce shading conflicts, particularly in mid-rise and high-rise developments. Renewable energy systems and material-based interventions further improve environmental performance without requiring structural reconstruction, demonstrating the feasibility of incremental retrofitting strategies. The findings suggest that sustainable redevelopment in Batıkent should prioritize site-specific, morphology-sensitive, and simulation-informed approaches rather than uniform planning solutions. By focusing on future scenarios rather than existing-condition evaluation, this study contributes a practical framework for guiding sustainable urban redevelopment in cooperative housing districts. The proposed strategies offer transferable insights for similar urban contexts seeking to enhance energy efficiency, environmental resilience, and long-term sustainability through simulation-based planning.

Keywords: Sustainable Urban Development, Parametric Simulation, Future Scenarios, Cooperative Housing, Batıkent, Solar Radiation

1. Introduction

Rapid urbanization, climate change, and increasing energy demand have intensified the need for sustainable development strategies in existing urban environments. Contemporary sustainability discourse increasingly emphasizes that the environmental transformation of cities cannot rely solely on new developments but must also address the performance of established residential districts (Eryıldız, 1996; Eryıldız, 2007). Large-scale housing areas developed during the late twentieth century, particularly cooperative housing settlements, represent a critical challenge in this regard due to their fixed morphology, aging building envelopes, and limited adaptability to current environmental standards (Ratti et al., 2005; Sharifi & Murayama, 2013; Eryıldız & Eryıldız, 2005).

Batıkent, one of Ankara's largest planned cooperative housing districts, exemplifies this condition. Developed through a cooperative-based planning model, Batıkent contains a wide range of residential typologies, including low-rise duplex housing, uniform mid-rise apartment blocks, high-rise residential towers, and mixed-height configurations distributed across both flat and gently sloped terrain (Eryıldız & Eryıldız, 2004). While the original planning approach prioritized housing provision and functional organization, contemporary sustainability goals require a reassessment of how such districts can adapt to current and future environmental challenges, particularly in relation to energy efficiency and climate responsiveness (Jenks & Burgess, 2000; Yeang et al., 2012).

In recent years, simulation-based urban analysis has emerged as a powerful approach for evaluating environmental performance and testing future development scenarios. Parametric tools allow the integration of climatic data, urban geometry, and design variables within a unified analytical framework, enabling the exploration of multiple alternatives under controlled conditions. Compared to conventional evaluation methods, simulation-based approaches provide higher spatial resolution and greater flexibility, making them particularly suitable for scenario-driven planning and sustainability assessment in complex urban contexts (Ng et al., 2012; Robinson et al., 2009; SuSan & Eryıldız, 2023).

Among the various environmental indicators used in urban sustainability studies, solar radiation performance plays a central role due to its direct influence on heating demand, cooling loads, renewable energy potential, and outdoor thermal comfort. The distribution of solar radiation within urban environments is strongly affected by building height, spacing, orientation, and terrain configuration, underscoring the need for spatially explicit and geometry-sensitive analytical methods (Compagnon, 2004; Lobaccaro & Frontini, 2014; Eryıldız, 2005). As cities increasingly pursue low-carbon development pathways, understanding and optimizing solar access at both building and neighborhood scales has become a fundamental planning concern (Yeang et al., 2012).

At the same time, sustainable urban development strategies are expanding beyond energy generation alone to include nature-based solutions and advanced building materials that enhance environmental performance without requiring extensive structural intervention. Green façades, high-performance insulation materials, and renewable energy systems are increasingly recognized as effective retrofitting measures capable of improving thermal comfort, reducing energy consumption, and mitigating urban heat effects in dense residential areas (Perini et al., 2011; Santamouris, 2014; Eryıldız, 2007). These approaches are particularly relevant for cooperative housing districts, where large-scale demolition or reconstruction is often impractical (Eryıldız & Eryıldız, 2005).

Within this broader context, the present study adopts a future-oriented, simulation-based perspective to explore sustainable development strategies for Batıkent, Ankara. Rather than focusing on the evaluation of existing conditions alone, the research investigates how Batıkent could perform under alternative future scenarios shaped by terrain-sensitive planning, renewable energy integration, and material-based interventions, consistent with principles of ecological urbanism and urban ecology (Eryıldız, 1996; Yeang et al., 2012). Four representative cooperative areas—3D Dubleks, Harp-İş, Tez-Koop, and Ortadoğulular—are selected to reflect the district's morphological diversity and to enable comparative analysis across low-rise, mid-rise, high-rise, and mixed-typology settlements (Eryıldız & Eryıldız, 2004).

The study is structured around three interconnected analytical dimensions. First, it examines the influence of topography by comparing flat and sloped terrain scenarios, recognizing terrain as a potential environmental asset rather than a planning constraint (Toparlar et al., 2017; Eryıldız, 2005). Second, it evaluates the integration of

renewable energy systems and nature-based solutions, including solar panels and green walls, as feasible strategies for enhancing environmental performance in existing residential contexts (Santamouris, 2014; SuSan & Eryıldız, 2023). Third, it employs visual before–after simulations to translate numerical results into spatially interpretable outcomes, strengthening the link between quantitative analysis and design-oriented decision-making (Yeang et al., 2012).

By focusing on future scenarios and simulation-informed strategies, this research contributes to the growing body of literature that frames sustainability as an adaptive and transformative process rather than a static performance benchmark. The findings from Batıkent provide transferable insights for similar cooperative housing districts and mass-housing developments seeking to improve environmental performance through incremental, context-sensitive, and technologically informed interventions.

2. Research Tools and Method

This study adopts a simulation-based, scenario-oriented methodological framework to explore future strategies for the sustainable development of Batıkent, Ankara. Rather than evaluating existing conditions alone, the methodology is designed to test alternative future configurations under controlled environmental assumptions, allowing the assessment of how spatial form, terrain, and technological interventions may influence long-term environmental performance. The approach combines parametric modeling, climatic data integration, and visual simulation to support evidence-based urban design and planning decisions.

2.1. Case Study Selection

Batıkent was selected as the case study due to its significance as a large-scale cooperative housing district and its morphological diversity. Four representative cooperative areas were chosen to reflect different building typologies and spatial configurations within the district:

- 3D Dubleks (Site A): Low-rise duplex housing with open courtyards and high spatial permeability.
- Harp-İş (Site B): Uniform mid-rise (5-story) apartment blocks with linear arrangements.
- Tez-Koop (Site C): High-rise (10-story) residential blocks representing vertical density.
- Ortadoğulular (Site D): A mixed configuration combining duplex units and 8-story apartment blocks.

The selection of these sites enables comparative analysis across low-rise, mid-rise, high-rise, and mixed typologies, which is essential for evaluating the transferability of future-oriented sustainability strategies.

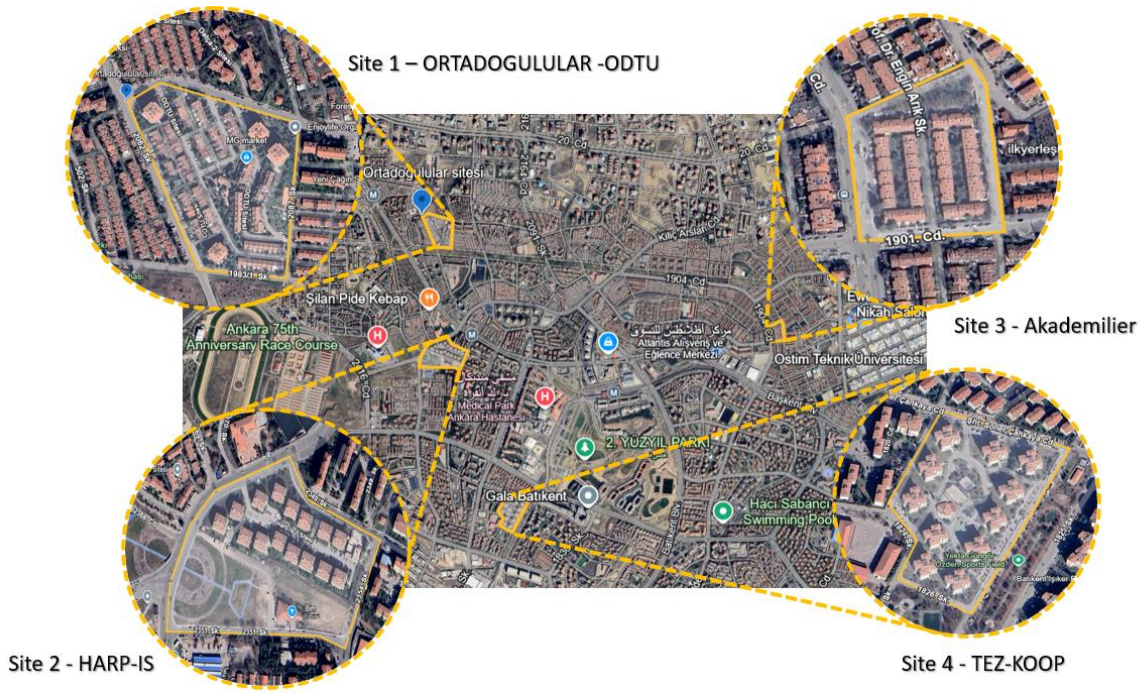

Figure 1: Locations in Batıkent-Ankara

2.2. Simulation Tools and Climatic Data

Parametric environmental simulations were conducted using Grasshopper as the core modeling platform, with Ladybug Tools employed for solar radiation analysis. These tools allow the integration of geometric parameters, orientation, and terrain conditions with real climatic data. Climate inputs were obtained from the EnergyPlus Weather (EPW) file for Ankara, ensuring that simulations reflect long-term local solar conditions rather than hypothetical or generalized climate assumptions.

Solar radiation was selected as the primary environmental performance indicator due to its direct relevance to energy efficiency, renewable energy potential, and thermal comfort. Incident radiation values (kWh/m²) were calculated for each site under multiple scenarios, enabling numerical comparison across different spatial and terrain configurations.

2.3. Terrain-Based Scenario Development

To assess the influence of topography on future environmental performance, two terrain scenarios were developed for each cooperative area:

1. Flat Terrain Scenario: All buildings are positioned on a uniform horizontal plane, reflecting conventional planning practices that prioritize land leveling and standardized layouts.
2. Sloped Terrain Scenario: Buildings follow natural topographical gradients, introducing elevation differences between blocks and façades. This scenario allows the evaluation of terrain-sensitive massing and its impact on solar exposure and shading behavior.

By keeping all other variables constant, the comparison between flat and sloped terrain scenarios isolates the effect of topography on environmental performance.

2.4. Future-Oriented Intervention Scenarios

Beyond terrain conditions, the methodology incorporates future-oriented design interventions aimed at improving sustainability without requiring structural reconstruction. Three categories of interventions were simulated and evaluated:

- Renewable Energy Integration: Rooftop and façade-based solar panels were proposed based on building height, orientation, and surface availability across the four sites.
- Nature-Based Solutions: Green walls were introduced on selected façades to improve thermal regulation, reduce surface temperatures, and enhance environmental quality, particularly in dense mid-rise and high-rise contexts.
- Material-Based Envelope Enhancement: The advanced insulation materials was applied as a façade treatment to improve thermal, acoustic, and fire performance. Its suitability for retrofitting existing buildings made it a key component of future redevelopment scenarios.

These interventions were applied consistently across sites, allowing comparative evaluation while accounting for typological differences.

2.5. Visual Simulation and Comparative Analysis

To complement numerical outputs, before–after visual simulations were generated for each site. The “before” condition represents the existing spatial configuration, while the “after” condition illustrates the proposed future scenario incorporating terrain adaptation and sustainability interventions. This visual approach enhances interpretability and supports the translation of simulation results into design-oriented insights.

Comparative analysis was conducted by examining differences in solar radiation values across scenarios and sites, supported by qualitative interpretation of visual outcomes. The methodology prioritizes relative performance trends rather than absolute optimization, aligning with the study's focus on strategic guidance rather than prescriptive design.

2.6. Methodological Scope and Limitations

The methodology is intentionally focused on future scenarios and solar radiation performance as a central indicator. While other environmental factors such as airflow and thermal comfort are relevant, they are addressed conceptually rather than through full multi-variable simulation to maintain methodological clarity and feasibility. The results should therefore be interpreted as strategic indicators rather than definitive performance predictions. Overall, this methodological framework enables a structured exploration of how Batıkent's cooperative housing areas could evolve toward sustainability through simulation-informed, terrain-sensitive, and intervention-based strategies.

3. Future-Oriented Strategies for the Sustainable Development of Batıkent

The sustainable development of Batıkent cannot be addressed solely through the evaluation of existing environmental performance; rather, it requires a forward-looking framework that integrates future design scenarios, terrain conditions, and advanced environmental technologies. Building on the comparative analyses and simulation results presented in the previous sections, this chapter shifts the focus from assessment to strategic projection, exploring how Batıkent's residential environments can evolve under alternative spatial, technological, and material-based interventions. The chapter emphasizes the role of topography-sensitive planning, renewable energy integration, and innovative façade and surface solutions in enhancing long-term environmental resilience and energy efficiency. By employing parametric simulations under varying terrain conditions and proposed design enhancements, the future perspective presented here aims to support informed decision-making for sustainable redevelopment, retrofitting strategies, and climate-responsive urban design across the four cooperative areas—3D Dubleks, Harp-İş, Tez-Koop, and Ortadoğulular.

3.1. Future Performance Scenarios under Different Terrain Conditions

Topography plays a decisive role in shaping long-term environmental performance in residential settlements, particularly in districts such as Batıkent where both flat and gently sloped terrains are present. While conventional planning approaches often treat terrain as a constraint to be neutralized through leveling, contemporary sustainability-oriented design recognizes topography as a spatial and environmental asset. In this context, the present section explores future performance scenarios for Batıkent by comparing flat terrain and sloped terrain conditions using parametric solar radiation simulations for the four cooperative areas—3D Dubleks, Harp-İş, Tez-Koop, and Ortadoğulular. The objective is to evaluate how terrain configuration influences solar exposure patterns and to identify forward-looking strategies for terrain-responsive urban redevelopment.

The flat terrain scenario represents a conventional planning assumption in which all buildings are positioned on a uniform horizontal plane. Under this condition, solar radiation performance is largely dictated by building orientation, height, and spacing. The simulation results show that settlements with open layouts or significant vertical differentiation perform more effectively, while uniform mid-rise arrangements experience notable reductions in solar access due to mutual shading.

Table 1: Solar Radiation Results under Flat Terrain Conditions for the Four Study Sites

	Incident Radiation [kWh/m2]							
	Site A		Site B		Site C		Site D	
	Original	Randomized	Original	Randomized	Original	Randomized	Original	Randomized
1	985.97	1002.65	948.92	979.41	995.55	996.97	988.66	998.9
2	887.37	902.39	858.61	887.35	899.88	897.8	889.79	899.01
3	788.78	802.12	768.3	795.29	804.22	798.63	790.93	799.12
4	690.18	701.86	677.98	703.24	708.55	699.46	692.06	699.23
5	591.58	601.59	587.67	611.18	612.89	600.29	593.2	599.34
6	492.98	501.33	497.36	519.12	517.22	501.12	494.33	499.45
7	394.39	401.06	407.05	427.06	421.56	401.95	395.46	399.56
8	295.79	300.8	316.74	335.01	325.89	302.77	296.6	299.67
9	197.19	200.53	223.43	242.95	230.23	203.6	197.73	199.78
10	98.6	100.27	136.11	150.89	134.25	104.43	98.87	99.89
11	0	0	45.8	58.83	38.9	5.26	0	0

The flat terrain results highlight clear performance distinctions among the four sites. High-rise configurations, such as Tez-Koop, benefit from unobstructed upper-level exposure, while low-rise but permeable layouts, such as 3D Dubleks, achieve comparable performance through horizontal openness. In contrast, Harp-İş, characterized by uniform 5-story blocks, consistently demonstrates lower radiation values, indicating sensitivity to shading accumulation in flat-grid configurations. These findings suggest that, under flat terrain assumptions, solar efficiency depends heavily on either vertical advantage or generous spacing—conditions not equally present across all cooperatives.

To extend this evaluation into a future-oriented framework, a sloped terrain scenario was introduced to examine how elevation differences influence solar radiation distribution. Rather than leveling the terrain, this scenario allows buildings to follow natural topographical gradients, creating vertical offsets between blocks and façades.

Table 2: Solar Radiation Results under Sloped Terrain Conditions for the Four Study Sites

	Incident Radiation [kWh/m2]							
	Site A		Site B		Site C		Site D	
	Original	Randomized	Original	Randomized	Original	Randomized	Original	Randomized
1	987.37	1002.95	987.59	987.59	999.47	997.95	986.14	998.69
2	888.63	902.65	888.83	888.83	899.53	898.15	887.53	898.82
3	789.9	802.36	790.07	790.07	799.58	798.36	788.91	798.95
4	691.16	702.06	691.31	691.31	699.63	698.56	690.3	699.08
5	592.42	601.77	592.55	592.55	599.68	598.77	591.69	599.21
6	493.68	501.47	493.79	493.79	499.74	498.97	493.07	499.34
7	394.95	401.18	395.04	395.04	399.79	399.18	394.46	399.48
8	296.21	300.88	296.28	296.28	299.84	299.38	295.84	299.61
9	197.47	200.59	197.52	197.52	199.89	199.59	197.23	199.74
10	98.74	100.29	98.76	98.76	99.95	99.79	98.61	99.87
11	0	0	0	0	0	0	0	0

The sloped terrain simulations reveal a generally more stable and, in several cases, improved solar performance compared to the flat scenario. This improvement is particularly evident in mid-rise and mixed-typology settlements. For Tez-Koop, the sloped condition enhances radiation consistency by reducing shading interactions between adjacent towers, especially at lower interfaces. The elevation gradient effectively increases sky exposure for lower façades without requiring additional building height. From a future planning perspective, this suggests that high-rise developments in Batıkent can achieve better environmental outcomes when aligned with topography rather than imposed on flattened terrain.

For Ortadoğulular, which combines duplex units with 8-story blocks, the sloped terrain scenario produces a more balanced radiation distribution across building types. Elevation differences mitigate the shadowing impact of taller blocks on adjacent low-rise units, supporting a more equitable solar environment. This finding is particularly significant for future redevelopment strategies in mixed-morphology areas, indicating that terrain-sensitive design can improve performance without altering building typology.

The 3D Dubleks site shows minimal variation between flat and sloped terrain scenarios. This stability confirms that open, low-rise configurations are inherently resilient to topographical change. From a future perspective, such layouts offer strong adaptability for redevelopment in sloped zones, as their performance does not depend on artificial leveling or complex height manipulation.

In contrast, Harp-İş benefits noticeably from the sloped terrain condition. The introduction of elevation differences reduces continuous shadow corridors formed under flat terrain assumptions, leading to improved radiation values across multiple rows. This outcome suggests that underperforming mid-rise settlements can achieve meaningful environmental gains through terrain-responsive reconfiguration rather than full-scale reconstruction.

Overall, the comparison between flat and sloped terrain scenarios demonstrates that topography-sensitive planning offers clear environmental advantages for Batıkent's future development. Flat terrain conditions tend to amplify the negative effects of dense and uniform block arrangements, while sloped terrain introduces spatial differentiation that enhances solar access, particularly in mid-rise and high-rise contexts. These results indicate that future redevelopment strategies should avoid excessive land leveling and instead adopt stepped massing, slope-aligned orientation, and terrain-integrated block layouts.

In conclusion, future performance scenarios based on terrain variation confirm that topography should be treated as an active design parameter rather than a passive constraint. By integrating slope-aware planning principles into Batıkent's redevelopment and infill strategies, it is possible to improve solar efficiency, reduce shading conflicts, and support long-term energy resilience across all four cooperative areas. This approach provides a critical foundation for subsequent future scenarios involving renewable energy systems and material-based interventions discussed in the following sections.

3.2. Integration of Renewable Energy and Nature-Based Solutions

Achieving long-term sustainability in Batıkent requires the integration of renewable energy systems and nature-based solutions that complement the existing urban morphology while enhancing environmental performance. Building on the terrain-sensitive future scenarios discussed in Section 4.1, this section explores three key intervention strategies—solar panels, green walls, and the advanced insulation material—as complementary measures to improve energy efficiency, thermal comfort, and environmental resilience across the four cooperative sites (3D Dubleks, Harp-İş, Tez-Koop, and Ortadoğulular). These strategies were selected due to their adaptability to different building typologies and their potential to be implemented through retrofitting rather than full-scale reconstruction.

3.2.1. Green Walls as Nature-Based Climate Moderators

Green walls constitute a nature-based solution that addresses multiple environmental challenges simultaneously, including thermal regulation, air quality improvement, and visual enhancement of dense urban façades. In the context of Batıkent, green walls are particularly relevant for mid-rise and high-rise blocks, where limited ground-level green space restricts conventional landscaping options.

Simulation-based projections indicate that green walls can significantly reduce surface temperatures by limiting direct solar absorption on façades, thereby decreasing cooling loads during summer periods. This intervention is especially valuable for Site B (Harp-İş) and Site C (Tez-Koop), where façade shading is more critical due to block density and building height. For Ortadoğulular, green walls can function as transitional elements between duplex units and taller blocks, contributing to microclimatic balance. In 3D Dubleks, green walls primarily serve as complementary features that enhance outdoor comfort and biodiversity rather than as primary thermal regulators.

Beyond thermal benefits, green walls contribute to acoustic buffering and visual softening of rigid building envelopes, improving residents' perception of environmental quality. Their modular nature allows phased implementation, making them feasible within cooperative-based redevelopment frameworks.

3.2.2. Advanced Insulation Material: Concept and Application

A key innovative component of the future development strategy is the integration of advanced fire insulation material, a perlite-based plaster and coating system that provides thermal insulation, acoustic performance, and fire resistance. Advanced Insulation material is free from chemical emissions, does not degrade under solar exposure, and contributes to indoor air quality while enhancing exterior durability. Thermal imaging evidence demonstrates its capacity to maintain significantly lower surface temperatures compared to untreated materials, even under extreme heat exposure.

Figure 2: Advanced Fire Insulation material

3.2.3. Easy Application

1. Advanced fire insulation coating is applied after the application of surface adhesion mortar on surfaces such as brick, gas concrete, lightweight concrete blocks, and concrete.
2. Advanced Insulation material is applied to the surface using 2.5-centimeter anode rods after proper mixing. Due to high plaster adhesion, the consumption is low, and application is easy.
3. It is recommended to use a mesh before applying the final coat of mineral decorative coating or paint. The mesh is applied by pressing it onto the surface of the coating that has been previously applied.
4. After applying the mesh, the desired decorative plaster or paint application completes the process.

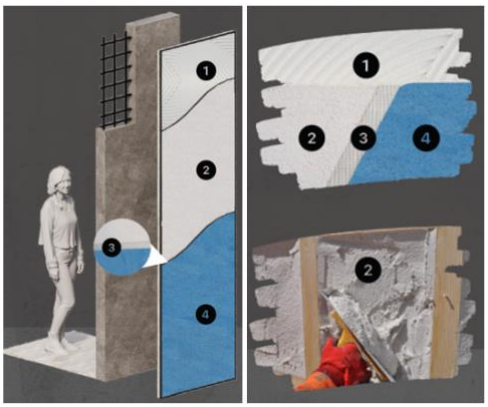

Figure 3: Advanced material Application

3.2.4. Free From Chemical Emissions

Advanced insulation material does not undergo chemical changes when exposed to sunlight and does not release harmful gases or chemicals into the air on the applied surface. This increases the durability of the exterior while maintaining indoor air quality.

3.2.5. Acoustic Effect

While absorbing noise with its sound insulation, Advanced insulation material also prevents sound from echoing indoors and provides acoustic comfort. This enables the creation of a quieter indoor environment or achieving desired sound characteristics.

3.2.6. Noise Insulation

Advanced insulation material limits the transmission of noise from outside to inside or from one room to another with the superior sound insulation it provides. Thus, it creates quieter and more comfortable interior spaces by reducing noise pollution. It reduces sound by 42 decibels in 3 cm thick applications.

Figure 4: Advanced material Specifications

Figure 5: How to install it

From a sustainable development perspective, Advanced insulation material is particularly suitable for retrofitting existing buildings in Batıkent. Its application process—surface preparation, plaster application, mesh reinforcement, and final coating—allows it to be integrated without structural alteration. This makes it highly applicable to Harp-İş and Ortadoğulular, where improving envelope performance is critical to compensating for lower solar efficiency. In Tez-Koop, Advanced insulation material can be combined with façade-mounted PV systems to enhance overall envelope performance, while in 3D Dubleks, it supports indoor comfort and fire safety without compromising architectural openness.

3.2.4. Permeable Outdoor Surfaces

In addition to façade applications, Advanced insulation material -compatible systems can be combined with permeable outdoor flooring solutions, such as self-draining surfaces, to improve stormwater management and thermal behavior in open spaces. These systems allow rainwater infiltration, reduce surface runoff, and mitigate urban heat accumulation—an increasingly important consideration under climate-change conditions.

Figure 6: Paving Stones and Building Components

Lack of drainage causes rainwater to spread uncontrollably into urban infrastructure, leading to environmental problems. Flash floods threaten life and property on streets and roads, while excess water accumulation that cannot be removed from retaining walls can threaten structural integrity. These situations highlight the importance of effective drainage systems and demonstrate their necessity for environmental sustainability and infrastructure safety.

Introducing the ecological paving stones, distinguished by their inherent water permeability. This innovative product combines aesthetics and durability while allowing rainwater to seep into the soil.

3.2.7. Cellular Drainage Technology (CDT)

Traditional paving stones have limited rainwater absorption capacity and, due to their generally hard surfaces, prevent water from penetrating the soil. However, this problem is eliminated with ecologically permeable paving stones. This special design, utilizing Cellular Drainage Technology, allows rainwater to directly seep into the soil, contributing to the natural water cycle and offering an environmentally friendly option.

This eco-friendly paving stone has a wide range of applications including landscaping, retaining walls, walkways, parking lots, pool sides, and car/carpet washing areas. If you are looking for an environmentally friendly and aesthetically pleasing solution for any of your outdoor projects, this specially designed paving stone will be the ideal choice for you.

Such applications are particularly relevant for courtyard spaces in 3D Dubleks and Ortadoğulular, as well as pedestrian zones in Harp-İş, where surface sealing currently limits environmental performance. Integrating permeable materials strengthens Batıkent’s capacity to adapt to extreme weather events while reinforcing ecological sustainability.

In summary, the combined integration of solar panels, green walls, and Advanced insulation material systems offers a multi-layered future strategy for sustainable development in Batıkent. Each intervention addresses different aspects of environmental performance—energy generation, thermal regulation, acoustic comfort, fire safety, and water management—while remaining adaptable to the distinct morphological conditions of the four cooperative sites. Together, these solutions form a coherent, scalable framework for climate-responsive urban regeneration that can be implemented incrementally and strategically across Batıkent.

3.3. Visual Simulation of Future Scenarios: Before–After Comparisons

Visual simulation constitutes a critical component of performance-based urban design, as it enables the translation of numerical and analytical results into spatially comprehensible representations. In the context of Batıkent's sustainable redevelopment, before–after visual simulations were employed to illustrate the potential impacts of proposed environmental interventions on the four cooperative areas—3D Dubleks, Harp-İş, Tez-Koop, and Ortadoğulular. These simulations complement the quantitative findings presented in previous sections by providing a clear visual narrative of how spatial form, building orientation, and material integration can transform environmental performance and urban quality.

For each site, the visual analysis follows a consistent structure. The "before" condition represents the current or baseline situation (status quo), reflecting existing building layouts, orientations, and envelope characteristics. The "after" condition illustrates a future-oriented scenario incorporating the proposed strategies discussed in Section 4.2, including adjusted building orientation, the integration of solar panels, green walls, and the application of Advanced insulation material. This standardized visual framework ensures comparability across the four sites and supports a coherent evaluation of design interventions under different morphological conditions.

In Ortadoğulular, the before–after visuals highlight how the integration of renewable energy systems and envelope improvements can mitigate the environmental limitations of mixed-height development. The existing condition shows a combination of duplex units and mid-rise blocks with limited rooftop utilization and conventional façade materials. In the future scenario, rooftop solar panels are added to both low-rise and mid-rise structures, while Advanced insulation material is applied to building envelopes to enhance thermal and fire performance. The visual outcome demonstrates a more coherent environmental identity, with improved energy-generation capacity and a visibly enhanced building envelope without altering the fundamental urban morphology.

Figure 7: Site 1 ORTADOGULULAR

Figure 8: Site 1 ORTADOGULULAR

In the case of Harp-İş, the before–after comparison plays a particularly important analytical role. The existing visuals reveal the limitations of uniform mid-rise blocks, including repetitive façades and limited environmental differentiation. The future scenario illustrates how targeted interventions—such as rooftop solar panel installation, façade-based green walls, and improved insulation through Advanced insulation material —can significantly enhance environmental quality without requiring structural reconstruction. The visual contrast clearly demonstrates that even morphologically constrained settlements can achieve substantial sustainability gains through strategic retrofitting.

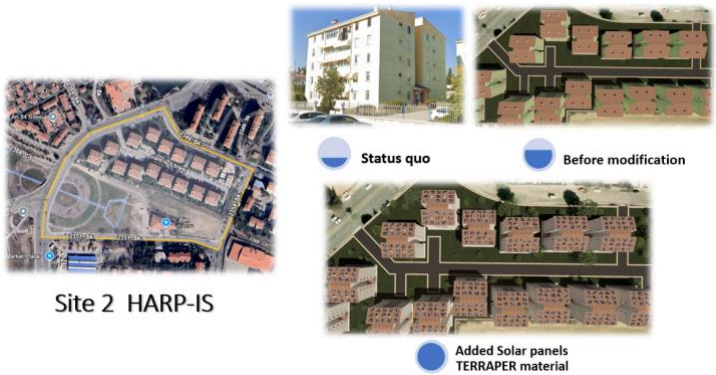

Figure 9: Site 2 HARP-IS

Figure 10: Site 2 HARP-IS

For Akademilier, the visual simulations emphasize the advantages of low-rise, open layouts when combined with renewable and nature-based solutions. The existing condition already exhibits strong spatial permeability and generous open spaces. The future scenario reinforces these qualities through the addition of solar panels on duplex roofs, green wall applications along selected façades, and permeable outdoor surfaces. Visually, the intervention maintains the human-scale character of the site while clearly communicating an upgrade in environmental performance and sustainability.

Figure 11: Site 3 Akademilier

Figure 12. Site 3 Akademilier

For Tez-Koop, the visual simulations focus on the vertical dimension of sustainability. The baseline condition highlights the dominance of high-rise blocks and their extensive façade surfaces. In the future scenario, these surfaces are reimagined as active environmental elements through the integration of photovoltaic systems and advanced insulation materials. The visual outcome underscores the potential of high-rise typologies to function as energy-producing structures, transforming perceived environmental challenges associated with height into long-term advantages.

Figure 13: Site 4 Tez-Koop

Figure 14: Site 4 Tez-Koop

Across all four sites, the before–after visual simulations serve three primary purposes. First, they validate the feasibility of the proposed interventions by demonstrating their spatial compatibility with existing urban forms. Second, they support comparative analysis, allowing differences in response between low-rise, mid-rise, high-rise,

and mixed typologies to be visually assessed. Third, they enhance communication, making complex environmental strategies accessible to planners, decision-makers, and non-technical stakeholders.

In summary, the visual simulation of future scenarios provides a critical bridge between analytical results and design-oriented interpretation. By presenting clear before–after comparisons for each cooperative area, this section reinforces the argument that Batıkent's sustainable transformation can be achieved through incremental, site-specific interventions that respect existing morphology while significantly improving environmental performance. These visuals not only illustrate possible futures for Batıkent but also function as decision-support tools for guiding sustainable urban redevelopment strategies.

3.4. Strategic Synthesis of Future Scenarios

The future-oriented scenarios developed in this study provide a comprehensive framework for guiding the sustainable transformation of Batıkent through performance-based, context-sensitive strategies. By synthesizing the findings from terrain-based simulations, renewable energy integration, nature-based solutions, and visual before–after comparisons, this section consolidates the key strategic insights that can inform both short-term interventions and long-term urban redevelopment policies for the four cooperative areas—3D Dubleks, Harp-İş, Tez-Koop, and Ortadoğulular.

A central outcome of the future scenarios is the recognition that morphological diversity requires differentiated strategies rather than uniform solutions. The comparison between flat and sloped terrain conditions demonstrates that topography significantly influences solar radiation performance, particularly in mid-rise and high-rise settlements. Sloped terrain scenarios consistently produced more balanced and stable solar exposure by reducing mutual shading and introducing vertical differentiation. This finding suggests that future planning in Batıkent should avoid excessive land leveling and instead adopt terrain-responsive massing, stepped building profiles, and slope-aligned orientations. Treating topography as an environmental asset rather than a constraint enables more efficient use of solar potential without increasing density or building height.

The integration of renewable energy systems, particularly solar panels, emerges as a second strategic pillar. Simulation results and visual scenarios confirm that all four sites possess varying but meaningful potential for decentralized solar energy production. High-rise façades and rooftops in Tez-Koop offer large, uninterrupted surfaces for photovoltaic systems, while the low-rise roofs of 3D Dubleks provide ideal conditions for efficient rooftop installations. Mixed-typology areas such as Ortadoğulular can benefit from hybrid deployment strategies, and even lower-performing sites like Harp-İş can achieve significant gains through selective rooftop and orientation-based applications. Strategically, this indicates that Batıkent can transition toward a distributed energy model, reducing reliance on centralized systems while enhancing neighborhood-level energy resilience.

Nature-based solutions, particularly green walls and permeable outdoor surfaces, constitute a third strategic dimension. These interventions address not only thermal performance but also microclimatic comfort, acoustic quality, and visual enhancement. The future scenarios demonstrate that green walls are especially valuable for dense mid-rise and high-rise blocks where ground-level green space is limited. Permeable flooring systems further contribute to sustainable stormwater management and urban heat mitigation, reinforcing Batıkent's adaptive capacity under climate-change pressures. Together, these solutions support a shift toward multifunctional urban surfaces that perform ecological, climatic, and social roles simultaneously.

The application of Advanced insulation material represents a critical enabling strategy that bridges environmental performance and practical feasibility. Its thermal, acoustic, and fire-resistant properties—combined with ease of application—make it particularly suitable for retrofitting existing cooperative housing stock. From a strategic standpoint, Advanced insulation material allows Batıkent to improve building-envelope performance without structural alteration, making sustainability upgrades achievable within legal, financial, and organizational constraints typical of cooperative developments. When combined with renewable energy systems, Advanced insulation material contributes to a holistic envelope strategy that enhances both energy efficiency and safety.

Finally, the visual simulation of before–after scenarios plays a key strategic role in translating analytical findings into actionable design guidance. These visuals demonstrate that meaningful environmental improvements can be achieved through incremental interventions rather than radical urban restructuring. They also provide a powerful communication tool for stakeholders, supporting informed decision-making and increasing the likelihood of implementation.

In synthesis, the future scenarios collectively indicate that Batıkent's sustainable development should be guided by four core principles: terrain-sensitive planning, distributed renewable energy integration, nature-based and material-based envelope enhancement, and incremental, site-specific transformation. By aligning these principles with the district's existing morphological structure, Batıkent can evolve into a resilient, energy-efficient, and climate-responsive urban environment while preserving its original cooperative planning identity. This strategic synthesis provides a transferable model for sustainable redevelopment in similar mass-housing contexts in Ankara and beyond.

4. Discussion

The findings of this study demonstrate that future-oriented, simulation-based strategies can play a decisive role in enhancing the environmental performance of existing cooperative housing districts such as Batıkent. By focusing on forward-looking scenarios rather than static evaluations of current conditions, the research contributes to an emerging body of literature that frames urban sustainability as a dynamic and adaptive process. The results highlight how spatial morphology, terrain configuration, and targeted environmental interventions interact to shape long-term solar performance and energy potential.

One of the most significant outcomes concerns the role of topography in future urban performance. The comparison between flat and sloped terrain scenarios reveals that terrain-sensitive configurations consistently improve or stabilize solar radiation distribution, particularly in mid-rise and high-rise developments. This finding aligns with previous studies demonstrating that elevation differences and stepped massing reduce mutual shading and enhance sky exposure in dense urban environments (Compagnon, 2004; Lobaccaro & Frontini, 2014). The results challenge conventional planning practices that prioritize land leveling and instead support approaches that integrate natural terrain as a design parameter. From a sustainability perspective, this reinforces the argument that topography should be leveraged as an environmental asset rather than treated as a constraint (Toparlar et al., 2017). The site-based comparisons further reveal that urban morphology strongly mediates environmental performance outcomes. Low-rise, permeable configurations such as the 3D Dubleks site show relative stability across terrain scenarios, confirming that horizontal openness and reduced building height inherently mitigate shading effects. In contrast, uniform mid-rise developments such as Harp-İş exhibit greater sensitivity to both terrain and orientation, resulting in lower baseline solar performance. High-rise typologies, represented by Tez-Koop, benefit from increased exposure at upper levels but require careful spatial coordination to avoid excessive shading at lower interfaces. These patterns are consistent with earlier research linking building height diversity and spatial articulation to improved solar access at the neighborhood scale (Ratti et al., 2005; Steemers, 2003).

The integration of renewable energy systems, particularly solar panels, emerges as a viable and scalable strategy across all four sites, albeit with varying degrees of effectiveness depending on morphology. The simulations indicate that both rooftop and façade-based photovoltaic installations can significantly enhance energy potential when aligned with building height and orientation. This finding supports existing literature emphasizing the importance of integrating solar energy considerations into early design and retrofit stages rather than treating renewable systems as add-on technologies (Kämpf et al., 2010; Mainzer et al., 2014). In the context of cooperative housing districts, where structural transformation is often limited, the ability to deploy solar systems incrementally is particularly valuable.

Nature-based solutions, including green walls, contribute an additional layer of environmental performance by addressing thermal regulation and microclimatic comfort. While green walls do not directly increase solar energy production, their capacity to reduce façade surface temperatures and mitigate heat accumulation enhances overall energy efficiency, especially in dense mid-rise and high-rise settings. This aligns with empirical studies demonstrating the cooling and insulating effects of vertical greening systems in urban environments (Perini et al.,

2011; Ng et al., 2012). In Batıkent, green walls are shown to be most effective as complementary interventions that enhance envelope performance rather than as standalone solutions.

The application of advanced insulation materials, such as Advanced insulation material, further strengthens the feasibility of future-oriented sustainability strategies. Material-based interventions play a critical role in bridging the gap between analytical potential and practical implementation. High-performance insulation has been widely recognized as one of the most cost-effective means of reducing energy demand in existing buildings (Santamouris, 2014). In this study, Advanced insulation material's suitability for retrofitting without structural modification positions it as a strategic enabler for cooperative housing contexts, where legal, financial, and organizational constraints often limit large-scale redevelopment.

A key methodological contribution of this study lies in the use of before–after visual simulations to support the interpretation of numerical results. Visual representations translate abstract performance metrics into spatially intelligible scenarios, facilitating communication between researchers, planners, and decision-makers. Previous studies have emphasized that visualization enhances stakeholder engagement and improves the uptake of sustainability-driven design strategies (Robinson et al., 2009; Sheppard, 2012). In the Batıkent case, the visual simulations confirm that meaningful environmental improvements can be achieved through incremental, site-specific interventions rather than radical urban restructuring.

From a broader perspective, the results reinforce the argument that there is no universally optimal urban form for sustainability. Instead, environmental performance emerges from the interaction between morphology, terrain, climate, and technological intervention. This finding supports adaptive planning frameworks that prioritize context-sensitive solutions over standardized design models (Sharifi & Murayama, 2013). For Batıkent, this implies that future development strategies should be differentiated across cooperative areas while guided by shared sustainability principles.

Despite its contributions, the study has limitations that should be acknowledged. The analysis focuses primarily on solar radiation as a key environmental indicator, while other factors such as wind comfort, indoor thermal performance, and user behavior are addressed conceptually rather than through full simulation. Future research could extend the framework by integrating multi-variable environmental modeling and socio-economic considerations to further refine strategic recommendations.

Overall, the discussion underscores that simulation-based, future-oriented strategies provide a robust foundation for sustainable redevelopment in cooperative housing districts. By combining terrain-sensitive planning, renewable energy integration, material-based interventions, and visual simulation, the study offers a transferable model for enhancing environmental performance in established urban contexts under increasing climatic and energy-related pressures.

5. Conclusion

This study has examined future-oriented, simulation-based strategies for the sustainable development of Batıkent, Ankara, with a particular focus on how existing cooperative housing areas can be environmentally enhanced through scenario-driven planning rather than large-scale reconstruction. By employing parametric simulation tools and visual scenario modeling, the research moves beyond conventional performance evaluation and demonstrates how alternative future configurations can inform sustainable urban transformation in established residential districts.

The findings confirm that urban morphology and terrain configuration play a decisive role in shaping environmental performance. The comparison between flat and sloped terrain scenarios clearly shows that terrain-sensitive planning improves the stability and distribution of solar radiation, particularly in mid-rise and high-rise settlements. Rather than treating topography as a constraint to be neutralized, the results support planning approaches that integrate natural elevation differences into massing and orientation strategies. This insight is especially relevant for districts such as Batıkent, where gentle slopes are present and can be leveraged to enhance solar access without increasing building height or density.

The study also demonstrates that renewable energy integration and nature-based solutions can significantly improve environmental performance when applied in a typology-sensitive manner. Solar panels, green walls, and advanced insulation materials such as Advanced insulation material were shown to be adaptable across low-rise, mid-rise, high-rise, and mixed-use configurations. Importantly, these interventions can be implemented through incremental retrofitting, making them feasible within the institutional and financial constraints typical of cooperative housing environments. The results underline that sustainability gains do not require radical urban restructuring but can be achieved through targeted, evidence-based interventions aligned with existing spatial conditions.

A key contribution of this research lies in the combined use of numerical simulation and visual before–after scenarios. While quantitative results provide objective performance indicators, visual simulations translate these outcomes into spatially intelligible representations that support communication and decision-making. This dual approach strengthens the applicability of simulation-based strategies by bridging the gap between technical analysis and design-oriented planning practice.

From a broader perspective, the study reinforces the understanding that there is no single optimal urban form for sustainability. Environmental performance emerges from the interaction between spatial configuration, terrain, climate, and technological intervention. Consequently, sustainable redevelopment strategies should prioritize flexibility, context sensitivity, and adaptability rather than uniform design prescriptions. In the case of Batıkent, this implies differentiated strategies for each cooperative area, guided by shared sustainability principles but tailored to local morphological characteristics.

In conclusion, the research demonstrates that future-oriented, simulation-based planning offers a robust framework for guiding sustainable development in existing cooperative housing districts. The strategies proposed for Batıkent provide transferable insights for similar urban contexts seeking to enhance energy efficiency, environmental resilience, and long-term sustainability through incremental, data-driven, and context-aware interventions.

Declaration of Competing Interest: The authors declare that they have no known competing financial interests or personal relationships that could have appeared to influence the work reported in this paper.

Funding Statement: No external funding was received for this research.

Data Availability: All data generated or analyzed during this study are included in the manuscript and supplementary material. Additional simulation data can be provided upon request.

Ethical Approval: Not applicable. The study involves no human subjects, animals, or sensitive data.

Declaration of Generative AI and AI-assisted Technologies: This study has not used any generative AI tools or technologies in the preparation of this manuscript.

References

Compagnon, R. (2004). Solar and daylight availability in the urban fabric. *Energy and Buildings*, 36(4), 321–328.

Eryildiz, D. I., & Eryildiz, S. (2004, September). A comparative analysis of the built and project. In *PLEA 2004—the 21st conference on passive and low energy architecture*.

Eryıldız, D., & Eryıldız, S. (2005). Ekolojik planlama ve tasarım ilişkisi. *Ege Üniversitesi Güneş Enerjisi Enstitüsü 4. Yenilenebilir Enerjiler Sempozyumu ve Sanayi Sergisi Bildiri Özetleri*, *45*.

Eryıldız, S. (1996). Kentsel Ekoloji. *Mimarlık Dergisi*, *25*(1), 25-30.

Eryıldız, S. (2005). Kentsel ekolojik yerleşim rehberi. *İBB Kentsel Dönüşüm Müdürlüğü çalışmaları*.

ErYıldız, S. (2007). Ekolojik mimarlıkla Çevreci Kentler Mümkün.

Jenks, M., & Burgess, R. (2000). *Compact cities: Sustainable urban forms for developing countries*. Spon Press.

Kämpf, J. H., Robinson, D., & Papadopoulos, S. (2010). Solar irradiation of buildings in urban environments: A comparison of modeling approaches. *Solar Energy, 84*(9), 1542–1558.

Lobaccaro, G., & Frontini, F. (2014). Solar energy in urban environment: How urban densification affects existing buildings. *Energy Procedia*, 48, 1559–1569.

Mainzer, K., Fath, K., McKenna, R., Stengel, J., Fichtner, W., & Schultmann, F. (2014). A high-resolution determination of the technical potential for residential-roof-mounted photovoltaic systems in Germany. *Energy and Buildings, 86*, 154–162.

Ng, E., Chen, L., Wang, Y., & Yuan, C. (2012). A study on the cooling effects of greening in a high-density city: An experience from Hong Kong. *Building and Environment, 55*, 39–48.

Perini, K., Ottelé, M., Fraaij, A. L. A., Haas, E. M., & Raiteri, R. (2011). Vertical greening systems and their effect on air flow and temperature on the building envelope. *Building and Environment, 46*(11), 2287–2294.

Ratti, C., Baker, N., & Steemers, K. (2005). Energy consumption and urban texture. *Energy and Buildings*, 37(7), 762–776.

Robinson, D., Campbell, N., Gaiser, W., Kabel, K., Le-Mouel, A., Morel, N., Page, J., Stankovic, S., & Stone, A. (2009). SUNtool—A new modeling paradigm for simulating and optimizing urban sustainability. *Building and Environment, 44*(6), 1181–1193.

Santamouris, M. (2014). Cooling the cities – A review of reflective and green roofs. *Energy and Buildings*, 103, 682–703.

Sharifi, A., & Murayama, A. (2013). A critical review of seven selected neighborhood sustainability assessment tools. *Environmental impact assessment review*, *38*, 73-87.

Steemers, K. (2003). Energy and the city: Density, buildings and transport. *Energy and Buildings, 35*(1), 3–15.

SuSan, M., & Eryıldız, H. S. (2023). Sustainable Eco-village for the Displaced Community of Hatay, Turkey. *Int. J. Sch. Res. Rev*, *2*, 54-72.

Toparlar, Y., Blocken, B., Maiheu, B., & van Heijst, G. J. F. (2017). A review on the CFD analysis of urban microclimate. *Building and Environment, 124*, 337–353.

Yeang, K., Eryıldız, S., & Eryıldız, D. (2012). *Ekotasarım: ekolojik tasarım rehberi*. Yem Yayın.